

WIND TUNNEL INVESTIGATION OF
JOINED WING CONFIGURATIONS

THESIS

JENNIFER CORNEILLE, LIEUTENANT, USAF

AFIT/GAE/ENY/99J-02

19990625 010

, Approved for public release; distribution unlimited

Disclaimer

The views expressed in this thesis are those of the author and do not reflect the official policy or position of the United States Air Force, the Department of Defense, or the United States Government.

AFIT/GAE/ENY/99J-02

WIND TUNNEL INVESTIGATION OF JOINED WING CONFIGURATIONS

THESIS

Presented to the Faculty of the Graduate School of Engineering
of the Air Force Institute of Technology
Air University in Partial Fulfillment of the
Requirements for the Degree of
Master of Aeronautical Engineering

Jennifer Corneille, B.ME
Lieutenant, USAF

June 1999

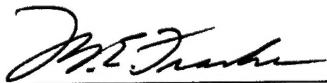
Approved for public release; distribution unlimited

AFIT/GAE/ENY/99J-02

WIND TUNNEL INVESTIGATION OF JOINED WING CONFIGURATIONS

Jennifer Corneille
First Lieutenant, USAF

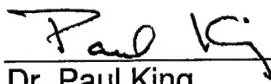
Approved:



Dr. Milt Franke
Committee Chairman

2 Jun 99

Date



Dr. Paul King
Committee Member

2 June 99

Date



Captain Jeffery Bons
Committee Member

3 June 99

Date

Acknowledgments

I would like to thank everyone who helped me immensely throughout this study. I would especially like to thank Charles McNeely for his constant help in the wind tunnel and trying to get the balance fixed as soon as possible. I would like to thank Jay Anderson for his constant pursuit in getting the balance fixed as well. Thanks to Dr. Milt Franke for his advice and recommendations on this thesis to make it the best one possible. And finally to Sean Krolikowski and my mom for their constant support and for always trying to keep me sane every time something went wrong.

Table of Contents

| | |
|----------------------------------|-----|
| Acknowledgments | iii |
| List of Figures | vi |
| List of Tables | xi |
| List of Symbols | xii |
| Abstract | xv |
| I. Introduction | 1 |
| Background | 1 |
| Current Studies | 1 |
| Problem Statement | 3 |
| II. Literature Review | 3 |
| Overview | 3 |
| Light Weight | 5 |
| Stiffness | 8 |
| Drag | 9 |
| Stability and Control | 13 |
| High Lift | 14 |
| Miscellaneous | 18 |
| As Compared to This Thesis | 19 |
| III. Methodology | 20 |
| Model | 20 |
| Equipment | 24 |
| Calibration | 25 |

| | |
|---------------------------------|-----|
| Test Plan | 25 |
| Computation of Parameters | 26 |
| Drag | 27 |
| Lift | 30 |
| Pitching Moment | 31 |
| Rolling Moment | 31 |
| Range | 32 |
| Compressibility Analysis | 32 |
| Data Reduction | 33 |
| Error Analysis | 35 |
| IV. Results | 37 |
| V. Summary | 59 |
| VI. Bibliography | 60 |
| Appendix A | 62 |
| Appendix B | 64 |
| Vita | 106 |

List of Figures

| | |
|--|----|
| Figure 1: CFD Analysis of Flow Over a Joined Wing Configuration..... | 2 |
| Figure 2: JW Joined Wing Configuration, Negative Stagger [14]..... | 4 |
| Figure 3: Swept Forward/Swept Rearward (SFSR) Joined Wing Configuration, Positive Stagger [14] | 4 |
| Figure 4: Single Wing Configuration [10] | 4 |
| Figure 5: Internal Structure of a Joined Wing [8] | 5 |
| Figure 6: Optimum Wing Structures [9] | 6 |
| Figure 7: Effective Wing Depth of Joined Wing [9] | 7 |
| Figure 8: Beam Depth of Single Wing [8] | 8 |
| Figure 9: Span Efficiency Factor for Joined Wings [18] | 10 |
| Figure 10: Control Deflections of the Joined Wing [8]..... | 15 |
| Figure 11: Measured Variation with Angle of Attack of Untrimmed Lift Coefficients Referred to Total Exposed Areas of All Lifting Surfaces [9] | 17 |
| Figure 12: Profiles for the 30° and 60° Swept Wing | 22 |
| Figure 13: Smart Missile with Wing Components | 22 |
| Figure 14: 60° Swept Joined Wing with Curved Connectors, Negative Stagger. | 23 |
| Figure 15: 30° Swept Joined Wing with Straight Connectors, Negative Stagger | 23 |
| Figure 16: Single Wing Configurations | 24 |
| Figure 17: AFIT 5' Wind Tunnel..... | 25 |
| Figure 18: Wind Axis and Body Axis Forces..... | 28 |
| Figure 19: Comparison of the Lift and Drag Relations for the 60° Swept Wings, Flown at 100 mph (44.7 m/s)..... | 39 |
| Figure 20: Comparison of the Lift and Drag Relations for the 30° Swept Wings, Flown at 100 mph (44.7 m/s)..... | 40 |

| | |
|--|----|
| Figure 21: Comparison of the Lift and Drag Relations for the 60° Swept Wings, Flown at 175 mph (78.2 m/s)..... | 41 |
| Figure 22: Comparison of the Lift and Drag Relations for the 30° Swept Wing, Flown at 175 mph (78.2 m/s)..... | 42 |
| Figure 23: Lift and Drag Relations of the 60° Swept Joined Wing with Curved Connectors, Negative Stagger | 43 |
| Figure 24: Lift and Drag Comparison of the Configurations, Flown at 175 mph (78.2 m/s) | 45 |
| Figure 25: Comparison of the Lift and Drag Coefficient Relations for the 60° Swept Wings | 46 |
| Figure 26: Comparison of the Drag Coefficient and Induced Drag Relations for the 60° Swept Wings | 47 |
| Figure 27: Comparison of the Lift and Drag Coefficient Relations for the 30° Swept Wings | 48 |
| Figure 28: Comparison of the Drag Coefficient and Induced Drag Relations for the 30° Swept Wings | 49 |
| Figure 29: Lift and Drag Coefficient Comparison of the Configurations..... | 51 |
| Figure 30: Error Analysis of the Lift and Drag Coefficients of the 60° Sweep Joined Wing with Straight Connectors, Negative Stagger | 58 |
| Figure 31: Lift and Drag Relations of the Bare Missile..... | 65 |
| Figure 32: Lift and Drag Relations of the 60° Swept Joined Wing with Curved Connectors, Negative Stagger | 66 |
| Figure 33: Pitch and Roll Relations of the 60° Swept Joined Wing with Curved Connectors, Negative Stagger | 67 |
| Figure 34: Lift and Drag Relations of the 60° Swept Joined Wing with Curved Connectors, Positive Stagger | 68 |
| Figure 35: Pitch and Roll Relations of the 60° Swept Joined Wing with Curved Connectors, Positive Stagger | 69 |
| Figure 36: Lift and Drag Relations of the 60° Swept Joined Wing with Straight Connectors, Negative Stagger | 70 |

| | |
|---|----|
| Figure 37: Pitch and Roll Relations of the 60° Swept Joined Wing with Straight Connectors, Negative Stagger | 71 |
| Figure 38: Lift and Drag Relations of the 60° Swept Joined Wing with Straight Connectors, Positive Stagger | 72 |
| Figure 39: Pitch and Roll Relations of the 60° Swept Joined Wing with Straight Connectors, Positive Stagger | 73 |
| Figure 40: Lift and Drag Relations of the 60° Swept Biplane, Negative Stagger | 74 |
| Figure 41: Pitch and Roll Relations of the 60° Swept Biplane, Negative Stagger | 75 |
| Figure 42: Lift and Drag Relations of the 60° Swept Biplane, Positive Stagger | 76 |
| Figure 43: Pitch and Roll Relations of the 60° Swept Biplane, Positive Stagger | 77 |
| Figure 44: Lift and Drag Relations of the 60° Swept Single Wing Located Aft of the CG, Wings on Bottom | 78 |
| Figure 45: Pitch and Roll Relations of the 60° Swept Single Wing Located Aft of the CG, Wings on Bottom | 79 |
| Figure 46: Lift and Drag Relations of the 60° Swept Single Wing Located Aft of the CG, Wings on Top..... | 80 |
| Figure 47: Pitch and Roll Relations of the 60° Swept Single Wing Located Aft of the CG, Wings on Top..... | 81 |
| Figure 48: Lift and Drag Relations of the 60° Swept Single Wing Located Forward of the CG, Wings on Bottom | 82 |
| Figure 49: Pitch and Roll Relations of the 60° Swept Single Wing Located Forward of the CG, Wings on Bottom | 83 |
| Figure 50: Lift and Drag Relations of the 60° Swept Single Wing Located Forward of the CG, Wings on Top | 84 |
| Figure 51: Pitch and Roll Relations of the 60° Swept Single Wing Located Forward of the CG, Wings on Top | 85 |

| | |
|---|-----|
| Figure 52: Lift and Drag Relations of the 30° Swept Joined Wing with Curved Connectors, Negative Stagger | 86 |
| Figure 53: Pitch and Roll Relations of the 30° Swept Joined Wing with Curved Connectors, Negative Stagger | 87 |
| Figure 54: Lift and Drag Relations of the 30° Swept Joined Wing with Curved Connectors, Positive Stagger | 88 |
| Figure 55: Pitch and Roll Relations of the 30° Swept Joined Wing with Curved Connectors, Positive Stagger | 89 |
| Figure 56: Lift and Drag Relations of the 30° Swept Joined Wing with Straight Connectors, Negative Stagger | 90 |
| Figure 57: Pitch and Roll Relations of the 30° Swept Joined Wing with Straight Connectors, Negative Stagger | 91 |
| Figure 58: Lift and Drag Relations of the 30° Swept Joined Wing with Straight Connectors, Positive Stagger | 92 |
| Figure 59: Pitch and Roll Relations of the 30° Swept Joined Wing with Straight Connectors, Positive Stagger | 93 |
| Figure 60: Lift and Drag Relations of the 30° Swept Biplane, Negative Stagger | 94 |
| Figure 61: Pitch and Roll Relations of the 30° Swept Biplane, Negative Stagger | 95 |
| Figure 62: Lift and Drag Relations of the 30° Swept Biplane, Positive Stagger | 96 |
| Figure 63: Pitch and Roll Relations of the 30° Swept Biplane, Positive Stagger | 97 |
| Figure 64: Lift and Drag Relations of the 30° Swept Single Wing Located Aft of the CG, Wings on Bottom | 98 |
| Figure 65: Pitch and Roll Relations of the 30° Swept Single Wing Located Aft of the CG, Wings on Bottom | 99 |
| Figure 66: Lift and Drag Relations of the 30° Swept Single Wing Located Aft of the CG, Wings on Top | 100 |

| | |
|---|-----|
| Figure 67: Pitch and Roll Relations of the 30° Swept Single Wing Located Aft of the CG, Wings on Top | 101 |
| Figure 68: Lift and Drag Relations of the 30° Swept Single Wing Located Forward of the CG, Wings on Bottom..... | 102 |
| Figure 69: Pitch and Roll Relations of the 30° Swept Single Wing Located Forward of the CG, Wings on Bottom | 103 |
| Figure 70: Lift and Drag Relations of the 30° Swept Single Wing Located Forward of the CG, Wings on Top | 104 |
| Figure 71: Pitch and Roll Relations of the 30° Swept Single Wing Located Forward of the CG, Wings on Top | 105 |

List of Tables

| | |
|--|----|
| Table 1: Various Parameters of the Model Configurations | 21 |
| Table 2: Model Test Configurations..... | 27 |
| Table 3: Legend Notation | 38 |
| Table 4: Range Ratio..... | 55 |
| Table 5: Calculation of the Error in the Drag Coefficient..... | 63 |

List of Symbols

- a - Distance from the force N_1 to the center of gravity
- A - Axial force
- AR - Aspect ratio
- AR_F - Aspect ratio of the front wing
- AR_R - Aspect ratio of the rear wing
- b - Span; Distance from the force N_2 to the center of gravity
- b_{longer} - Span of the longer wing
- c - Chord
- C - Specific fuel consumption
- C_D - Drag coefficient
- C_{Di} - Induced drag coefficient
- C_{D0} - Incompressible drag coefficient
- C_f - Skin friction drag coefficient
- CG - Center of gravity
- C_L - Lift coefficient
- $C_{L\text{max}}$ - Maximum lift coefficient
- C_{L0} - Incompressible lift coefficient
- d - Beam depth for single wing
- d' - Effective beam depth for joined wing
- D - Drag
- D_{jw} - Drag of the joined wing
- D_{sw} - Drag of the single wing

e - Span efficiency factor

h - Maximum distance between joined wings

L - Lift

L' - Rolling moment

L_{jw} - Lift of the joined wing

L_{sw} - Lift of the single wing

M - Pitching moment

M_∞ - Freestream Mach number

N - Total normal force

N_1 - Normal force measured at location 1

N_2 - Normal force measured at location 2

r - Area of the shorter wing/area of the longer wing

R - Range

Re_c - Reynolds number based on the total plate length c

Re_x - Reynolds number based on the distance from the entrance of the tunnel to the test section

S - Reference area

S_F - Area of the front wing

S_R - Area of the back wing

V_∞ - Free stream velocity

W_0 - Initial weight

W_1 - Final weight

x - Distance from the entrance of the tunnel to the test section

α - Angle of attack

δ^* - Displacement thickness

ε_t - Total blockage

Λ_{LE} - Sweep angle of the leading edge of the wing

μ - Shorter span/longer span

ρ_∞ - Freestream density

σ - Interference factor

Abstract

The Air Force Research Laboratory's Munitions Directorate is looking to extend the range of its small smart bomb. One proposed idea is to retrofit the bombs with a wing kit, particularly a joined wing configuration. A typical joined wing configuration is one where the wings are positioned in such a way that they form a diamond in both plan and front views. The purpose of this study is to conduct low speed wind tunnel testing of the joined wing configuration to help determine if the joined wing is more beneficial than a single wing configuration. Configurations with differing sweep angles and tip interconnects will be tested in the AFIT 5' wind tunnel. The lift, drag, and pitching moment coefficients will be ascertained. All researched literature indicates that certain joined wing configuration outperforms its single wing counterpart.

WIND TUNNEL INVESTIGATION OF JOINED WING CONFIGURATIONS

I. Introduction

Background

Early aircraft designers realized the benefits of a biplane — it had more lifting surfaces and therefore could produce more lift. Unfortunately, the wires that structurally held the wings together created a lot of profile drag, which practically voided the added benefit of the extra lifting surfaces [1]. The movement was then towards the commonly seen single wing of today. It was structurally sound and did not have the incredible profile drag the biplanes had. Today, however, with the advent of new materials and structural ideas, the biplane concept is no longer plagued by the high profile drag. One of the upcoming configurations for the biplane is the joined wing. The joined wing not only creates a more structurally sound wing system, it also cuts down on the vortices shedding off the wingtips, thus helping reduce the induced drag [1]. The joined wing also offers more area for control surfaces, making it very stable. With this increase in lift and stability and reduction in drag, the plane could theoretically have a longer range or be lighter in weight compared to its single counterpart.

Current Studies

During the 1980's, Julian Wolkovitch was a leading expert and advocate of the joined wing [1]. Today, many companies and organizations are continuing his work to make the joined wing configuration a flying reality. Lockheed Martin

is looking to incorporate the joined wing design on the next generation tankers. The hope is that the joined wing tanker, designated the New Strategic Aircraft, will be able to carry more fuel and have a two-boom system, thereby allowing the Air Force to refuel more planes with fewer tankers. A radio-scaled model has flown eleven successful flights, validating Lockheed Martin's choice of the joined wing configuration [2,3]. Other companies are looking to validate the joined wing as well. NASA Langley (LaRC) has been working with the Boeing Military Airplane Company to verify Boeing's joined wing design. So far, tests have been run in the LaRC 16-foot transonic tunnel at Mach 0.32 to 0.9. The Boeing configuration is proposed to replace the Navy's E-2C Hawkeye [4]. Aside from the experimental tests, many people are developing CFD programs to analyze the joined wing configuration [5-7]. Figure 1 shows a picture of such a CFD analysis conducted by Boeing [7].

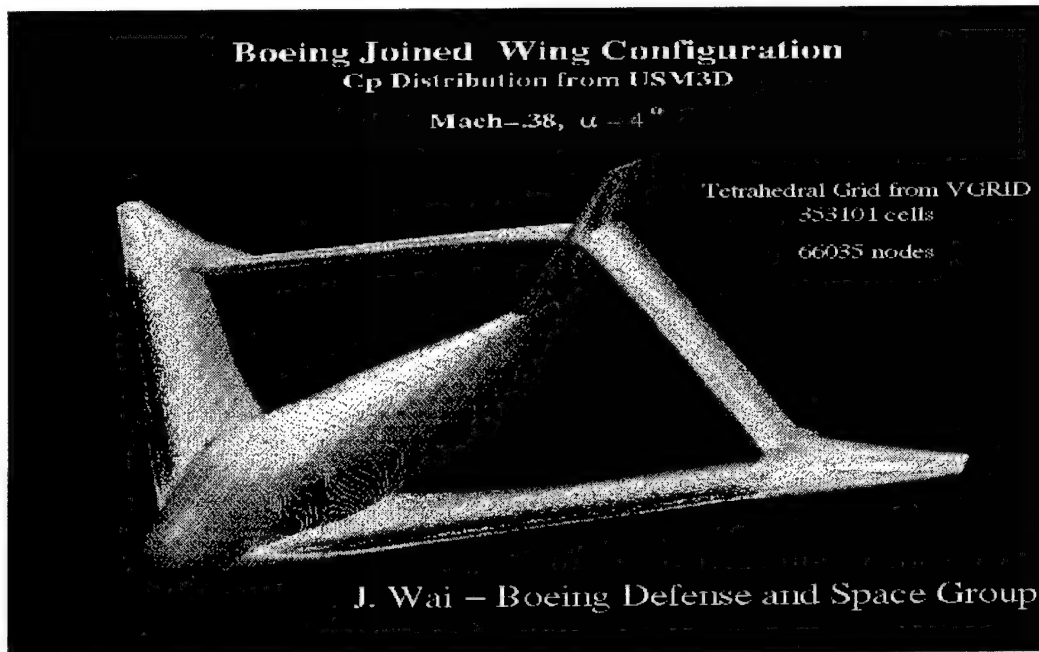


Figure 1: CFD Analysis of Flow Over a Joined Wing Configuration

Despite all of this research into the joined wing configuration, there is still much to learn and study.

Problem Statement

The Air Force Research Laboratory (AFRL) Munitions Division is looking to extend the range of a 250-pound smart bomb [16]. With the bomb able to travel that much farther, the pilot can release the payload and fly out of the war zone that much sooner -- possibly preventing the aircraft from being shot down. One of the proposed ideas is to retrofit smart bombs with wing kits for range extension. Instead of adding just a single wing system, the Munitions Division is interested in finding out if the joined wing configuration is substantially more beneficial than its single counterpart. In addition, it is desired to determine what type of wing tip connectors, curved or straight, will maximize the aerodynamic performance of the joined wing. It is the scope of this study to determine the lift and drag and pitching moment of several joined wing configurations. These results could help determine if the joined wing is indeed more beneficial than the single wing.

II. Literature Review

Overview

Julian Wolkovitch defines the joined wing as "arranged such that the wings form diamond shapes both in plan view and front view" [8]. Figures 2-4 depict two types of joined wing and the single wing. Biplanes and joined wings can be described in terms of the stagger of the wings. Stagger is the longitudinal offset of the two wings relative to each other. A positive stagger configuration is one

where the top wing is closer to the nose. Differing staggers can be seen in Figures 2 and 3. The joined wing configurations, if designed correctly, have many benefits over the single wing. This chapter will discuss those benefits, as related by various researchers, in terms of aerodynamics, stability, design options, and in comparison to the single wing

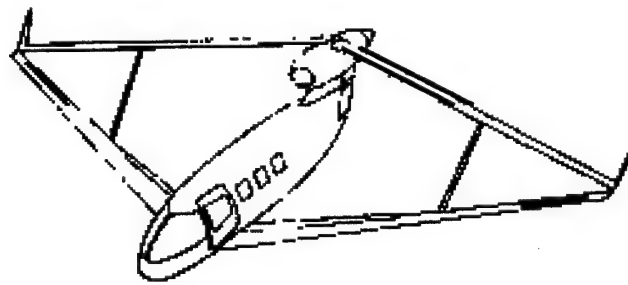


Figure 2: JW Joined Wing Configuration, Negative Stagger [14]

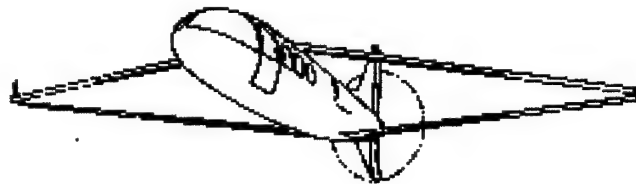


Figure 3: Swept Forward/Swept Rearward (SFSR) Joined Wing Configuration, Positive Stagger [14]

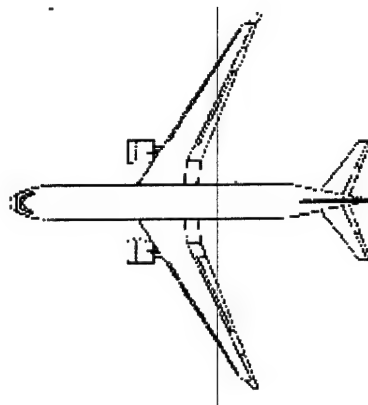


Figure 4: Single Wing Configuration [10]

Light Weight

The joined wing can offer great weight savings based on a number of factors. Just comparing a joined wing with a single wing that has the same airfoil, equal parasite and induced drag, and taper ratios, the joined wing is about 24% lighter than the single wing plane [8]. This has a lot to do with the chordwise tapering. Skin thickness helps to provide structural stability in the wings. Less skin thickness is required in the joined wing because of its bracing of the wings. This reduces the overall weight of the wing [9]. Figure 5 shows the chordwise tapering of the wingbox and the skin thickness for the joined wing.

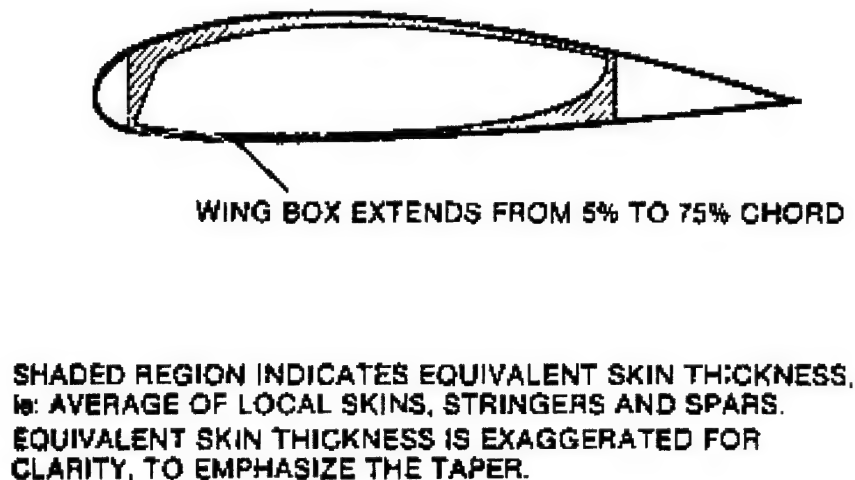


Figure 5: Internal Structure of a Joined Wing [8]

An added benefit besides the weight savings that the smaller skin thickness offers is that a larger wing box can be employed – one that extends from 5% to 75% of the chord [8,9]. This adds to the amount of fuel that can be carried, thus extending the range. Figure 6 shows the optimum wing structures for the single wing and the joined wing – depicting the extended wing box, and

the chordwise tapering. As can be seen, the single wing has a more rectangular wingbox that is positioned in the thickest part of the airfoil. The joined wing has a wingbox that follows the contours of the airfoil and encompasses the entire airfoil. With this enlarged wingbox in the joined wing, more fuel can be carried. It must be noted that this design point may not always be needed. For instance, in this study the wings are solid and are not used to carry fuel. Consequently, there would not be the added weight savings from the smaller skin thickness.

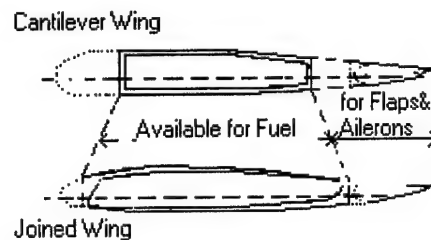


Figure 6: Optimum Wing Structures [9]

In another study, the weight of the joined wing was 65 to 78% less than the single wing system that had the same gross projected area, equal taper ratio and magnitude of sweep angle, and equal ratio of front to rear lifting surface projected area [9,10]. This is one of the first examples of how hard it can be to compare the joined wing and single wing configurations. Depending on which parameters one tries to match can give quite different results. As indicated above, in the first case the joined wing was 24% lighter where in Reference 9, the joined wing was 65% lighter. Each study equated different parameters between the joined wing and the single wing, causing this disparity. This shows

the importance of paying attention to the parameters cited in order to compare different sources accurately.

Other factors that tend to reduce the weight of the joined wing are reduction in sweep, large dihedrals, and joining the wings inboard of the tips. While joining the wings inboard will reduce the weight, the tip joined configurations tends to have more aerodynamic advantages that may be more beneficial to have over the weight savings [8,9]. These advantages, such as higher span efficiency factor, will be discussed further in a later section.

The effective beam depth, d' , is defined from the root centerline chords of the front and rear wings as seen in Figure 7 [8,9]. The effective beam depth is a way to refer to the "total" depth of the joined wing system as opposed to the depth defined on the single wing shown in Figure 8. Because of this effective beam depth, it was found that the weight of the joined wing is not as sensitive to the thickness/chord ratio as a single wing. Therefore, thin airfoils can be applied, allowing this wing system to be effective during supersonic flight. With thin airfoils comes even more weight savings [8].

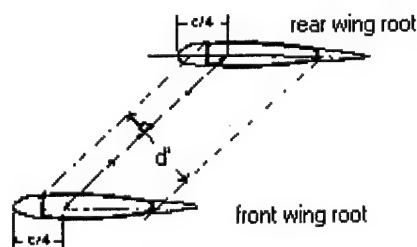


Figure 7: Effective Wing Depth of Joined Wing [9]

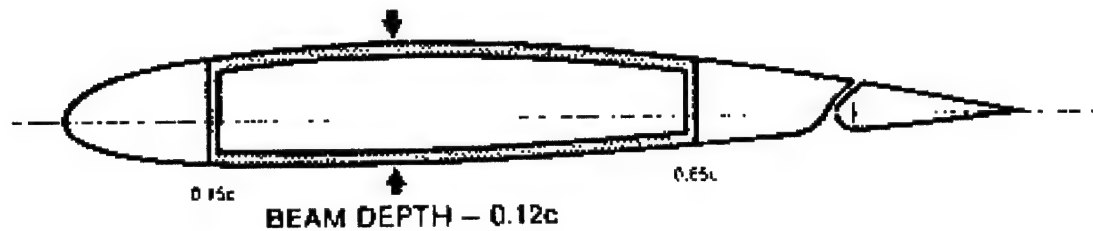


Figure 8: Beam Depth of Single Wing [8]

Joined wings are not always necessarily lighter than single wings. Weight will be saved only if the geometric parameters of the joined wing are properly chosen and if the internal wing structure is optimized [9]. In general, though, the standard joined wing and swept forward/swept rearward configurations tends to be lighter than the single wing with the same flight mission.

Stiffness

Since the two wings form a box-like structure, they tend to prevent each other from bending or twisting. This gives the joined wing a very high stiffness, both torsionally and flexurally [11]. Reference 8 conducted a study on the tip deflection of a joined wing compared with a single wing. The tip deflection of the single wing can be up to 2.8 times that of the joined wing when both systems experience equal vertical loading at the same lift to drag ratio. This can be attributed to the stiff, box-like structure of the joined wing system. This added stiffness of the joined wing allows higher aileron effectiveness, probably due to the fact the "flapping" of the wings would tend to counter the force of an aileron deflection [9].

In a negative stagger configuration the rear wing is in compression during positive "g" loading. Since many aircraft and missile maneuvers experience

positive g's, it was feared that the wing could buckle under such a loading. However, this has not been a factor for any negative stagger, joined wing configuration studied thus far [8,9]. The added support of the front wing more than likely prevents the rear wing from failing.

Drag

The main concern of the early biplanes was the large amounts of profile drag the wings would experience due to the structural wires. As it turns out, in most design considerations the joined wing will have a lower overall drag than the single wing. This is mainly because it does not need the wiring that caused the high profile drag a biplane did for structural purposes. In addition, the joined wing produces a much lower induced drag -- also contributing to the low total drag. Many other drag-reducing elements are discussed below.

Most will concur that the induced drag on the joined wing is lower than the single wing when comparing systems of equal lift, span, and dynamic pressure [6,8,9,11,12]. Two factors make this possible. First, swept wings tend to have a higher induced drag because the lift distribution cannot be approximated as elliptical. However, "swept wings can have the same induced drag as straight wings of the same aspect ratio -- provided that the lift distribution is the same" [13]. By choosing the proper twist and camber, the adverse effect from the swept wings can be improved [8]. Secondly, the Prandtl-Munk biplane theory shows that the span efficiency factor, e , can be greater than one for biplanes, especially with winglets [8,9,10,11]. This is because the vortex sheet shed by the front wing remains undistorted and parallel to the freestream. Two corrections must be

applied to the Prandtl-Munk theory: one for the downward drift of the vortex sheet shed by the front wing and the other for wing-body interference and for loss of leading edge suction. However, for most joined wings these two approximately cancel out, so no real modifications are necessary [8]. Unfortunately, because of the large stagger for joined wings, the theory predicts span efficiency factors much lower than those obtained in wind tunnel tests [8,9]. Kuhlman and Ku were able to develop a computer program that would theoretically calculate the span efficiency factor for joined wings [18]. Figure 9 depicts the span efficiency factor as it varies with winglet size and the dimensions of the wing. The fact that the span efficiency factor is greater than one is good for the joined wing -- the higher the efficiency factor, the lower the induced drag. Joining the wings inboard of the tips drastically reduces the span efficiency factor to the point the induced drag is within 2-3% of the single wing [9]. The large dihedrals used for reducing the weight also help reduce the induced drag [8].

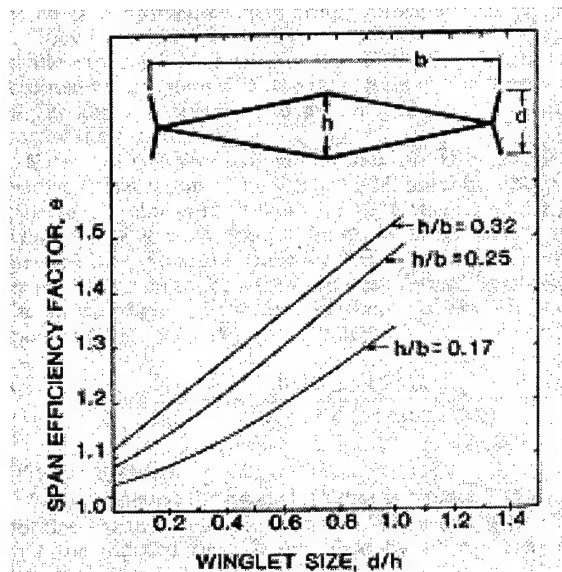


Figure 9: Span Efficiency Factor for Joined Wings [18]

In Reference 14, the induced drag of a single wing, the JW joined wing, and the swept rearward/swept forward (SFSR) joined wing configurations were examined. Each configuration had differing aspect ratios of 12, 17.8 and 16, respectively. It was found that the JW joined wing had the highest induced drag, even with the highest aspect ratio. The single wing had the second highest induced drag followed by the SFSR. While only the SFSR had a lower induced drag than the single wing in this study, looking at the JW joined wing in other design conditions may yield results that the JW joined wing has a lower induced drag than the single wing.

Profile drag is the sum of skin friction drag and pressure drag due to separation for a two-dimensional body. For a three-dimensional body, this sum is typically known as the parasite drag [17]. Overall, the parasite drag for joined wings tends to be lower than that of the single wing due to the reduced wetted area of joined wing configurations. With less area comes less frictional drag. However, close attention must be paid to the adverse effects. The Reynolds number based on chord can be 60 to 65% that of a single wing of the same area and span. To achieve the same area with the same span, the chord on the joined wing must be smaller thus giving the lower Reynolds number. Another adverse effect is the increased ratio of wetted area to lifting area due to the dihedral cosine effect. This can increase wetted area by 3.5%. These adverse effects must be balanced and ultimately exceeded by the positive effects. Among the positive effects of the joined wing are reduced wing area due to high trimmed C_{Lmax} , reduced fuselage wetted area due to reduced length, and

improved wing-fuselage interference [8]. To optimize the reduction of parasite drag for joined wings the configuration should be designed such that the wings do not overlap in plan view. This can induce a venturi effect that in turn increases drag. The front wing root should be placed in a favorable pressure gradient on the fuselage to reduce separation. In addition, natural laminar airfoils should be chosen when using tip joined configurations to increase the wing Reynolds number. Finally, to minimize separation, fillet the junction of the rear wing undersurface [9].

Even though the consensus is that parasite drag is lower for joined wings, it is still open if the skin friction drag, commonly called the viscous drag, is lower than its single wing counterpart. Since the skin friction drag is part of the parasite drag, it follows that the pressure drag must be that much lower for the joined wing in order to make the parasite drag lower for the joined wing configuration. Some have stated that under the best of conditions the joined wing does indeed have a lower viscous drag [1,6]. However, the other thought is that because the Reynolds number can be so significantly lower for the joined wing, the viscous drag is higher than that for the single wing. It can be seen in Reference 17, that for the top surface of a flat plate, the skin friction drag coefficient for laminar flow is given as:

$$C_f = \frac{1.328}{\sqrt{Re_c}} \quad (1)$$

where the Reynolds number is based on the total plate length c . Therefore, as the Reynolds number decreases the skin friction drag coefficient increases,

causing a higher skin friction drag. Because the skin friction drag is also based on the reference area, there may be a point where, as one is decreasing the area to obtain a lower Reynolds number for a higher skin friction drag coefficient, the skin friction drag is ultimately reduced. The swept forward/swept rearward configuration can offer a reduction in viscous drag over the JW joined wing configuration. The JW joined wing has an even higher viscous drag, not only because of the low Reynolds number due to the shorter chord, but also because of the negative stagger. According to Reference 14, negative stagger configurations tend to have early boundary layer separation that contributes to drag. Unfortunately, because of these adverse effects none of the joined wings tested in Reference 14 have a lower viscous drag than the single wing.

Two other types of drag to consider are wave drag and trim drag. Low wave drag is advantageous for transonic and supersonic flight [8]. Thin airfoils are a primary factor in reducing wave drag. The fact that thin airfoils can be applied to joined wings makes them a great choice for the transonic or supersonic regime. Joined wings are also noted for their good transonic area distribution. Trim drag can essentially be disregarded for equal span wings during cruise. In general, the trim drag is approximately 1% of the induced drag [8,9].

Stability and Control

One of the obvious benefits of the joined wing is the availability of more control surfaces than the typical single wing as shown in Figure 10. With the control surfaces on each wing, there are added maneuverability and control

capabilities. Direct lift control and direct side force control can be achieved [8]. Since the joined wing has effectively four places for control surfaces as compared with two for a single wing, the joined wing can offer more stabilizing features. Inherent in the joined wing configuration is a pitch damping value twice of a single wing. Also, longitudinal stability is achieved with very little static margin. There is good spiral stability and no Dutch roll to speak of. The only problem that has occurred is a modest pitch down at high lift coefficients [8]. This can be solved by either shifting the aerodynamic center, which could need large control deflections, or by adding strakes. The strakes tended to reduce the pitch down motion while slightly increasing the maximum lift coefficient [9].

Because of the great stability of this configuration, there is no longer the need for the tail to be so far downstream in order to produce a long moment arm. Thus, the fuselage can be shortened, thereby reducing the weight a great deal.

High Lift

One of the major benefits reaped by the joined wing is its high trimmed $C_{L_{max}}$ [8,9,11]. In general, for a statically stable joined wing configuration, when the front wing reaches its $C_{L_{max}}$, the rear wing has generated much less lift than it is capable. While, this does give good recovery properties, with the rear wing not reaching its $C_{L_{max}}$ implies that the rear wing is oversized, unnecessarily adding weight. In addition, the rear wing loading is 50-60% of the front wing. If the wing system can be designed to let the front wing stall when the rear wing is at its optimum point, the system as a whole will be more efficient. This can enable the

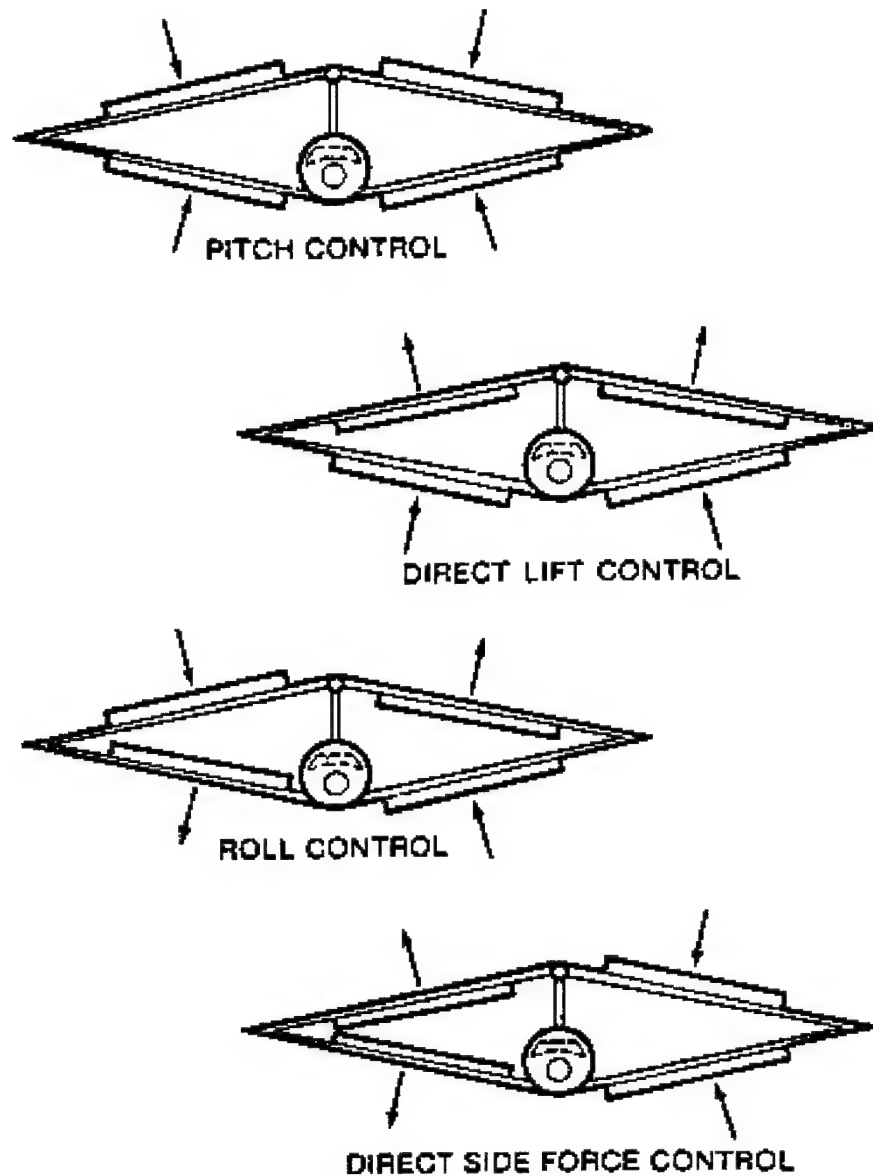


Figure 10: Control Deflections of the Joined Wing [8]

joined wing to have less wing wetted area than the single wing and still achieve the same lift as the single wing plane. The less area can also go towards a large weight reduction or, since range is a function of lift coefficient, towards an extended range [6,15]. Conversely, the span of the joined wing could be increased, maintaining the same weight, thereby reducing the induced drag, allowing for thin airfoils and a faster cruise [9]. As stated before, one must keep

in mind the mission of the plane in order to design the joined wing optimally for the desired features. One must be careful, however, in comparing the joined wing and the single wing configurations. For starters, the reference areas used to define the lift coefficients must be equal [9]. Secondly, it has been shown that for biplane airfoils, it is necessary that the camber be increased in order to get a C_{Lmax} equal to that of single airfoils. The joined wing configuration has a unique characteristic of inducing camber. The induced camber is a result of the flow being curved by each wing and can be either positive or negative. It will vary based on the spanwise variations in gap and stagger angles [8,9]. This tends to make it impossible to compare the joined wing and single wing if the same airfoils are used. In using the same airfoil, it has been shown that the joined wing configuration will suffer from premature flow detachment [8]. A variable camber has been suggested for optimum performance, especially for missiles. As the fuel is consumed, the wing loading is decreased. If the camber is reduced in such a way as to maintain the highest lift to drag, the range will be at a maximum [8].

Other ways to increase the lift is to add a canard of low aspect ratio, high sweep, and a sharp leading edge [8]. Not only does it augment the lift as seen in Figure 11, it adds to the stability of the craft. It helps correct the shift of the aerodynamic center giving a more constant static margin [8]. It also helps delay the front wing from stalling so early [9]. As stated before, this can ultimately lead to a weight reduction. Adding a canard is a win-win situation in that it helps the stall features as well as adding lift [8,9,11].

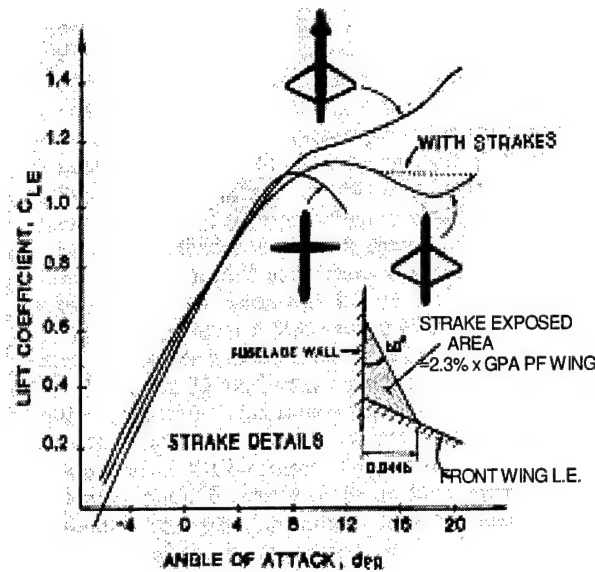


Figure 11: Measured Variation with Angle of Attack of Untrimmed Lift Coefficients Referred to Total Exposed Areas of All Lifting Surfaces [9]

A proper choice of twist and cant angles can give a higher lift to induced drag ratio than the single wing. In comparing swept forward/swept rearward joined wing configurations, it was shown that larger gaps gave the highest lift to induced drag ratios [14]. In a separate comparison, the joined wing with a positive stagger and a cant angle of 30° yields the highest lift to induced drag [1]. One final note is that in comparing lift to induced drag coefficients, the positive stagger joined wing with 30° cant is significantly better at the lower lift coefficients than the single wing of differing aspect ratios. As the lift coefficient increases the joined wing and the single wing have about the same performance [1]. Once again, optimization of the joined wing is essential in determining the best configuration.

Miscellaneous

There are many other benefits that can be realized with the joined wing. A number do not fit into the categories above and will be described here.

The joined wing outdistances the single wing, especially at high altitude [8]. The Brequeut range formula can be used to compare the two configurations flying at the same condition [19]. It is assumed that the configuration has a power plant and expends fuel. The range formula is given as:

$$\frac{dR}{dW} = \frac{V}{-CT} = \frac{V}{-CD} = \frac{V(L/D)}{-CW} \quad (2)$$

and once integrated yields:

$$R = \frac{V_{\infty}}{C} \frac{L}{D} \ln \frac{W_0}{W_1} \quad (3)$$

where V_{∞} is the free stream velocity, C is the specific fuel consumption, L is the lift, D is the drag, W_0 is the initial weight, and W_1 is the final weight. Taking a range ratio between two configurations can predict by what percent a configuration can outdistance another.

Unfortunately, the advantages of the joined wing decrease as its wing area is reduced. It has also been shown that among the different joined wing configurations, the swept forward/swept rearward (SFSR) system can travel 13.8% farther than the standard joined wing [14]. If it is necessary to fly at low altitudes, the joined wing plane is more maneuverable than the single wing plane, especially when flying above 3g's [8].

It is best to keep in mind that not all advantages can be gained at once. There is a lot of optimization and design that must be done [11]. It is recommended that a new fuselage is design specifically for the joined wing – not retrofitting a current fuselage with a joined wing configuration [9]. Other recommendations include locating the ailerons outboard of the wing connectors, placing the flap on the rear wing and the elevators on the front wing so that trimming the wing also increases lift, do not use the canard for trim, pick airfoils such that the rear wing produces the most lift possible when the front wing is stalled, and finally, reduce sweep [11]. These recommendations were to help stabilize and improve the flying qualities of a joined wing aircraft. While they may be helpful for the design in Reference 11, they may not be the best for a different design or mission, such as for this study.

As Compared to This Thesis

The main goal of this thesis is to determine if the range can be extended with the joined wing configuration. Based on the literature, the range will indeed be increased, especially when the model is in its positive stagger arrangement. Other design considerations were made to the model to increase its range, such as joining the wings at the tips and a high angle of sweep. According to the literature, with these aspects, the modified, joined wing bomb should have no problem outdistancing the bare model.

In most of the literature read the joined and single wing configurations have the same span and wing area. This leads to different chords for the joined wing and the single wing leading to a lower Reynolds number based on chord for

the joined wing. In other studies the aspect ratios are equal. For this study, since the same basic wings are used for both the single and joined configurations, the spans will be equal in the same sweep family. Also, since the chords are the same, the Reynolds numbers based on chord will also be equal in the same sweep family. However, since the joined wing will have nearly twice the area of the single wing, the aspect ratios will differ. The fact that the joined wing will have that much more lifting surface should allow the joined wing to outperform the single wing. Previous studies that have the same design characteristics as this study -- equal spans and chords between the joined and single wing configurations -- can be directly compared. Otherwise, educated adjustments will have to be made to relate the literature with the data obtained.

III. Methodology

Model

The models, shown in Figures 13-16, made of aluminum, has a fuselage 28.44 in. (0.72 m) long with a projected diameter of 2 in. (0.0508 m). There are two sweep families -- a 30° swept wing set and a 60° swept wing set. Sweep is defined as the angle from the horizontal line perpendicular to the fuselage to the wing. The weight, span, reference area, aspect ratios, and efficiency factors of the various wing configurations in this study are presented in Table 1. The weight did not vary between the curved joined wing connectors and the straight joined wing connectors. The reference area is defined as the projected area for the bare missile and the total wing planform area for the winged configurations. The area of the connectors was not taken into account. The total area for the

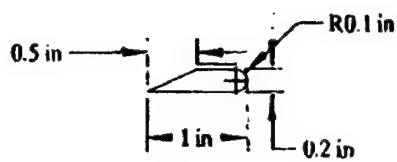
curved and straight connectors for the 60° swept joined wing is the same, 0.062 ft². This is 22.7% the area of the reference area. The total area for the curved and straight connectors for the 30° swept wing is also the same, 0.034 ft². This is 13.3 % the area of the reference area. The aspect ratios and efficiency factors are calculated using equations or figures specific for each configuration that are discussed later.

Table 1: Various Parameters of the Model Configurations

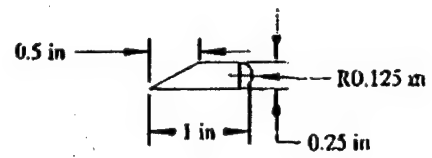
| | Weight | Span | Reference Area * | Aspect Ratio | Efficiency Factor |
|-----------------------|-----------------------|------------------------|--|--------------|-------------------|
| Bare Model | 6.81 lbm (3.09 kg) | N/A | 0.4 ft ² (0.0372 m ²) | N/A | N/A |
| 60° Swept Joined Wing | 7.63 lbm (3.46 kg) | 9 in (0.2286 m) | 0.275 ft ² (0.0245 m ²) | 4.5 | 1.45 |
| 30° Swept Joined Wing | 7.56 lbm (3.43 kg) | 15.588 in (0.396 m) | 0.265 ft ² (0.0239 m ²) | 7.79 | 1.2 |
| 60° Swept Biplane | 7.44 lbm (3.37 kg) | 9 in (0.2286 m) | 0.275 ft ² (0.0245 m ²) | 4.5 | 0.676 |
| 30° Swept Biplane | 7.46 lbm (3.38 kg) | 15.588 in (0.396 m) | 0.265 ft ² (0.0239 m ²) | 7.79 | 0.613 |
| 60° Swept Single Wing | 7.12 lbm (3.23 kg) | 9 in (0.2286 m) | 0.1375 ft ² (0.0124 m ²) | 9 | 0.222 |
| 30° Swept Single Wing | 7.14 lbm (3.24 kg) | 15.588 in (0.396 m) | 0.133 ft ² (0.012 m ²) | 15.58 | 0.098 |

*The area of the connectors are not taken into account.

The airfoil for all wings is a tear drop shape, shown in Figure 12. The chord is 1 in (0.0254 m) for all wings. There was no twist in any of the wings. There was no dihedral so the wing gap is the diameter of the fuselage -- 2 in (0.0508 m). The wing connectors are mounted at an angle and are considered winglets for computing the efficiency factor from Figure 9.



Chord for 30° Swept Wing



Chord for 60° Swept Wing

Figure 12: Profiles for the 30° and 60° Swept Wing

For a visual understanding of the configurations see Figures 13-16.

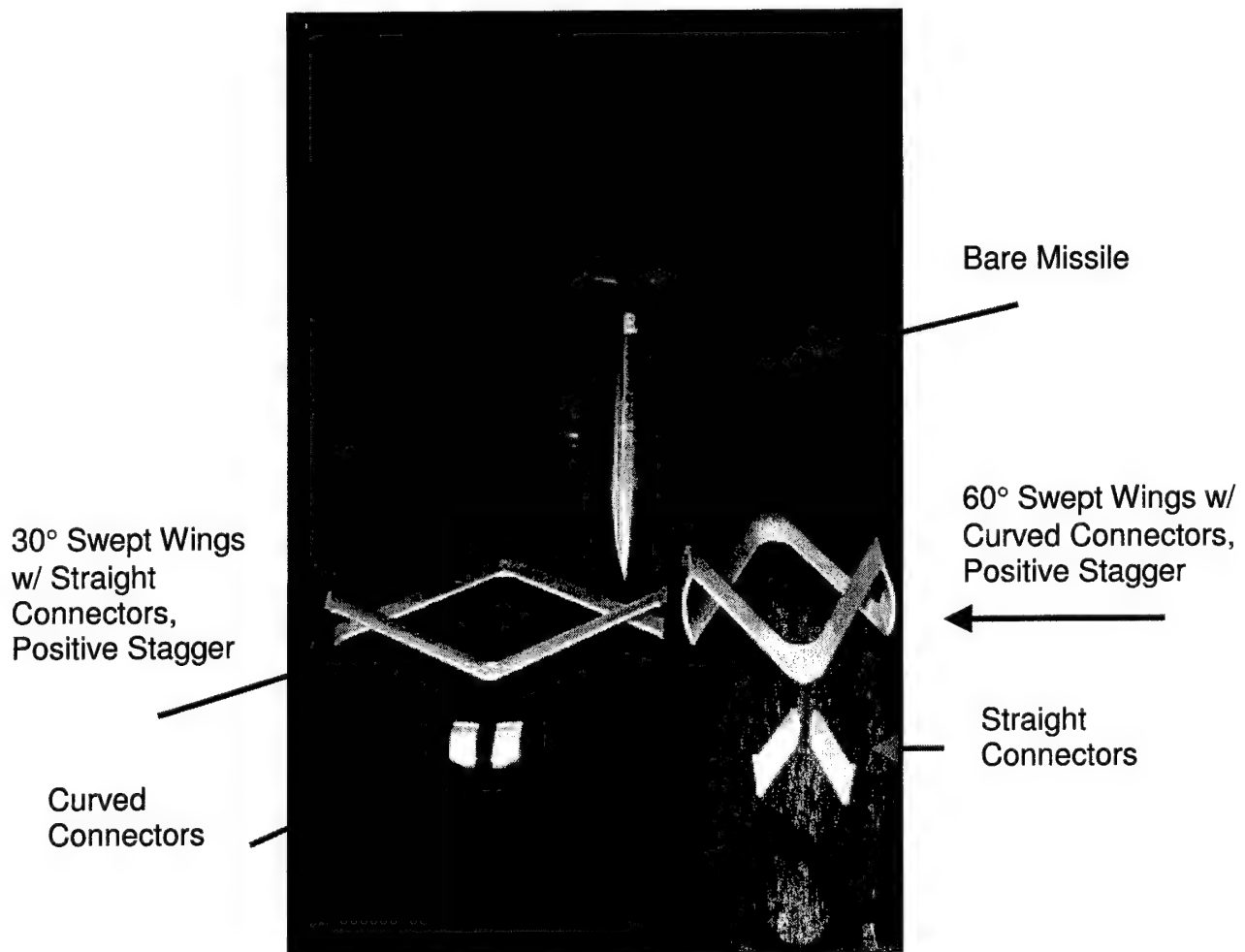


Figure 13: Smart Missile with Wing Components

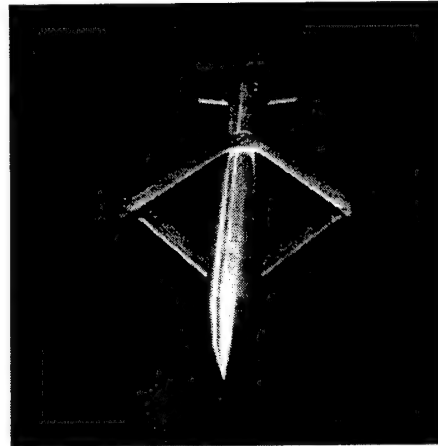
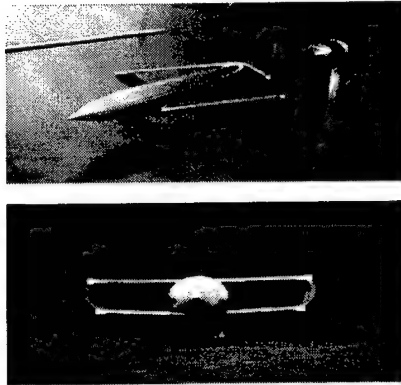


Figure 14: 60° Swept Joined Wing with Curved Connectors, Negative Stagger

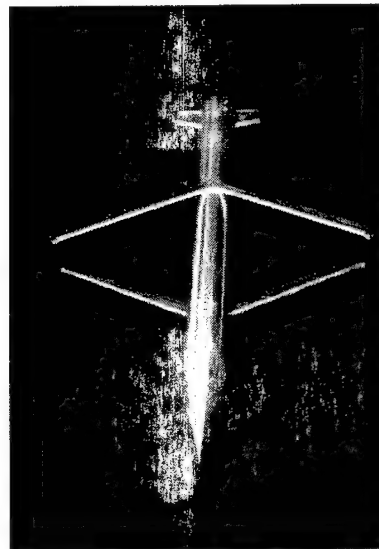
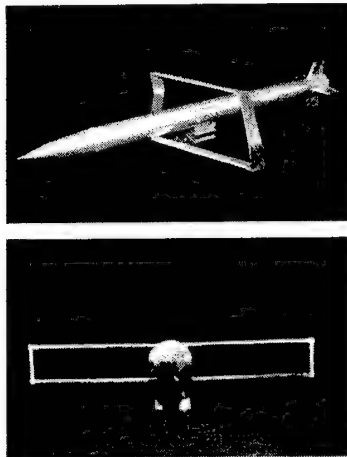
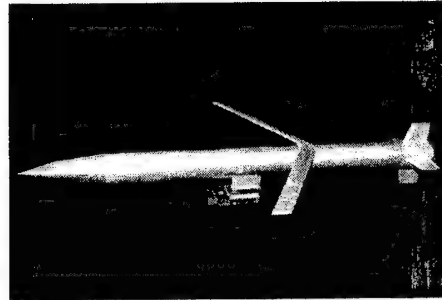
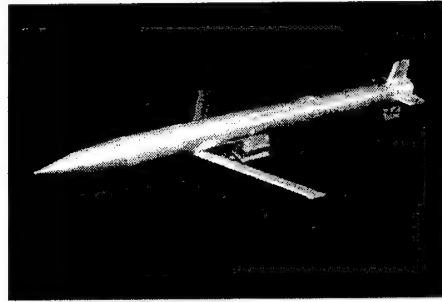


Figure 15: 30° Swept Joined Wing with Straight Connectors, Negative Stagger

30° Swept
Single Wing,
Forward of the
CG, Wings on
Bottom



30° Swept Single
Wing, Aft of the
CG, Wings on
Top

Figure 16: Single Wing Configurations

Equipment

The AFIT five-foot (1.5 m) diameter, subsonic wind tunnel, shown in Figure 17, was used to test the various configurations of the joined wing model. The missile model was mounted on a sting that could sweep through various angles of attack. The forces were measured by a balance system. The balance was inserted through the sting and shrouded by a metal cylinder to increase the balance's diameter. The balance was directly pinned to the model once inserted into the model. The electrical center of gravity of the balance coincides with the center of gravity of the bare model. The forces experienced by the balance were sent as a voltage to Labview. Labview, a software package that can be used to write programs for calibration and data acquisition, then converted the voltages into forces that are used to calculate the lift and drag.

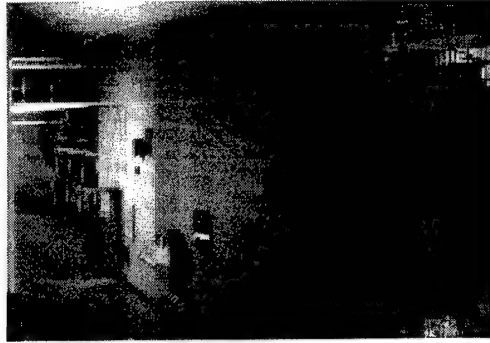


Figure 17: AFIT 5' Wind Tunnel

Calibration

The balance was calibrated by applying weights in each of the six degrees of freedom and in both the positive and negative directions. The normal forces were calibrated to 80 lbf (355.96 N), side forces to 40 lbf (177.93 N), roll moments to 32 lbf-in (3.62 N-m), and axial force to 50 lbf (222.41 N). The weight with its corresponding voltage was recorded in Balcal – a program written in Labview. The data was then taken into the program Curvefit to determine if the balance was within acceptable parameters. All calibration curves achieved approximately a 0.9999 correlation coefficient. Curvefit then provided a slope of the voltage with weight line to be used in Calslop2. Calslop2 developed a volt-to-force matrix that was inserted into the data acquisition program, SB 1998. This matrix contained the interaction sensitivities of the balance to the loading.

Test Plan

Low speed, incompressible wind tunnel testing was performed on twenty-one configurations of the missile model. A new configuration was obtained by interchanging the parts. Converting the positive stagger to a negative stagger was achieved by turning the model 180°. Each configuration, specified in Table

2, was tested at three speeds -- 100 mph (44.7 m/s), 130 mph (58.1 m/s), and tunnel maximum of 175 mph (78.2 m/s). During each run, the model was swept through angles of attack from -4 deg to a tunnel maximum of 13 deg. Beyond 13 deg the back end of the sting system would hit the bottom of the tunnel wall. Data was collected in 2-degree increments, except close to the stall angle where data was taken at each degree until the tunnel maximum was reached. The lift, drag, and pitching and rolling moments were determined for each configuration.

Computation of Parameters

There are a number of parameters that were calculated in this study. Those are lift, drag, pitching and rolling moments, and range ratio. Since the missile will more than likely fly at high speeds a compressibility analysis can be extrapolated from the incompressible data obtained. The balance measures the normal force forward and aft of the center of gravity, the side force on either side of the center of gravity, the axial force and the rolling moment. Adding the two normal forces measured gives the total normal force, or the summation of forces in the body axis y-direction. Likewise, adding the two measured side forces gives the total side force, or the summation of forces in the body axis x-direction. It is from these measurements that the parameters are obtained.

Table 2: Model Test Configurations

| | | |
|------------|------------------------------|--|
| Bare Model | | |
| 30° Sweep | | |
| | Single Wing | |
| | Aft of CG (Swept Forward) | |
| | | Wings on Top Wings on Bottom |
| | Forward of CG (Swept Aft) | |
| | | Wings on Top Wings on Bottom |
| | Biplane | |
| | Positive Stagger | |
| | | No Joining Plate Curved Joining Plate Straight Joining Plate |
| | Negative Stagger | |
| | | No Joining Plate Curved Joining Plate Straight Joining Plate |
| 60° Sweep | | |
| | Single Wing | |
| | Aft of CG (Swept Forward) | |
| | | Wings on Top Wings on Bottom |
| | Forward of CG (Swept Aft) | |
| | | Wings on Top Wings on Bottom |
| | Biplane | |
| | Positive Stagger | |
| | | No Joining Plate Curved Joining Plate Straight Joining Plate |
| | Negative Stagger | |
| | | No Joining Plate Curved Joining Plate Straight Joining Plate |

Drag. The drag is the component of the force that is parallel to the freestream velocity, as seen in Figure 18. However, the forces measured by the

balance are body axis forces. Therefore, to calculate the drag, the body axis forces must be transformed to the wind axis. This is done by:

$$D = N \sin \alpha + A \cos \alpha \quad (4)$$

where D is drag, N is the total normal force, A is the axial force and α is the angle of attack.

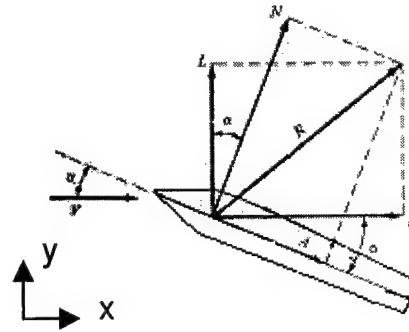


Figure 18: Wind Axis and Body Axis Forces

Once the drag has been measured the drag coefficient can be obtained:

$$C_D = \frac{D}{1/2 \rho_{\infty} V_{\infty}^2 S} \quad (5)$$

where ρ_{∞} is the freestream density, V_{∞} is the freestream velocity and S is the reference area. See Table 1 for the reference areas of each configuration. The total drag is also the sum of the induced drag and the profile drag. The profile drag is typically obtained from experimental data. The induced drag, which is drag due to lift from winged surfaces, can be calculated from:

$$C_{D,i} = \frac{C_L^2}{\pi e A R} \quad (6)$$

where C_L is the lift coefficient, e is the span efficiency factor, and AR is the aspect ratio. The span efficiency factor used for the joined wings can be found in Table 1. The efficiency factor for joined wings can be taken from Figure 9. For swept single wing aircraft the efficiency factor is found by [19]:

$$e = 4.61(1 - 0.045AR^{0.68})(\cos \Lambda_{LE})^{0.15} - 3.1 \quad (7)$$

where Λ_{LE} is the sweep angle and must be greater than 30° . The efficiency factor for a biplane is given as [19]:

$$e = \frac{\mu^2(1+r^2)}{\mu^2 + 2\sigma\mu r + r^2} \quad (8)$$

where μ is the ratio of the shorter span/longer span, r is approximately ratio of the area of the shorter wing/area of the longer wing and σ is the interference factor. These values can be obtained from Figure 12.32 in Reference 19. The aspect ratio for a single wing is given as:

$$AR = \frac{b^2}{S} \quad (9)$$

where b is the span and S is the reference area. For a joined wing the aspect ratio is, as cited in Reference 6,

$$AR_T = \frac{AR_F \left(\frac{S_F}{S_R} \right) + AR_R \left(\frac{S_R}{S_F} \right)}{\left(\frac{S_F}{S_R} + 1 \right) \left(\frac{S_R}{S_F} + 1 \right)} \quad (10)$$

where AR_F is the aspect ratio of the front wing, AR_R is the aspect ratio of the rear wing, S_F is the area of the front wing, and S_R is the area of the back wing.

Typically for a biplane, the aspect ratio is determined as:

$$AR = \frac{b_{longer}^2}{S} \quad (11)$$

where b_{longer} is the span of the longer wing and S is the total area of both wings [19]. If Equation (11) is used for the biplanes in this study, the 30° swept wing has an aspect ratio of 6.36 and the 60° swept wing a value of 2.05. This is a huge deviation from the joined wing aspect ratio values in Table 1 considering the only difference in this study between the joined wings and the biplanes was the removal of the connectors. Therefore, Equation (10) was used to calculate the aspect ratios for both the biplane and joined wing configurations.

The values for the aspect ratio and the efficiency factors given in Table 1 were evaluated using Equations (7) to (11) and Figure 9.

Lift. From Figure 18, one can see that the lift is perpendicular to the freestream velocity and is in the wind axis. Again, the body axis forces must be transformed into the wind axis. This gives lift as:

$$L = N \cos \alpha - A \sin \alpha \quad (12)$$

where N is the total normal force, A is the axial force and α is the angle of attack.

The lift coefficient can be found from:

$$C_L = \frac{L}{1/2 \rho_{\infty} V_{\infty}^2 S} \quad (13)$$

where ρ_{∞} is the freestream density, V_{∞} is the freestream velocity and S is the reference area. The lift coefficient can be used to calculate the induced drag from Equation (6).

Pitching Moment. The pitching moment is found by calculating the moment the individual normal forces produce on the center of gravity of the model. This is given by:

$$M = N_1 a + N_2 b \quad (14)$$

where a is the distance from the force N_1 to the center of gravity and b is the distance from the force N_2 to the center of gravity. The moment coefficient is found by:

$$C_M = \frac{M}{1/2 \rho_{\infty} V_{\infty}^2 S c} \quad (15)$$

where ρ_{∞} is the freestream density, V_{∞} is the freestream velocity, S is the reference area and c is the chord.

Rolling Moment. One of the items the balance detects is the rolling moment. To determine the rolling moment coefficient, the following equation is used:

$$C_{L'} = \frac{L'}{1/2 \rho_{\infty} V_{\infty}^2 S c} \quad (16)$$

where L' is the rolling moment, ρ_∞ is the freestream density, V_∞ is the freestream velocity, S is the reference area and c is the chord.

Range. The percentage increase, or decrease, in range that the joined wing configuration can achieve over the single wing can be found by taking a range ratio. Using Equation (3), the ratio is given as:

$$\frac{R_{jw}}{R_{sw}} = \frac{\frac{V_\infty}{C} \frac{L_{jw}}{D_{jw}} \ln \frac{W_0}{W_1}}{\frac{V_\infty}{C} \frac{L_{sw}}{D_{sw}} \ln \frac{W_0}{W_1}} \quad (17)$$

which, given that both flight vehicles are flying the same mission, with the same power plant and have the same initial/final weight ratio, can simplify to:

$$\frac{R_{jw}}{R_{sw}} = \frac{L_{jw} / D_{jw}}{L_{sw} / D_{sw}} \quad (18)$$

where V_∞ is the free stream velocity, C is the specific fuel consumption, L_{jw} is the lift of the joined wing, D_{jw} is the drag of the joined wing, L_{sw} is the lift of the single wing and, D_{sw} is the drag of the single wing. If the initial/final weight ratio is 1 for either configuration, such as for a glider, Equation 3 can no longer be used and alternative methods for a range ratio analysis must be used.

Compressibility Analysis. While the model is being tested at low air speeds, the actual missile will more than likely be flying at higher velocities. Because of this, many of the incompressible assumptions are no longer valid. In order to get a feel for how the missile will fly in the compressible regime, it is

possible to modify the data to accommodate the higher speeds. Prandtl and Glauert developed a compressibility correction for inviscid flow over an airfoil. This is given as:

$$c_L = \frac{c_{L,0}}{\sqrt{1 - M_\infty^2}} \quad (19)$$

where c_L is the compressible lift coefficient, $c_{L,0}$ is the incompressible lift coefficient and M_∞ is the freestream Mach number. The compressible drag coefficient can be found in the same way:

$$c_D = \frac{c_{D,0}}{\sqrt{1 - M_\infty^2}} \quad (20)$$

where c_D is the compressible drag coefficient, $c_{D,0}$ is the incompressible drag coefficient and M_∞ is the freestream Mach number. The above equations start to fall apart as the Mach number reaches 0.8 and then should no longer be used. One thing the compressibility correction equation does relay readily is that the compressible lift and drag coefficients will be larger than the incompressible lift and drag coefficients. It should be noted, however, that this analysis is only meant to be a first cut approximation for the behavior in compressible flow. Actual testing in the compressible regime should be conducted.

Data Reduction. It is a given that the number obtained from the data acquisition system are not the actual values that the model would experience during flight. Therefore, the data must be modified to give the actual forces the model is under.

One of the major reductions that must be considered is tare. This is a result of the model being on the sting. As the model is pitched, a portion of its weight will show up in the balance readings. This especially affects the axial readings. To subtract this value out, the model must be "flown" in the tunnel under zero velocity and at each angle of attack that will be measured. These values are then subtracted from those from the test. This effectively zeros out the data. Because the model was so heavy -- 7.63 lbm (3.46 kg) when fully loaded -- the tare values could be substantial. For the 60° swept joined wing configuration, the tare in the axial direction ranged from 0.04 lbf (0.178 N) at 0° angle of attack to 1.88 lbf (8.36 N) at 13° angle of attack. For this case, the tare makes up 63% of the measurement at 13 angle of attack. If it had not been subtracted out, the error at the higher angles of attack would be significant.

Because the model blocks a portion of the airflow, it causes the velocity to increase over the model. As a result of this blockage, the velocity over the model is no longer the freestream velocity measured upstream. Since the velocity is part of the lift and drag coefficients, this change in velocity will modify them. To account for this change the total blockage is given as:

$$\epsilon_t = \frac{1}{4} \frac{\text{model frontal area}}{\text{test section area}} \frac{\Delta V}{V} \quad (21)$$

where ϵ_t is the total blockage, ΔV is the change in freestream velocity, and V is the freestream velocity. Included in the model frontal area are the model and the sting system. The total blockage typically had a value around 0.005 for most

configurations. The total blockage accounts for buoyancy effects. The streamline curvature was not accounted for but is considered to be very small. While the test section area is generally the size of the tunnel, it too must be modified to account for boundary layer growth. For a flat plate in laminar flow, which is used in this analysis since the tunnel has such a large diameter, the displacement thickness is given as:

$$\delta^* = \frac{1.721x}{\sqrt{\text{Re}_x}} \quad (22)$$

where x is the distance from the entrance of the tunnel to the test section, and Re_x is the Reynolds number based on the distance from the entrance of the tunnel to the test section. The boundary layer, δ^* , grew at most 1 in (0.0254 m). Needless to say when taking the blockage and boundary layer growth into account, the change in velocity is very small, less than 1%. However, taking these two corrections into account reduces the error in the data.

Error Analysis. Kline and McClintock developed a method to determine the uncertainty in one's data. This procedure is presented below and can be found in Reference 20.

If the parameter is a function of independent variables x_1 through x_n ,

$$R = R(x_1, x_2, x_3, \dots, x_n) \quad (23)$$

then the uncertainty of the parameter, w_R , is a function of the uncertainty of each of the independent variables, w_i , and the sensitivity of R to change each variable:

$$w_R = \left[\left(\frac{\partial R}{\partial x_1} w_1 \right)^2 + \left(\frac{\partial R}{\partial x_2} w_2 \right)^2 + \dots + \left(\frac{\partial R}{\partial x_n} w_n \right)^2 \right]^{1/2} \quad (24)$$

To determine the uncertainty in the drag coefficient in this study, the basic measurements must be inserted into the drag coefficient equation.

$$C_D = \frac{D}{qS} = \frac{(N_1 + N_2) \sin \alpha + A \cos \alpha}{qS} = \frac{\left[V_{N_1} \frac{\partial N_1}{\partial V_{N_1}} + V_{N_2} \frac{\partial N_2}{\partial V_{N_2}} \right] \sin \alpha + V_A \frac{\partial A}{\partial V_A} \cos \alpha}{qS} \quad (25)$$

where V_{N1} is the voltage measured by the N_1 component of the balance, V_{N2} is the voltage measured by the N_2 component of the balance and V_A is the axial component of the balance. The partial derivative of the drag coefficient with respect to the independent variables, V_{N1} , V_{N2} , V_A , and q , must then be taken and are as follows:

$$\frac{\partial C_D}{\partial V_{N_1}} = \frac{\frac{\partial N_1}{\partial V_{N_1}} \sin \alpha}{qS} \quad (26)$$

$$\frac{\partial C_D}{\partial V_{N_2}} = \frac{\frac{\partial N_2}{\partial V_{N_2}} \sin \alpha}{qS} \quad (27)$$

$$\frac{\partial C_D}{\partial V_A} = \frac{\frac{\partial A}{\partial V_A} \cos \alpha}{qS} \quad (28)$$

$$\frac{\partial C_D}{\partial q} = \frac{- \left[V_{N_1} \frac{\partial N_1}{\partial V_{N_1}} + V_{N_2} \frac{\partial N_2}{\partial V_{N_2}} \right] \sin \alpha - V_A \frac{\partial A}{\partial V_A} \cos \alpha}{q^2 S} \quad (29)$$

The uncertainty analysis for the lift coefficient was performed in the same way. Appendix A contains the actual numerical analysis for the drag coefficient.

IV. Results

With the tools established in Chapter 3, the data was analyzed to determine the aerodynamic properties of the different configurations. The lift and drag were found using Equations (5) and (12) for each angle of attack tested. From these values the lift and drag coefficients were then calculated. Using the lift and drag curves, the positive and negative stagger configurations were compared first with each other and then within their sweep family. The lift and drag relations curves for each sweep family are found on the next few pages. See Figures 20-23. Table 3 contains the nomenclature found in the legends.

Typically, the negative stagger configurations outperformed its positive stagger counterparts. This is contradictory to Reference 14. This could be because of the model Reference 14 used for its negative stagger case. In their model, the wings were connected to the tail, where in this study they are not. See Appendix B for the graphs of each configuration.

Table 3: Legend Notation

| | |
|---------------------|---|
| 30 or 60bf curved | 30° or 60° Swept Joined Wing with Curved Connectors, Negative Stagger |
| 30 or 60tf curved | 30° or 60° Swept Joined Wing with Curved Connectors, Positive Stagger |
| 30 or 60bf straight | 30° or 60° Swept Joined Wing with Straight Connectors, Negative Stagger |
| 30 or 60tf straight | 30° or 60° Swept Joined Wing with Straight Connectors, Positive Stagger |
| 30 or 60bf biplane | 30° or 60° Swept Biplane, Negative Stagger |
| 30 or 60tf biplane | 30° or 60° Swept Biplane, Positive Stagger |
| 30 or 60sin aft bot | 30° or 60° Swept Single Wing Located Aft of the CG, Wings on Bottom |
| 30 or 60sin aft top | 30° or 60° Swept Single Wing Located Aft of the CG, Wings on Top |
| 30 or 60sin for bot | 30° or 60° Swept Single Wing Located Forward of the CG, Wings on Bottom |
| 30 or 60sin for top | 30° or 60° Swept Single Wing Located Forward of the CG, Wings on Top |

One thing to notice is that the lift and drag are directly proportional to the velocity squared. As the velocity is increased the lift and drag increase accordingly. This can be seen specifically in Figure 23 with the lift and drag coefficients for the 60° swept joined wing with curved connectors with a negative stagger. The lift and drag coefficients have the same values for a given angle of attack regardless of velocity. This also shows excellent repeatability among the tests.

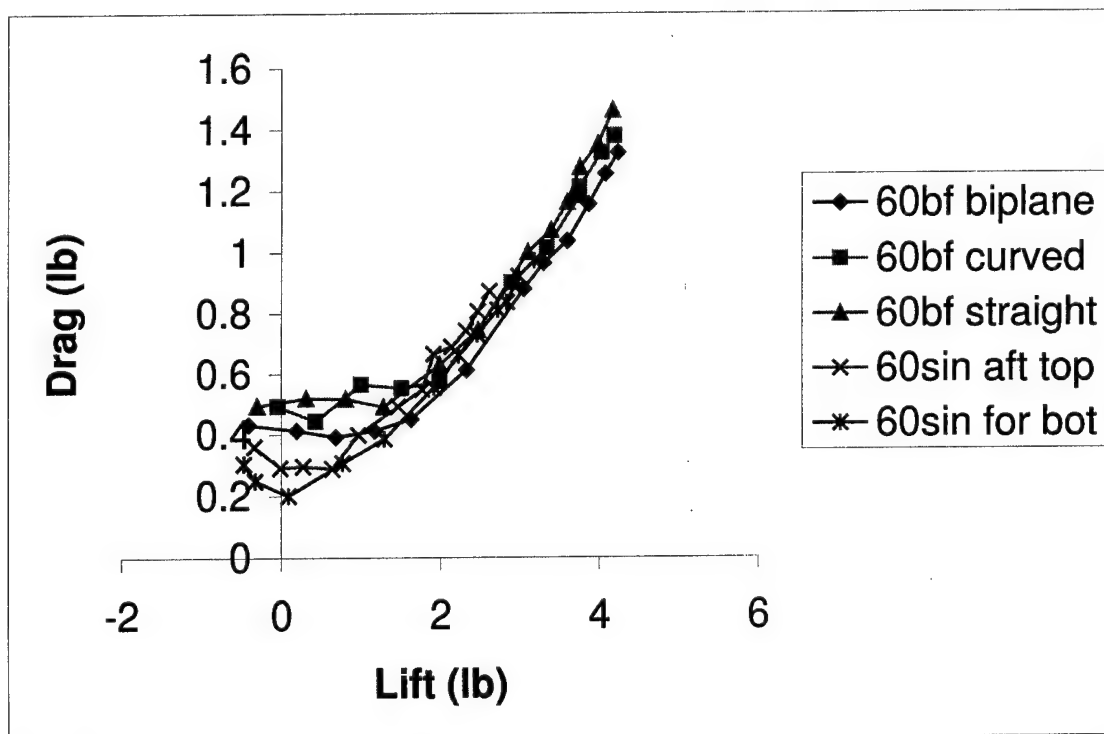
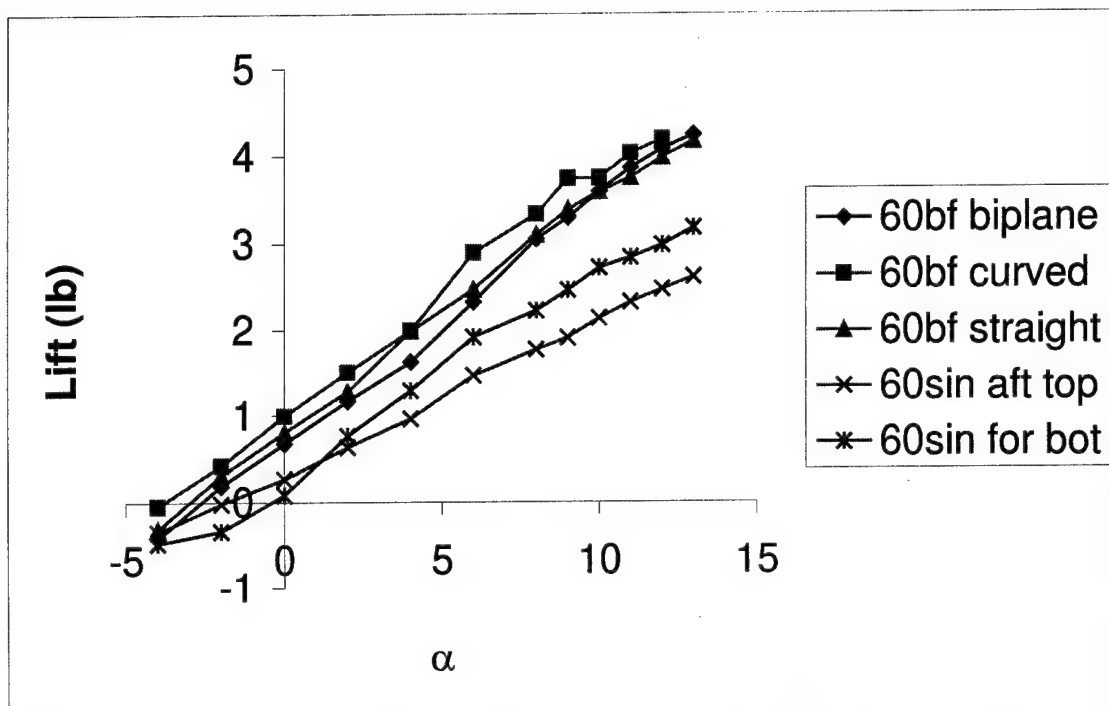


Figure 19: Comparison of the Lift and Drag Relations for the 60° Swept Wings, Flown at 100 mph (44.7 m/s)

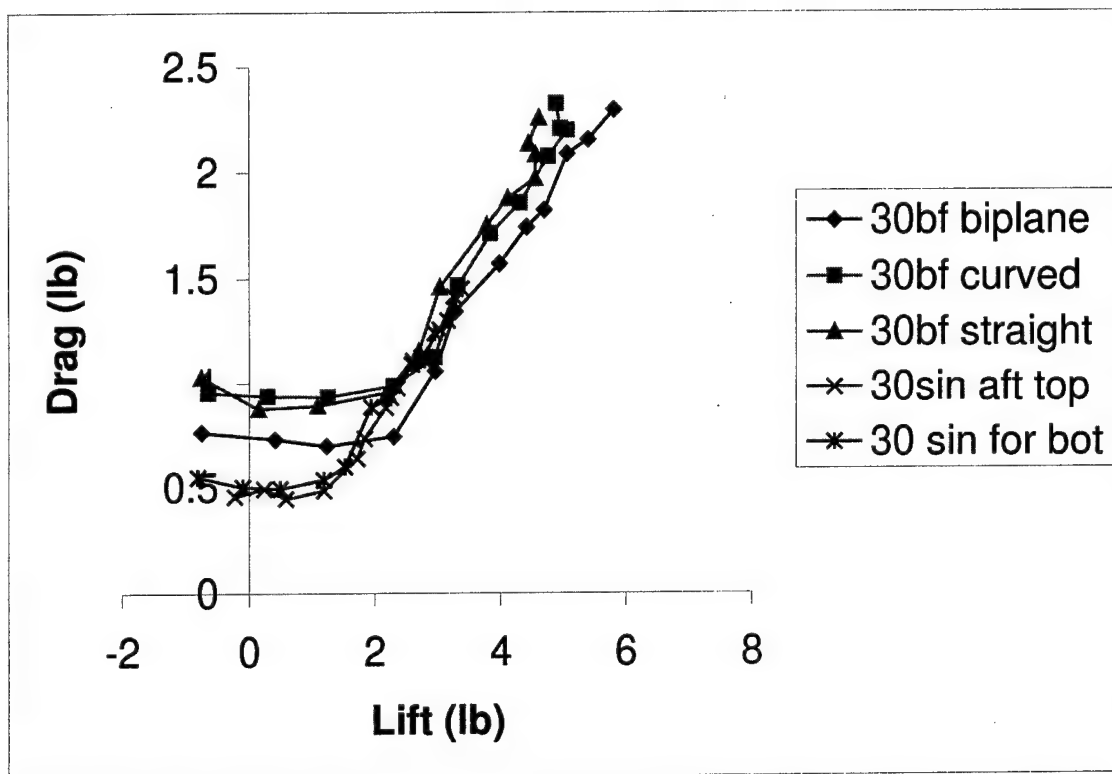
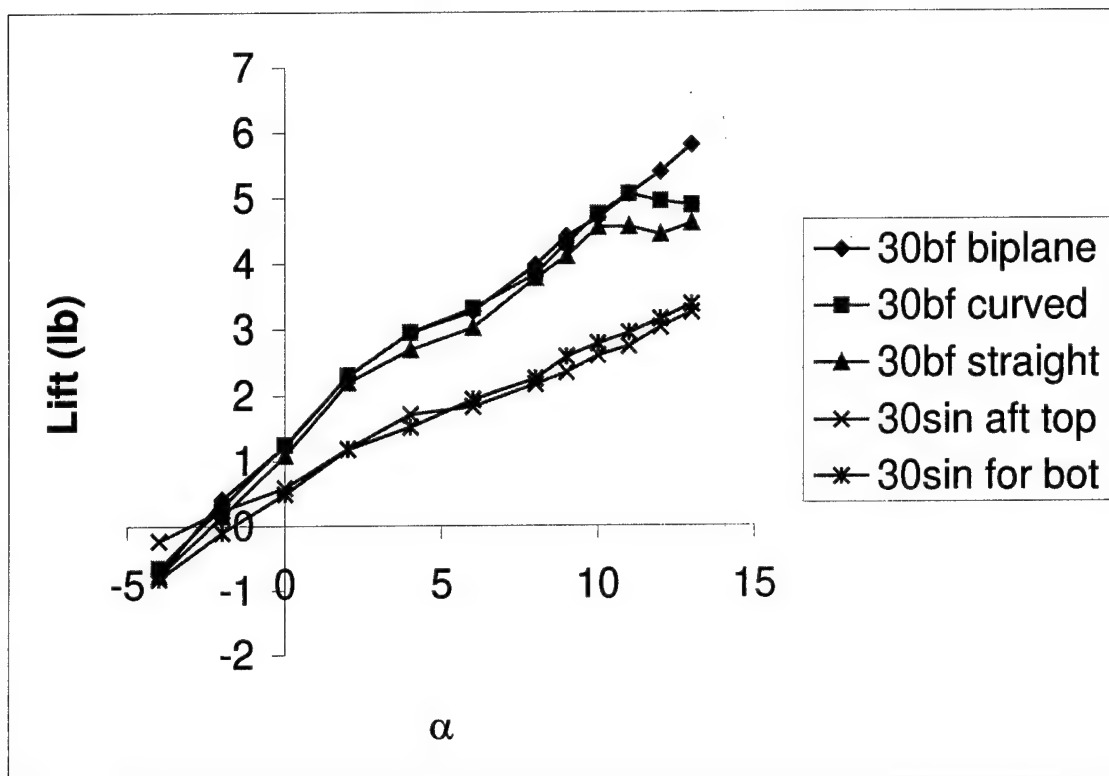


Figure 20: Comparison of the Lift and Drag Relations for the 30° Swept Wings, Flown at 100 mph (44.7 m/s)

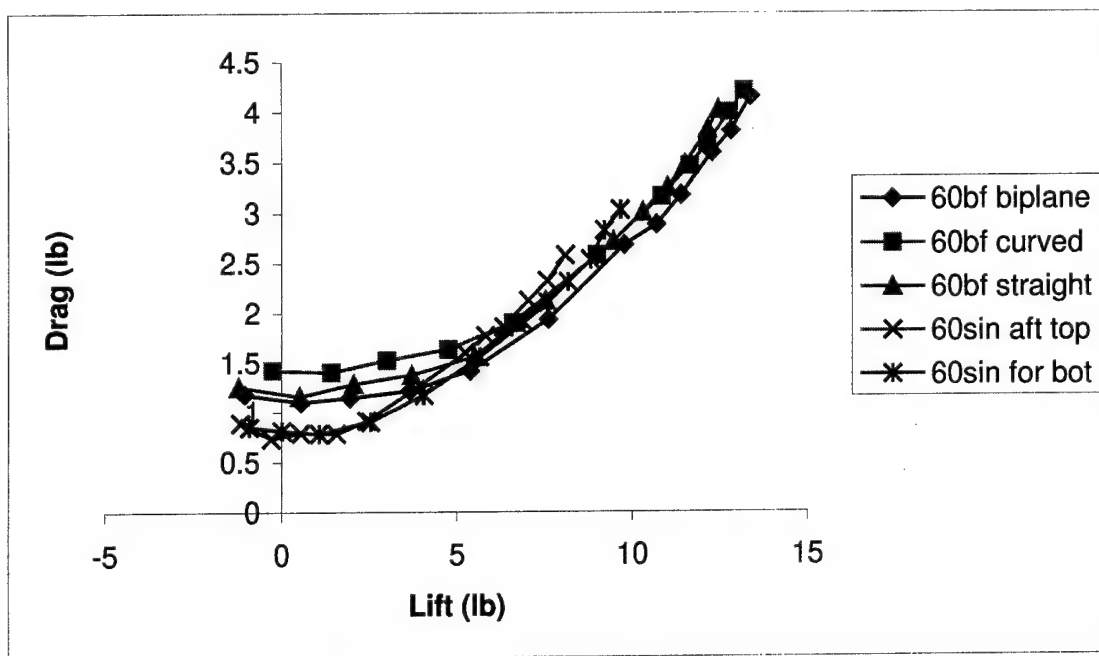
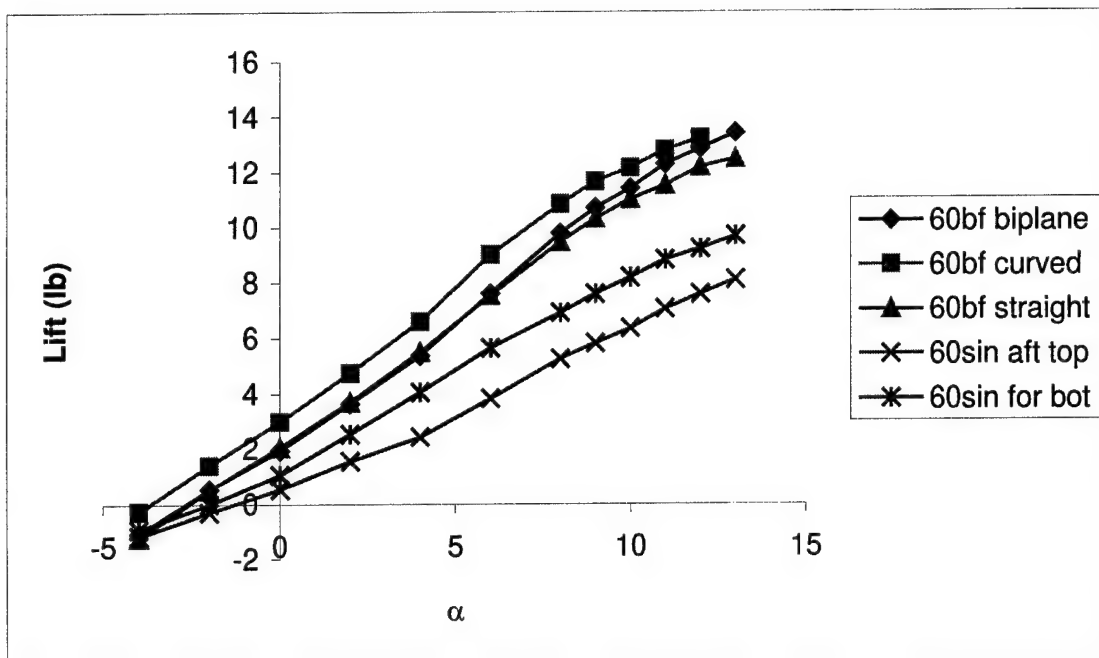


Figure 21: Comparison of the Lift and Drag Relations for the 60° Swept Wings, Flown at 175 mph (78.2 m/s)

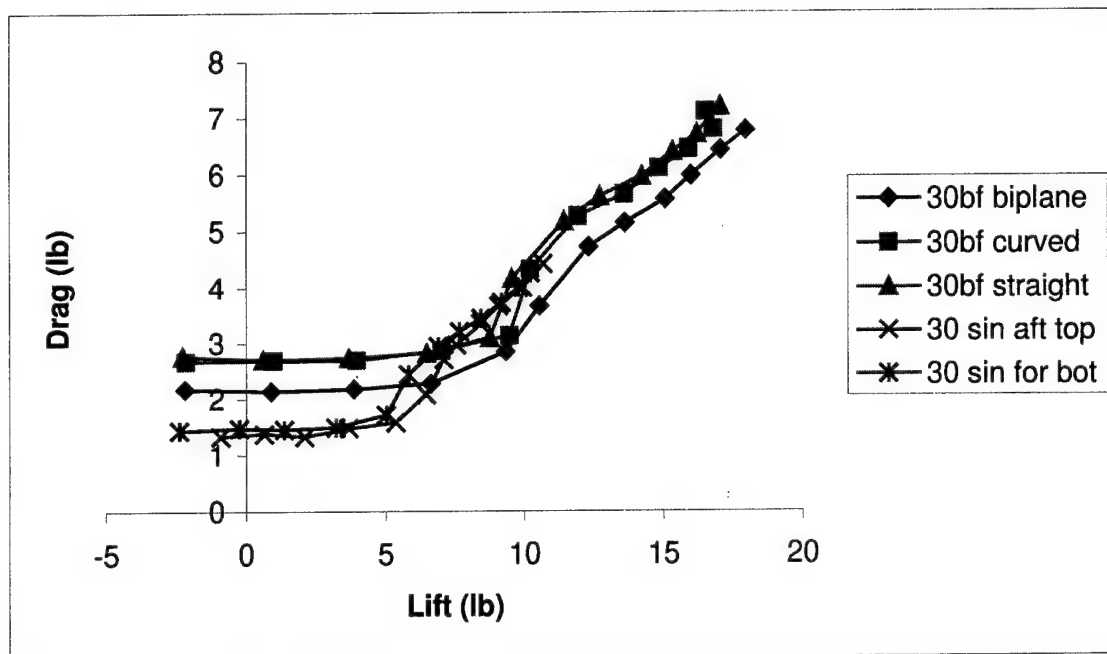
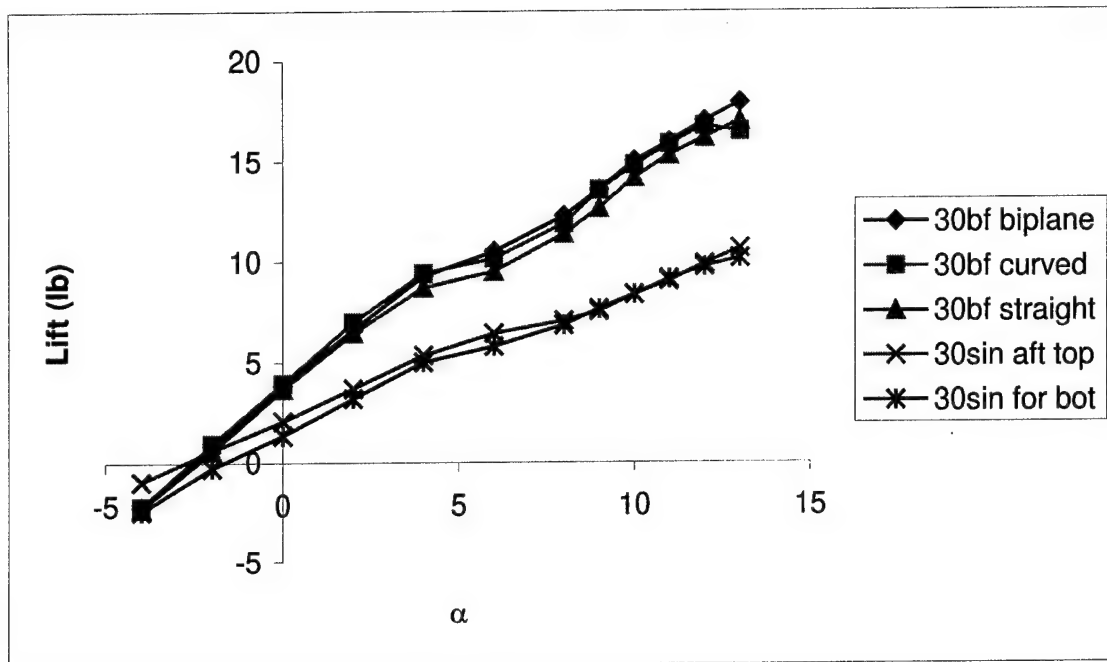


Figure 22: Comparison of the Lift and Drag Relations for the 30° Swept Wing, Flown at 175 mph (78.2 m/s)

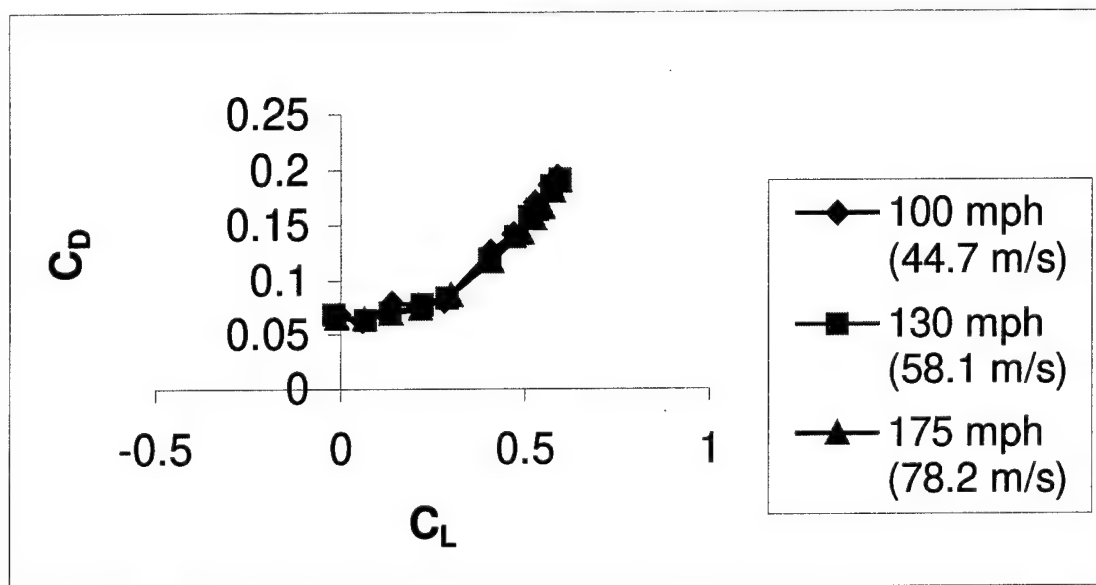
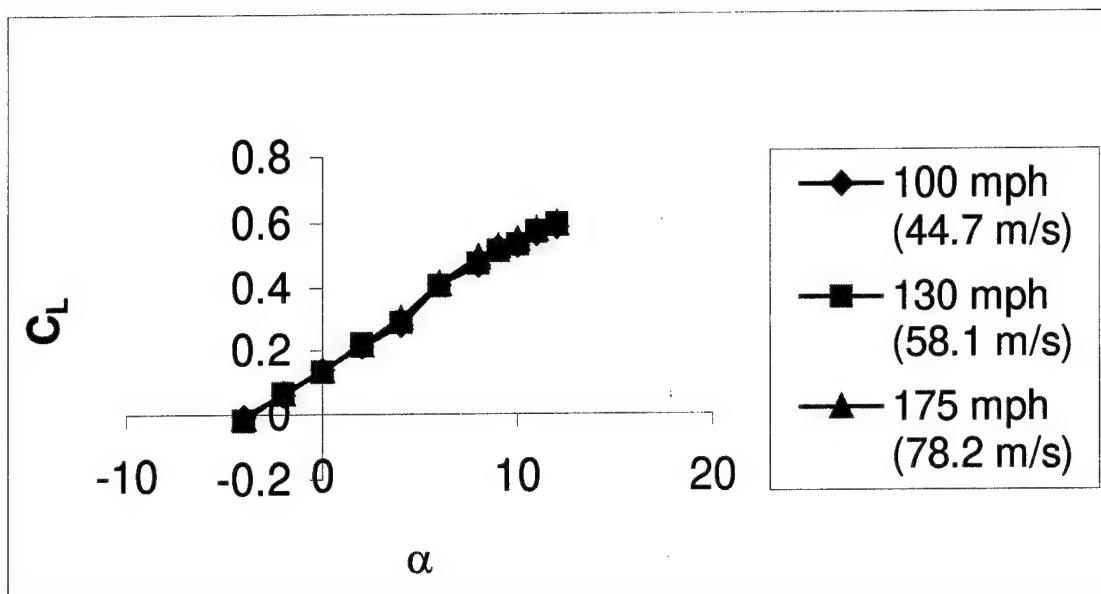


Figure 23: Lift and Drag Relations of the 60° Swept Jointed Wing with Curved Connectors, Negative Stagger

Upon analyzing Figures 20-23, it can be determined that the 60° swept joined wing with curved connectors, negative stagger and the 30° swept biplane were the better configurations in their sweep family. These configurations were chosen because they produced the greatest overall lift. However, there are a number of configurations that have nearly the same values as the chosen configuration making it difficult to distinguish one configuration as the outstanding choice. The chosen configurations are then compared with the bare missile in Figure 24. From this figure it is apparent that the winged configurations produce much more lift than the bare missile. In addition, the 30° swept biplane has a good deal more lift than the 60° swept joined wing with curved connectors. However, as a down side, the biplane does have significantly more drag.

Typically when trying to compare configurations, the lift and drag and pitch and rolling moments are non-dimensionalized to produce a common ground for comparison. This analysis was done for each configuration. These coefficient curves can be found in Appendix B. The same procedure used to compare configurations for the lift and drag relations was done for the lift and drag coefficient relations. Each positive stagger configuration was compared to its negative stagger counterpart. The better configuration was then stacked against the rest of its sweep family. With the lift and drag coefficient relations are the induced drag relations. The induced drag was calculated using Equation (6) with the aspect ratio and efficiency factor values for a given configuration found in Table 1. Figures 25-28 depict the result of this analysis.

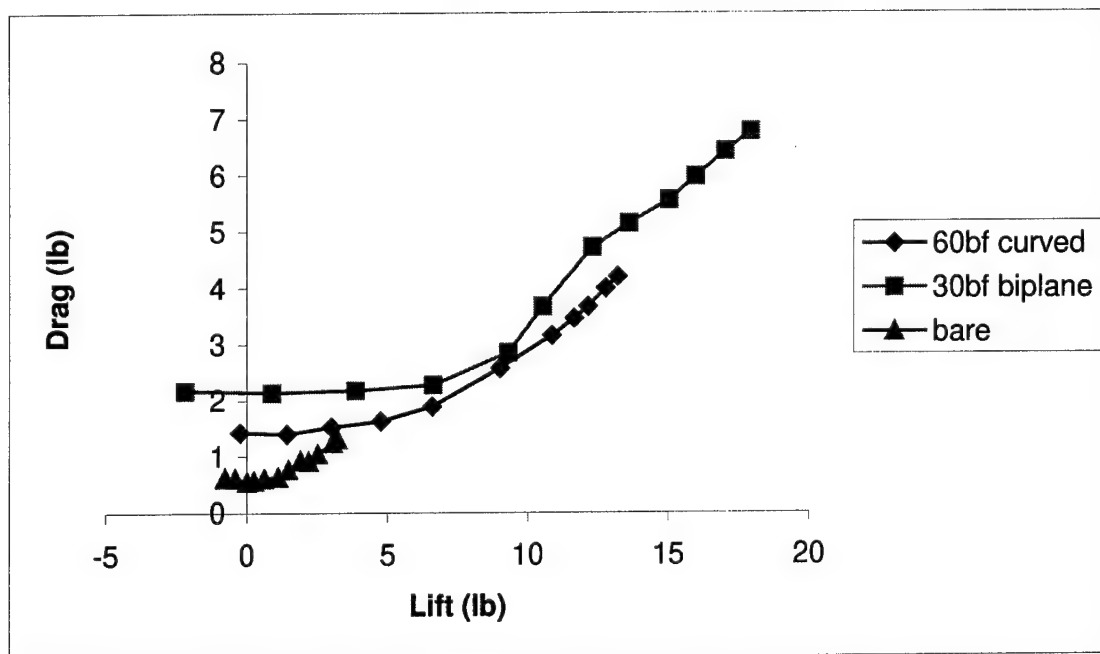
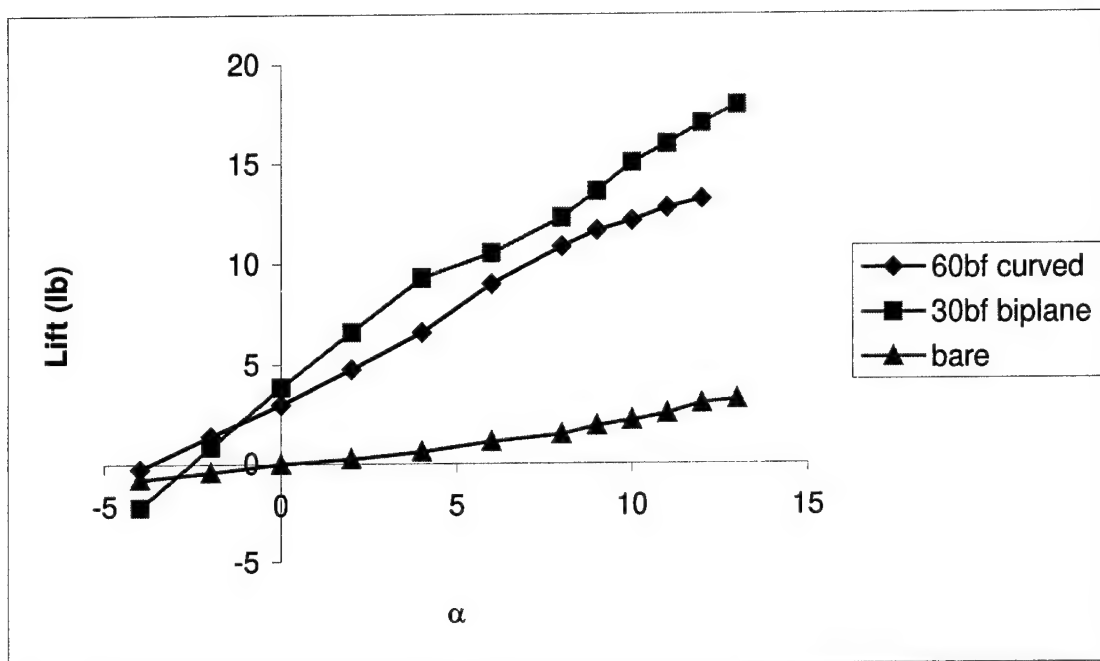


Figure 24: Lift and Drag Comparison of the Configurations, Flown at 175 mph (78.2 m/s)

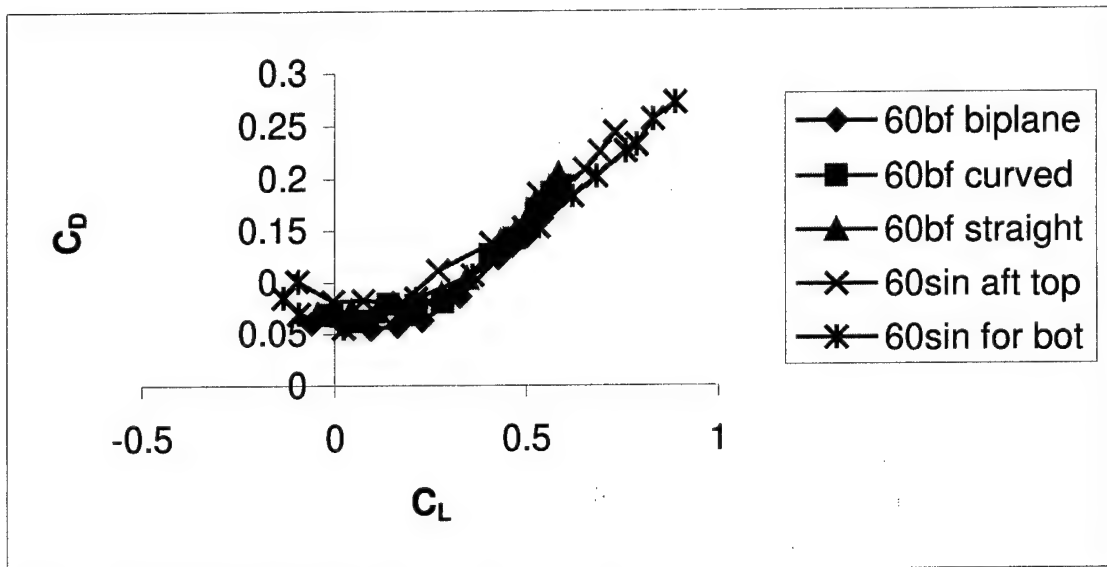
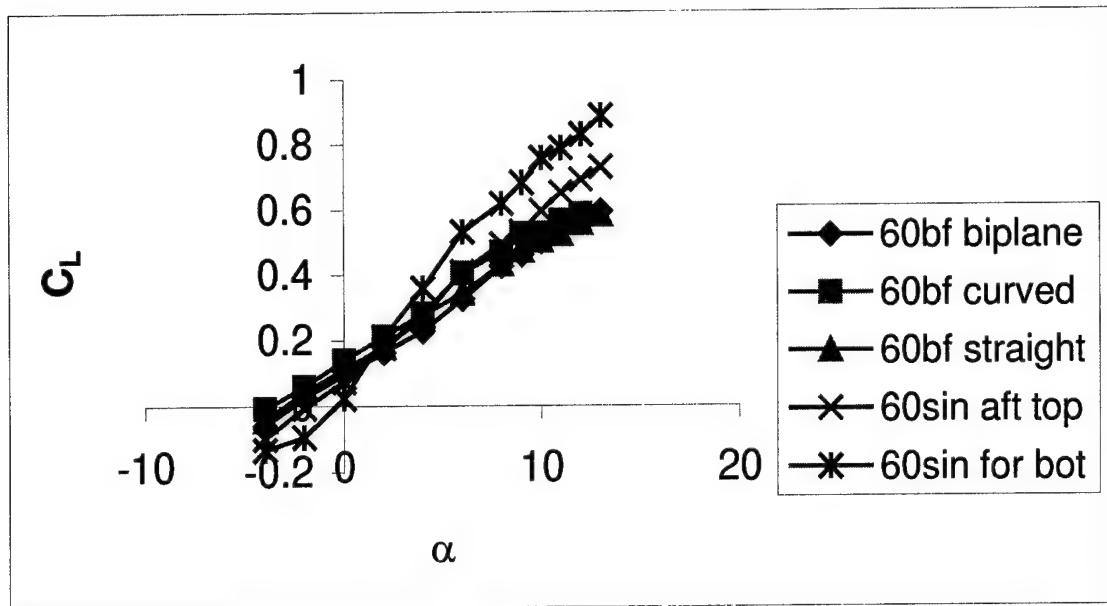


Figure 25: Comparison of the Lift and Drag Coefficient Relations for the 60° Swept Wings

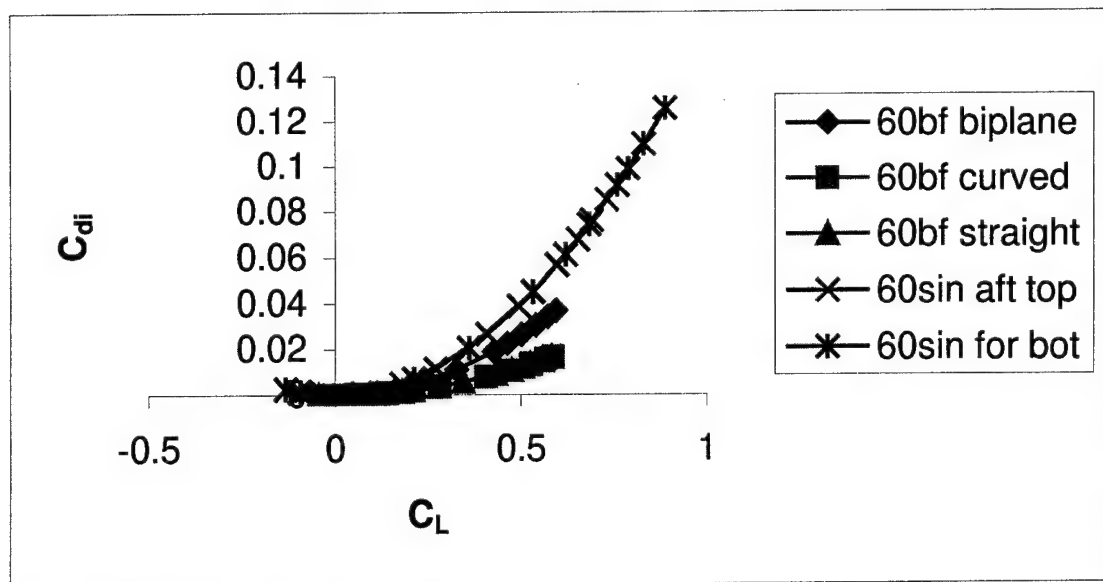
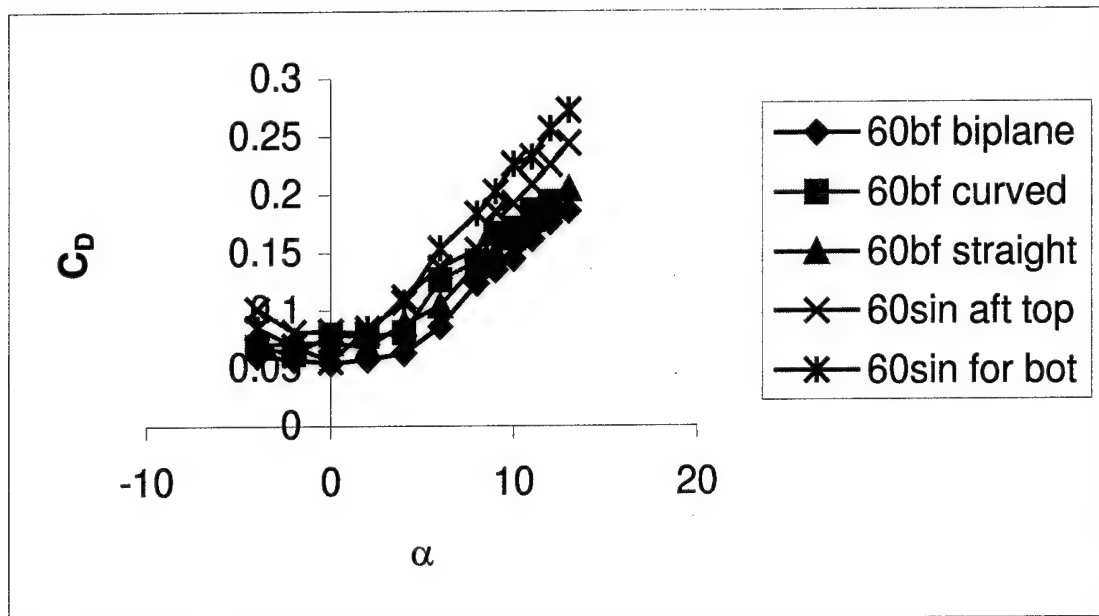


Figure 26: Comparison of the Drag Coefficient and Induced Drag Relations for the 60° Swept Wings

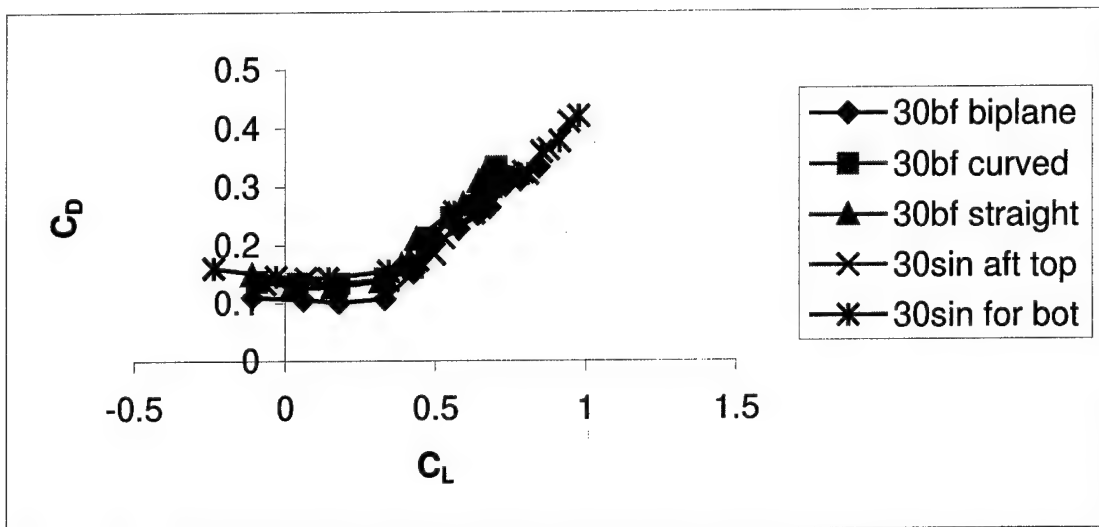
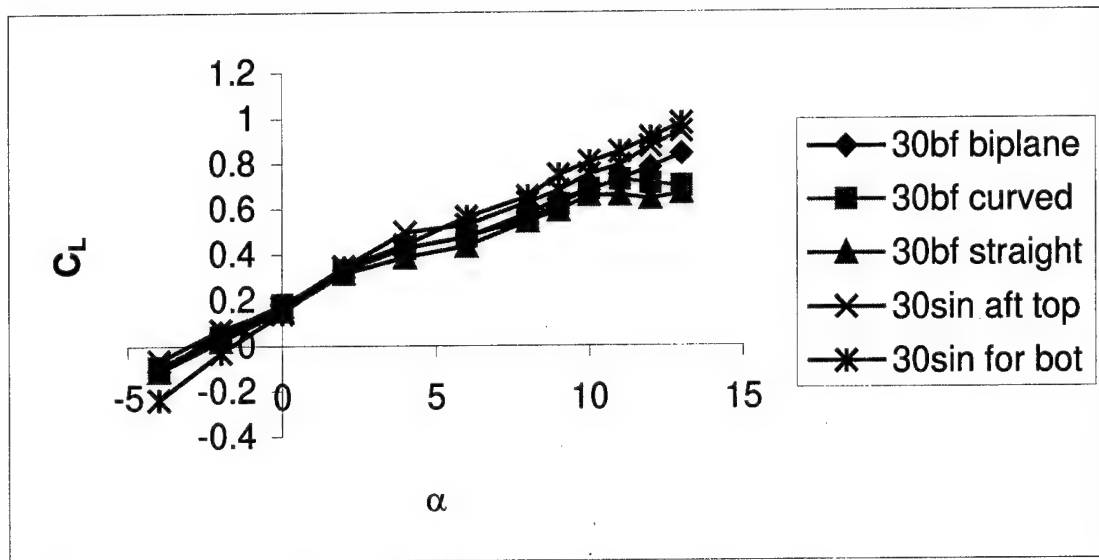


Figure 27: Comparison of the Lift and Drag Coefficient Relations for the 30° Swept Wings

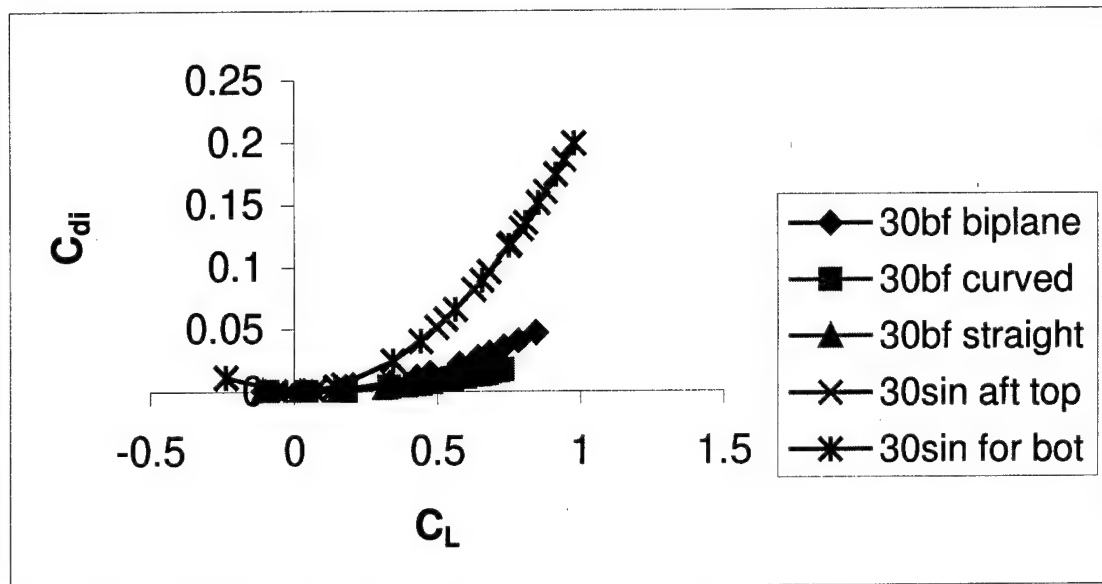
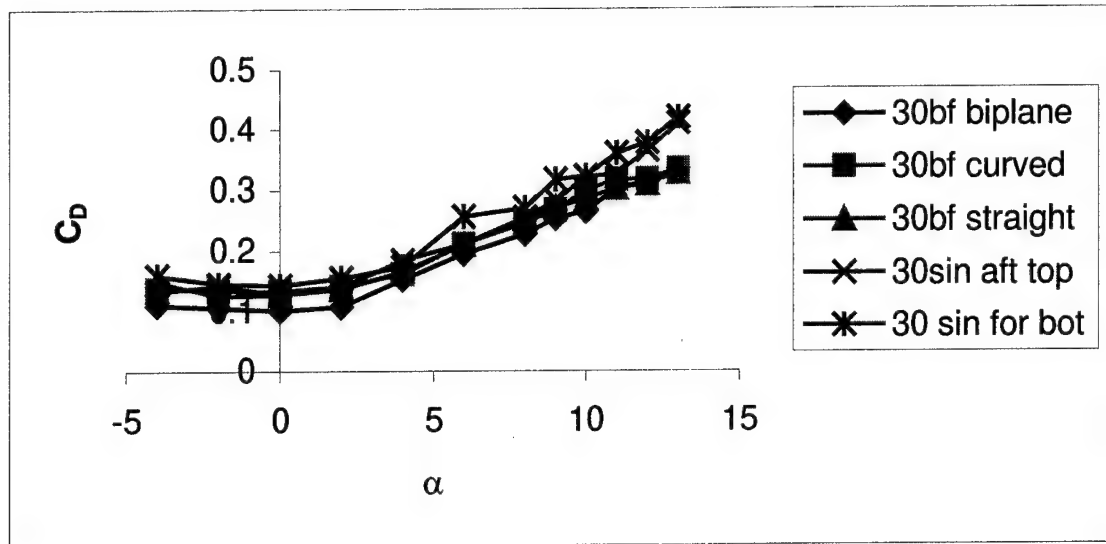


Figure 28: Comparison of the Drag Coefficient and Induced Drag Relations for the 30° Swept Wings

Looking at the lift and drag coefficients, it appears that the single wings located forward of the CG with the wings on the bottom are slightly better than their biplane counterparts in both sweep families. One explanation for this is the inflation of their coefficients because of their smaller wing area -- half that of their sweep family biplanes. With the area in the denominator in Equations 5 and 13, it may be erroneously portraying the single wings as better. Correcting for aspect ratio brings the single wing and the joined wing lines closer together and in some cases switches which gives higher lift. As stated in earlier chapters, it is important to keep track of how the joined wing and single wing are being compared. It may be that maintaining equal spans within the same sweep family, as in this case, is not the best method. Having equal areas or the same aspect ratio could be a better approach. In any event, the coefficient analysis portrays the single wings as being better configurations for lift shown in Figures 25 and 27.

One can notice in Figures 26 and 28 that the single wings in both sweep families produce more drag, especially induced drag. The 30° and 60° sweep biplanes produced the least amount of drag in each of their respective families. While the joined wings experienced very small amounts of induced drag, as to be expected, they did have a relatively high overall drag. This could be due to the additional area of the connectors which increased the profile drag.

From the sweep family comparison graphs, the "best" configuration was chosen in each sweep family. These configurations, along with the bare missile data, were compared to determine an "ultimate" configuration. This can be seen in Figure 29.

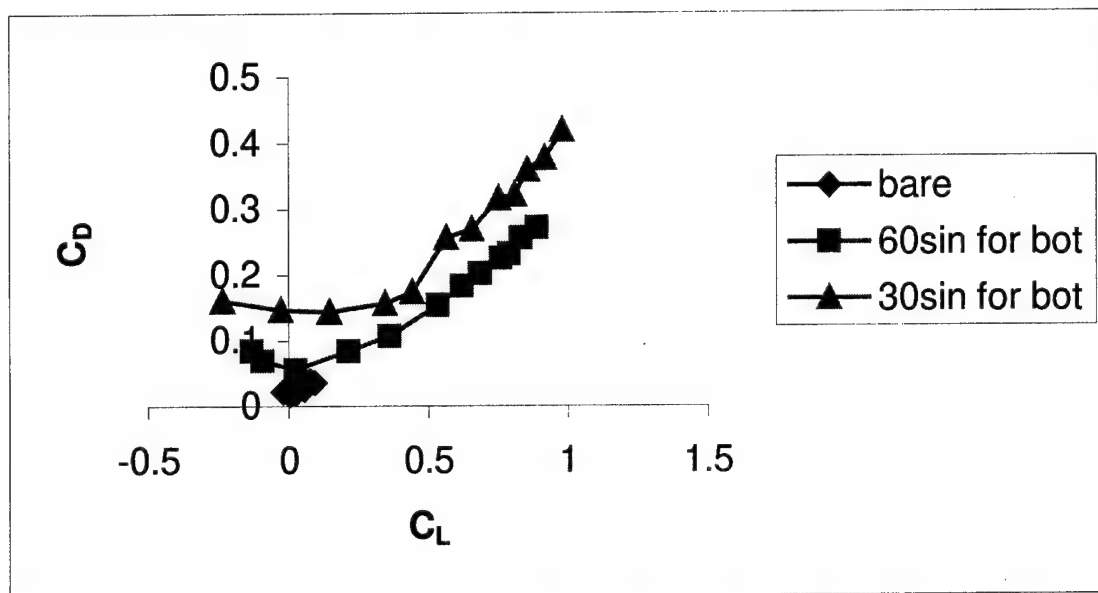
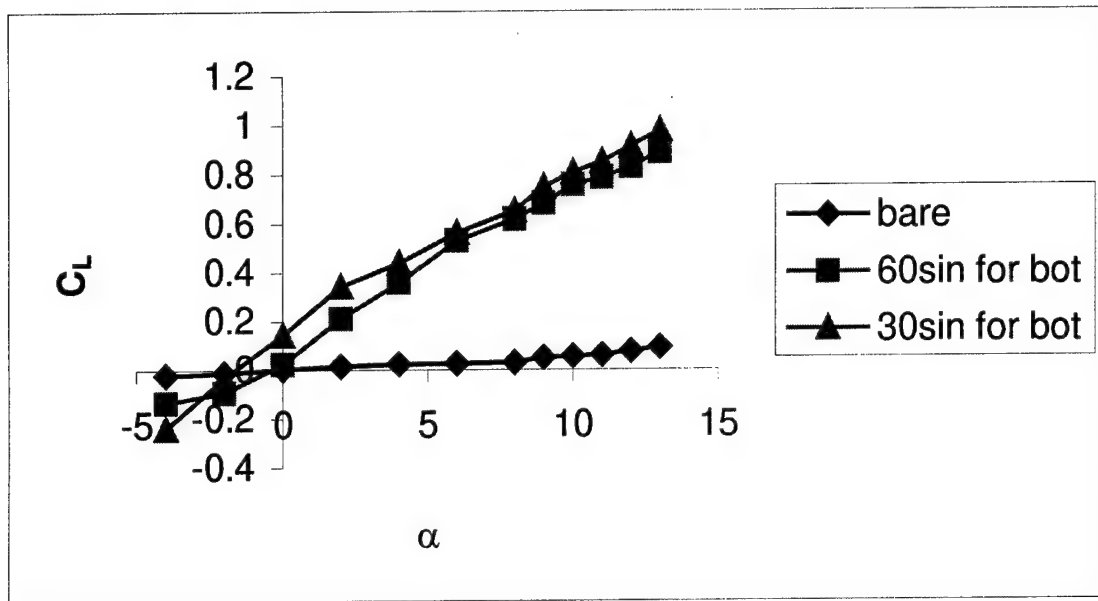


Figure 29: Lift and Drag Coefficient Comparison of the Configurations

It appears that the 30° swept aft single wing located forward of the CG is the better configuration for lift. This coincides with the recommendation by Reference 11 to have a smaller sweep. However, the 60° swept single wing is not far behind and tends to have better other properties, such as a lower drag and more favorable pitch and roll curve. It must be kept in mind that the area and span of the different swept wings are different. Therefore, because the 30° swept single wing had a smaller sweep does not inevitably make it a better wing -- it also has a 0.6 in² larger area.

Because the joined and single wing configurations are so drastically different, the traditional comparison of the non-dimension lift and drag coefficients may not be appropriate.

One other thing to note is that the type of connector does not appear to make much of a difference. Neither joined wing configuration tends to really outperform the other. Any difference in the curves between the two configurations can be accounted for in the error band.

On a more general note, there are some basic trends that the configurations follow when looking at the coefficient curves. All of these trends can be found when looking at the figures in Appendix B. As stated before, the different speeds flown line up with each other. This shows superb repeatability among the runs. As typical for most negative stagger configurations tested, the stall point was not found -- the curve continues upward. Conversely, the positive stagger configurations, specifically those in the 30° sweep family, have a distinct stall point. The curves in the lift to drag graphs for all configurations have the

traditional "bucket" shape. This shows excellent correlation with historical findings. It is ideal to have a pitching moment graph with a negative slope that allows the negative angles to pitch up and the higher positive angles to pitch down. Unfortunately, this was not the case for all configurations. Some of the 60° swept wings with positive stagger continually pitch down. This causes interesting stability issues. The single wing configuration placed aft of the CG with wings on top had a very steep negative slope. While the slope is in the desired direction, the steepness indicates an extreme pitch can occur. The pitch was measured about the electrical center of gravity of the balance, which coincides with the center of gravity of most of the configurations. In the case of the single wings, the missile center of gravity shifts from the electrical center of gravity as much as 0.25 in (0.635 cm), potentially causing the readings to be skewed. This could be one explanation as to why the single wings, especially, tend to pitch severely. This instability could be a deciding factor in choosing one configuration over another. All of the configurations besides the bare missile show some rolling moment. This could be related to the slight vibration during testing or to an off centering of the model when assembled. The amount of roll appears to be rather insignificant in most cases.

One final form of comparison is the range ratio, or essentially the ratio of lift to drag. See Equation (18). A lift of $0.7\text{lift}_{\text{max}}$ was taken with its corresponding drag. In some cases, especially with the 30° swept wings in positive stagger, there was a clear stall point and that lift_{max} used. For the rest of the configurations, the highest lift recorded was used. This produces some error in

the range ratios in Table 4. It may be that some configurations will outperform others at higher angles, giving them a better range ratio. For now, Table 4 gives the range ratios for all of the configurations as compared to each other. The range of the configurations across the top is divided by the range of the configurations along the left-hand side. Based on this analysis, the 60° swept biplane performs the best with a 76% increase in range over the bare missile. However, many configurations are within 5% of the biplane, including a few of the single wings.

One other aspect to look at is the fact that the missile will more than likely fly in the compressible regime around Mach 0.7. The Mach number in this study did not exceed 0.23 which is within the incompressible range. While no actual tests were conducted in the compressible regime, it is believed that Equations (19) to (20), the equations that convert incompressible values into compressible estimates, will give a good prediction of the lift and drag coefficients at the higher Mach numbers. For this study, the lift and drag coefficients could increase approximately 70% based on a Mach of 0.7. Keep in mind that while this increase is good for the lift, it is also increasing drag, which is typically a bad thing.

Table 4: Range Ratio

| | bare | 60bf curved | 60tf curved | 60bf straight | 60tf straight | 60bf biplane | 60tf biplane | 60sin aft bot | 60sin aft top | 60sin for bot | 60sin for top |
|---------------|-------|----------------|----------------|------------------|------------------|-----------------|-----------------|------------------|------------------|------------------|------------------|
| bare | 1.000 | 1.693 | 1.517 | 1.521 | 1.373 | 1.757 | 1.508 | 1.465 | 1.570 | 1.752 | 1.387 |
| 60bf curved | 0.591 | 1.000 | 0.896 | 0.898 | 0.811 | 1.038 | 0.890 | 0.865 | 0.927 | 1.034 | 0.819 |
| 60tf curved | 0.659 | 1.116 | 1.000 | 1.002 | 0.905 | 1.159 | 0.994 | 0.965 | 1.035 | 1.155 | 0.915 |
| 60bf straight | 0.658 | 1.114 | 0.998 | 1.000 | 0.903 | 1.156 | 0.992 | 0.963 | 1.032 | 1.152 | 0.912 |
| 60tf straight | 0.728 | 1.233 | 1.105 | 1.107 | 1.000 | 1.280 | 1.098 | 1.066 | 1.143 | 1.275 | 1.010 |
| 60bf biplane | 0.569 | 0.964 | 0.863 | 0.865 | 0.997 | 1.000 | 0.858 | 0.833 | 0.893 | 0.997 | 0.789 |
| 60tf biplane | 0.663 | 1.123 | 1.006 | 1.008 | 0.911 | 1.166 | 1.000 | 0.971 | 0.513 | 1.162 | 0.920 |
| 60sin aft bot | 0.683 | 1.156 | 1.036 | 1.038 | 0.938 | 1.200 | 1.030 | 1.000 | 1.072 | 1.196 | 0.947 |
| 60sin aft top | 0.637 | 1.079 | 0.966 | 0.969 | 0.875 | 1.119 | 0.960 | 0.933 | 1.000 | 1.116 | 0.884 |
| 60sin for bot | 0.571 | 0.967 | 0.866 | 0.868 | 0.784 | 1.003 | 0.861 | 0.836 | 0.539 | 1.000 | 0.792 |
| 60sin for top | 0.721 | 1.221 | 1.093 | 1.096 | 0.990 | 1.267 | 1.087 | 1.056 | 1.132 | 1.262 | 1.000 |
| 30bf curved | 0.863 | 1.461 | 1.308 | 1.312 | 1.185 | 1.516 | 1.301 | 1.263 | 1.354 | 1.511 | 1.197 |
| 30tf curved | 1.269 | 2.148 | 1.924 | 1.929 | 1.742 | 2.230 | 1.913 | 1.858 | 1.992 | 2.222 | 1.760 |
| 30bf straight | 0.915 | 1.550 | 1.388 | 1.391 | 1.257 | 1.608 | 1.380 | 1.340 | 1.437 | 1.603 | 1.270 |
| 30tf straight | 1.292 | 2.188 | 1.960 | 1.965 | 1.775 | 2.271 | 1.949 | 1.893 | 2.029 | 2.264 | 1.793 |
| 30bf biplane | 0.743 | 1.258 | 1.127 | 1.129 | 1.020 | 1.305 | 1.120 | 1.088 | 1.166 | 1.301 | 1.030 |
| 30tf biplane | 1.029 | 1.742 | 1.561 | 1.564 | 1.413 | 1.808 | 1.551 | 1.507 | 1.615 | 1.802 | 1.427 |
| 30sin aft bot | 1.059 | 1.793 | 1.606 | 1.610 | 1.454 | 1.861 | 1.597 | 1.551 | 1.662 | 1.855 | 1.469 |
| 30sin aft top | 0.783 | 1.326 | 1.188 | 1.191 | 1.076 | 1.377 | 1.181 | 1.147 | 1.230 | 1.372 | 1.087 |
| 30sin for bot | 1.142 | 1.935 | 1.733 | 1.737 | 1.569 | 2.008 | 1.723 | 1.673 | 1.794 | 2.001 | 1.142 |
| 30sin for top | 1.056 | 1.789 | 1.603 | 1.606 | 1.451 | 1.857 | 1.593 | 1.547 | 1.658 | 1.850 | 1.466 |

Table 3: Range Ratio (cont'd)

| | 30bf curved | 30tf curved | 30bf straight | 30tf straight | 30bf biplane | 30tf biplane | 30sin aft bot | 30sin aft top | 30sin for bot | 30sin for top |
|---------------|----------------|----------------|------------------|------------------|-----------------|-----------------|------------------|------------------|------------------|------------------|
| bare | 1.159 | 0.788 | 1.093 | 0.774 | 1.347 | 0.972 | 0.944 | 1.277 | 0.875 | 0.947 |
| 60bf curved | 0.685 | 0.465 | 0.645 | 0.457 | 0.795 | 0.574 | 0.558 | 0.754 | 0.517 | 0.559 |
| 60tf curved | 0.764 | 0.520 | 0.720 | 0.510 | 0.888 | 0.641 | 0.623 | 0.842 | 0.577 | 0.624 |
| 60bf straight | 0.762 | 0.518 | 0.719 | 0.509 | 1.156 | 0.639 | 0.621 | 0.840 | 0.576 | 0.623 |
| 60tf straight | 0.844 | 0.574 | 0.796 | 0.563 | 0.981 | 0.708 | 0.688 | 0.930 | 0.637 | 0.689 |
| 60bf biplane | 0.660 | 0.449 | 0.622 | 0.440 | 0.766 | 0.553 | 0.537 | 0.726 | 0.498 | 0.539 |
| 60tf biplane | 0.769 | 0.523 | 0.725 | 0.513 | 0.893 | 0.645 | 0.626 | 0.000 | 0.581 | 0.628 |
| 60sin aft bot | 0.792 | 0.538 | 0.746 | 0.528 | 0.919 | 0.664 | 0.645 | 0.872 | 0.598 | 0.646 |
| 60sin aft top | 0.738 | 0.502 | 0.696 | 0.493 | 0.858 | 0.619 | 0.602 | 0.813 | 0.558 | 0.603 |
| 60sin for bot | 0.662 | 0.450 | 0.624 | 0.442 | 0.769 | 0.555 | 0.539 | 0.729 | 0.500 | 0.540 |
| 60sin for top | 0.836 | 0.568 | 0.788 | 0.558 | 0.971 | 0.701 | 0.681 | 0.920 | 0.631 | 0.682 |
| 30bf curved | 1.000 | 0.680 | 0.943 | 0.667 | 1.162 | 0.838 | 0.815 | 1.101 | 0.755 | 0.817 |
| 30tf curved | 1.471 | 1.000 | 1.386 | 0.982 | 1.708 | 1.233 | 1.198 | 1.620 | 1.110 | 1.201 |
| 30bf straight | 1.061 | 0.721 | 1.000 | 0.708 | 1.232 | 0.889 | 0.864 | 1.168 | 0.801 | 0.866 |
| 30tf straight | 1.498 | 1.019 | 1.412 | 1.000 | 1.740 | 1.256 | 1.220 | 1.650 | 1.131 | 1.223 |
| 30bf biplane | 0.861 | 0.585 | 0.812 | 0.575 | 1.000 | 0.722 | 0.701 | 0.948 | 0.650 | 0.703 |
| 30tf biplane | 1.193 | 0.811 | 1.124 | 0.796 | 1.385 | 1.000 | 0.972 | 1.313 | 0.900 | 0.974 |
| 30sin aft bot | 1.228 | 0.835 | 1.157 | 0.819 | 1.426 | 1.029 | 1.000 | 1.352 | 0.927 | 1.002 |
| 30sin aft top | 0.908 | 0.617 | 0.856 | 0.606 | 1.055 | 0.761 | 0.740 | 1.000 | 0.686 | 0.742 |
| 30sin for bot | 1.325 | 0.901 | 1.249 | 1.569 | 1.538 | 1.111 | 1.079 | 1.459 | 1.000 | 1.082 |
| 30sin for top | 1.225 | 0.833 | 1.154 | 0.817 | 1.423 | 1.027 | 0.998 | 1.349 | 0.925 | 1.000 |

The final analysis to be discussed is error. Inherent in data collection is some degree of error. Obtaining the smallest error possible will add to the reliability of the data. Upon conducting the error analysis discussed above using the 60° sweep joined wing with straight connectors, the best error calculated was 3.7% for the drag coefficient and 2.8% for the lift coefficient, shown in Figure 30. The error bands are approximately the size of the data point markers. This was using data received during the 175 mph (78.2 m/s) test. As the speed was reduced the error increased. The error bands for the 100 mph (44.7 m/s) test overlap the 175 mph (78.2 m/s) error bands, further proving the reliability of this data. With the small error percentage, it is with confidence that the conclusions are presented.

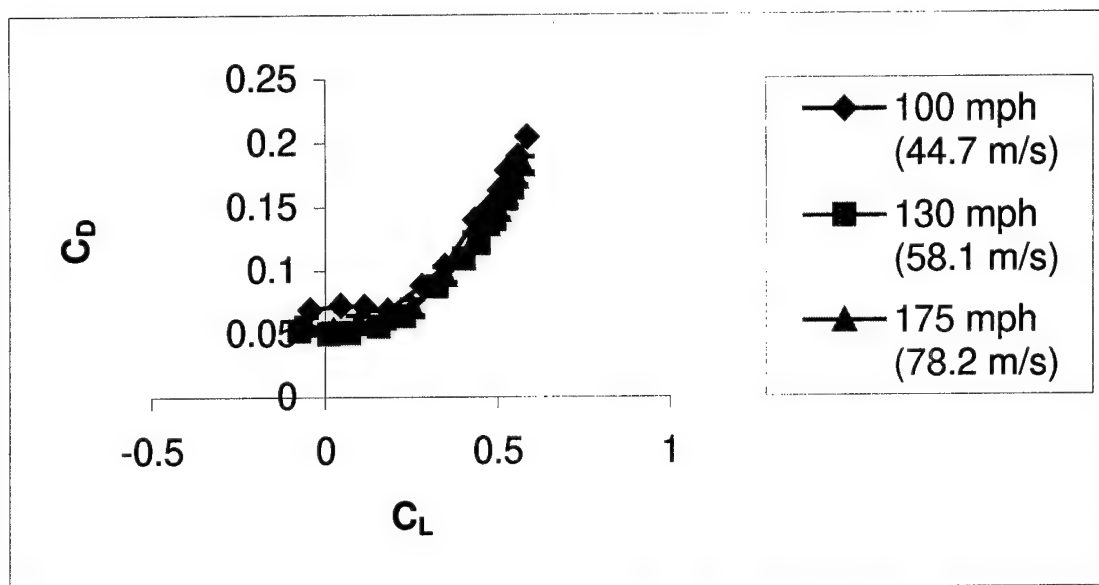
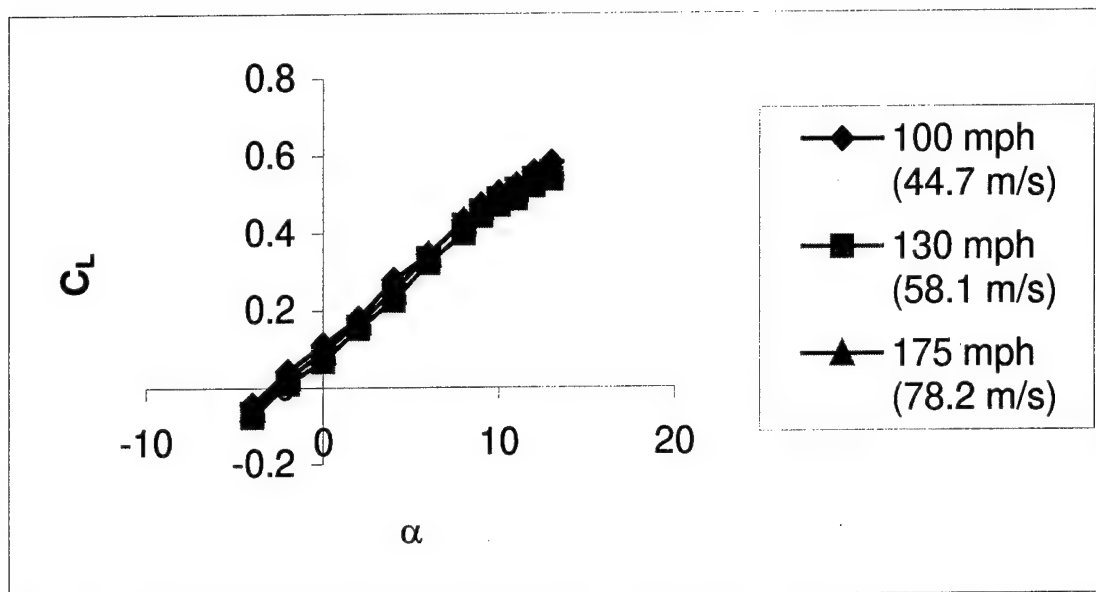


Figure 30: Error Analysis of the Lift and Drag Coefficients of the 60° Sweep Joined Wing with Straight Connectors, Negative Stagger

V. Summary

The main thrust of this study was to determine if adding a wing kit, specifically a joined wing system, would increase the range of a smart bomb. It can be maintained that adding wings will increase the range in some cases over 30%. It is not conclusive from this study which configuration is the best. There is no one system that overwhelmingly stands out in any of analysis conducted. Also, there was a different "best" configuration in each of the three comparison analyses. Further research must be conducted to determine if a joined wing configuration is the most beneficial system. It is recommended that a future study be conducted where all configurations have the same reference area. Currently there are too many variables to be able to make secure conclusions. For instance, one cannot conclude which sweep is better because they have differing reference areas. Therefore, it can not be determined if it is the sweep or the area that is making the difference. Future studies will need more design consideration and reduction of variables to produce results that are more reliable and conclusive.

VI. Bibliography

1. Bagwell, Tracy and Selberg, Bruce, "Aerodynamic Investigation of Twist and Cant angles for Joined Wing Transport Aircraft", 35th Aerospace Sciences Meeting & Exhibit, AIAA 97-0037.
2. Morrocco, John and Fulghum, David, "Partners Sought for New transport Designs", Aviation Week & Space Technology, August 11, 1997, p. 76.
3. "Aeronautical Systems Tests Progressive Joined-Wing Aircraft", www.lmco.com/files2/lmtoday/9707/aero.html, posted August 7, 1997.
4. ad-www.larc.nasa.gov/cib/People/jay.html, December 1, 1998.
5. Wai, J., Herling, W.W., Muilenburg, D.A., "Analysis of a Joined-Wing Configuration", 32nd Aerospace Sciences Meeting & Exhibit, AIAA 94-0657.
6. Bagwell, Tracy and Selberg, Bruce, "Aerodynamic Investigation of Joined Wing Configurations for Transport Aircraft" AIAA 96-2373-CP.
7. ad-www.larc.nasa.gov/tsab/tetruss/images/joined.html, December 1, 1998.
8. Wolkovitch, Julian, Application of the Joined Wing to Cruise Missiles: Final Report for Phase I, Contract N00014-79-C-0953, Rancho Palos Verdes, CA: Aeronautical Consultant Associates, November 1980 (AD-A096450).
9. Wolkovitch, Julian, "The Joined Wing: An Overview", Journal of Aircraft, Vol. 23, No. 3, 1986, pages 161-178.
10. Hoang, T, and Soban, D., "Technology Advancements as Applied to Six Subsonic Transports", Aircraft Design, Systems and Operations Meeting, AIAA 93-3950.
11. Perkins, J.N., et. al., "The Design and Testing of Several Joined Wing RPV's", 23rd Aerospace Sciences Meeting, AIAA 85-0275.
12. Kroo, Ilan, and Gallman, John, "Aerodynamic and Structural Studies of Joined Wing Aircraft", Journal of Aircraft, Vol. 28, No. 1, January 1991, page 74.
13. Hoerner, S. F., Fluid Dynamic Drag, published by the author, 1965.
14. Selberg, B. P., and Cronin, D. L., "Aerodynamic-Structural Optimization of Positive/Negative Stagger Joined Wing Configurations", Aircraft Systems, Design, & technology Meeting, AIAA 86-2626.
15. Anderson, John, Introduction to Flight, New York, McGraw-Hill, 1989.

16. Kruggel, Benjamin, AFRL Munitions Directorate, Eglin AFB, FL. Personal Correspondence, 20 Jan 1998.
17. Anderson, John, Fundamentals of Aerodynamics, New York, McGraw-Hill, 1991.
18. Kulhman, J.M, and Ku, T.J., " Numerical Optimization Techniques for Bound Circulation Distribution for Minimum Induced drag of Non-Planar Wings: Computer Program Documentation," NASA CR-3458, 1982.
19. Raymer, Daniel, Aircraft Design: A Conceptual Approach, Washington, DC, AIAA, 1992.
20. Holman, J.P. and W.J. Gajda, Jr., Experimental Methods for Engineers (Fifth Edition), New York, McGraw-Hill, 1989.

Appendix A

The error in the drag coefficient calculations can be found using Equations (25-29). The actual numbers used are located on the following page.

The first three columns are the voltages sensed by the balance in the N_1 , N_2 and axial gages, respectively, for a given angle of attack. The fourth and fifth columns are the angle of attack in degrees and radians, respectively. The sixth column is the calculation of Equation (26); the seventh is the calculation of Equation (27); the eighth is the calculation of Equation (28); and the ninth column is the calculation of Equation (29). Column ten is the summation of the squares of columns six through nine. Column eleven is the square root of column ten and is the uncertainty of the drag coefficient. In column twelve is the calculated drag coefficient for a given angle of attack. The final column, thirteen, gives the percent error of the drag coefficient. Despite the fact that angle of attack can be found in the error equations, as the angle of attack increases, the percent error decreases. This is because the drag coefficient becomes much larger at the greater angles quicker than the angle of attack can affect the value of the uncertainty. Comparing the larger drag coefficients to essentially the same uncertainty as those found at the lower angles of attack produce smaller errors.

The error also increases significantly as the velocity decreases.

Table 5: Calculation of the Error in the Drag Coefficient

| Vn1 | Vn2 | Va | Alpha (in deg) | Alpha (in rad) | Cd/Vn1 | Cd/Vn2 | Cd/Va | Cd/q | total^2 | Cd un- certainty | Cd | % error |
|-------|--------|--------|-------------------|-------------------|---------|---------|--------|---------|----------|---------------------|--------|---------|
| 0.055 | -0.095 | 0.0456 | -4 | -0.0698 | -0.0819 | -0.0832 | 0.6612 | -0.0004 | 3.44E-05 | 0.0059 | 0.0575 | 0.1020 |
| 0.083 | -0.057 | 0.064 | -2 | -0.0349 | -0.0410 | -0.0416 | 0.6624 | -0.0005 | 3.36E-05 | 0.0058 | 0.0530 | 0.1093 |
| 0.107 | -0.024 | 0.091 | 0 | 0.0000 | 0.0000 | 0.0000 | 0.6628 | -0.0008 | 3.33E-05 | 0.0058 | 0.0588 | 0.0981 |
| 0.136 | 0.009 | 0.107 | 2 | 0.0349 | 0.0410 | 0.0416 | 0.6624 | -0.0010 | 3.36E-05 | 0.0058 | 0.0629 | 0.0921 |
| 0.168 | 0.047 | 0.122 | 4 | 0.0698 | 0.0819 | 0.0832 | 0.6612 | -0.0012 | 3.45E-05 | 0.0059 | 0.0711 | 0.0825 |
| 0.199 | 0.099 | 0.154 | 6 | 0.1047 | 0.1227 | 0.1246 | 0.6592 | -0.0018 | 3.59E-05 | 0.0060 | 0.0971 | 0.0617 |
| 0.216 | 0.162 | 0.175 | 8 | 0.1396 | 0.1634 | 0.1659 | 0.6564 | -0.0022 | 3.80E-05 | 0.0062 | 0.1239 | 0.0498 |
| 0.225 | 0.184 | 0.184 | 9 | 0.1571 | 0.1836 | 0.1865 | 0.6547 | -0.0025 | 3.93E-05 | 0.0063 | 0.1365 | 0.0459 |
| 0.233 | 0.205 | 0.185 | 10 | 0.1745 | 0.2038 | 0.2070 | 0.6528 | -0.0027 | 4.06E-05 | 0.0064 | 0.1477 | 0.0432 |
| 0.238 | 0.224 | 0.19 | 11 | 0.1920 | 0.2240 | 0.2275 | 0.6507 | -0.0029 | 4.21E-05 | 0.0065 | 0.1576 | 0.0412 |
| 0.245 | 0.243 | 0.198 | 12 | 0.2094 | 0.2440 | 0.2479 | 0.6483 | -0.0031 | 4.38E-05 | 0.0066 | 0.1736 | 0.0381 |
| 0.241 | 0.262 | 0.202 | 13 | 0.2269 | 0.2640 | 0.2682 | 0.6458 | -0.0033 | 4.56E-05 | 0.0068 | 0.1833 | 0.0368 |

Appendix B

The following pages contain the lift and drag coefficient relations and the pitch and roll coefficient relations for all of the configurations tested.

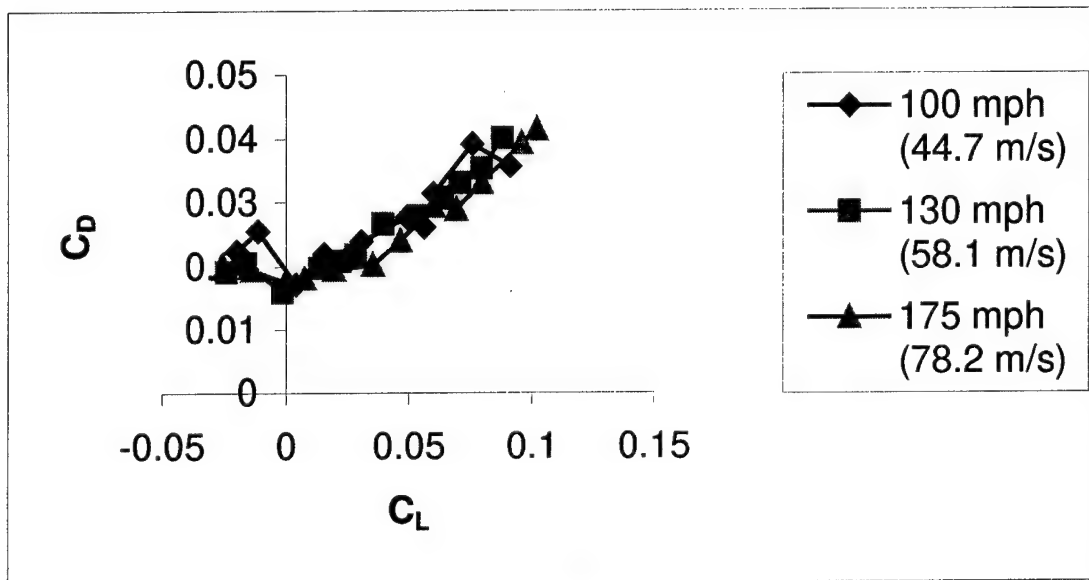
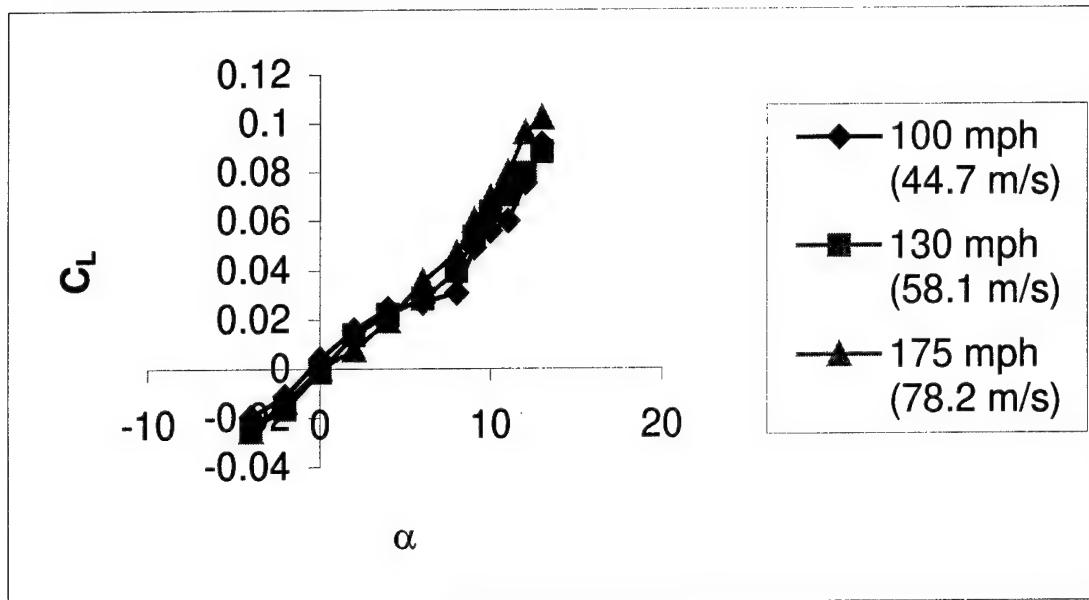


Figure 31: Lift and Drag Relations of the Bare Missile

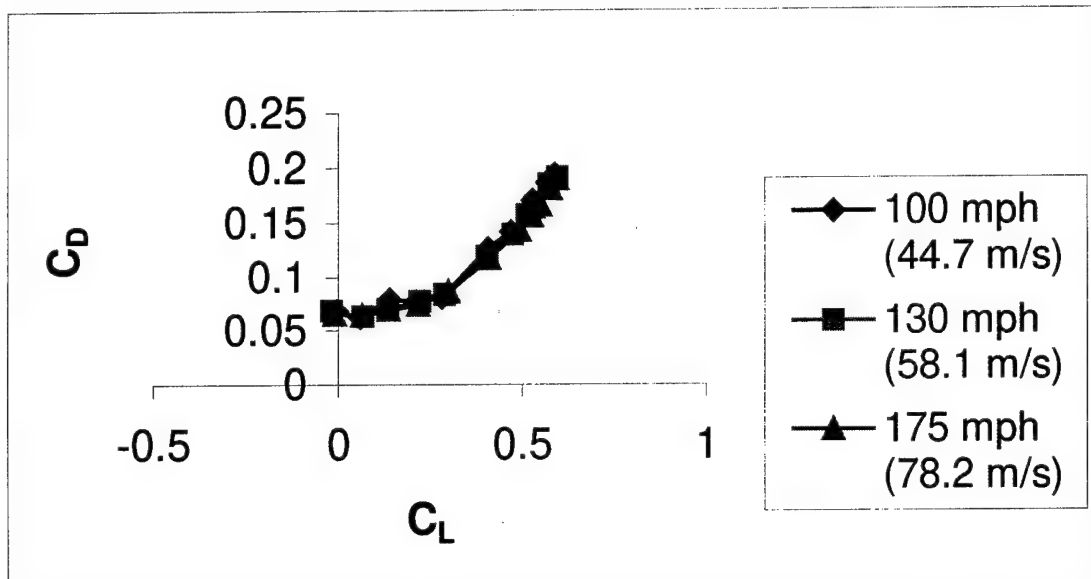
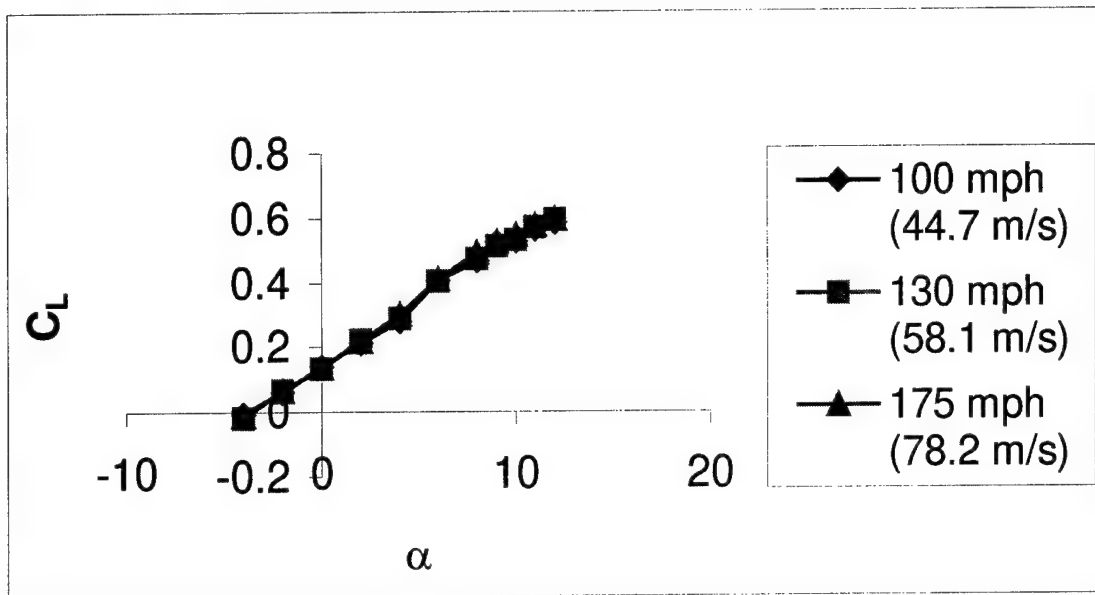


Figure 32: Lift and Drag Relations of the 60° Swept Joined Wing with Curved Connectors, Negative Stagger

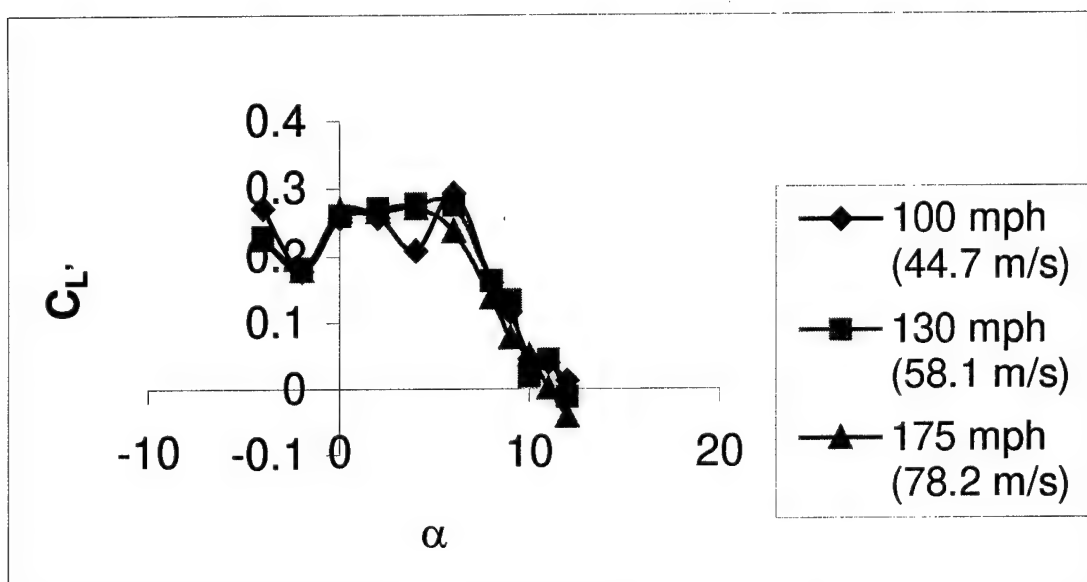
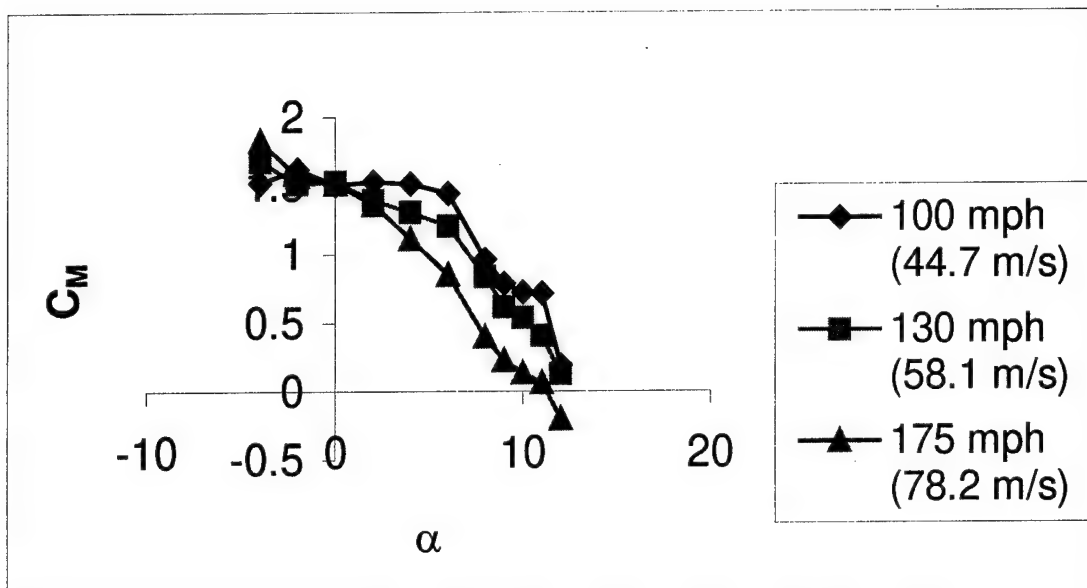


Figure 33: Pitch and Roll Relations of the 60° Swept Joined Wing with Curved Connectors, Negative Stagger

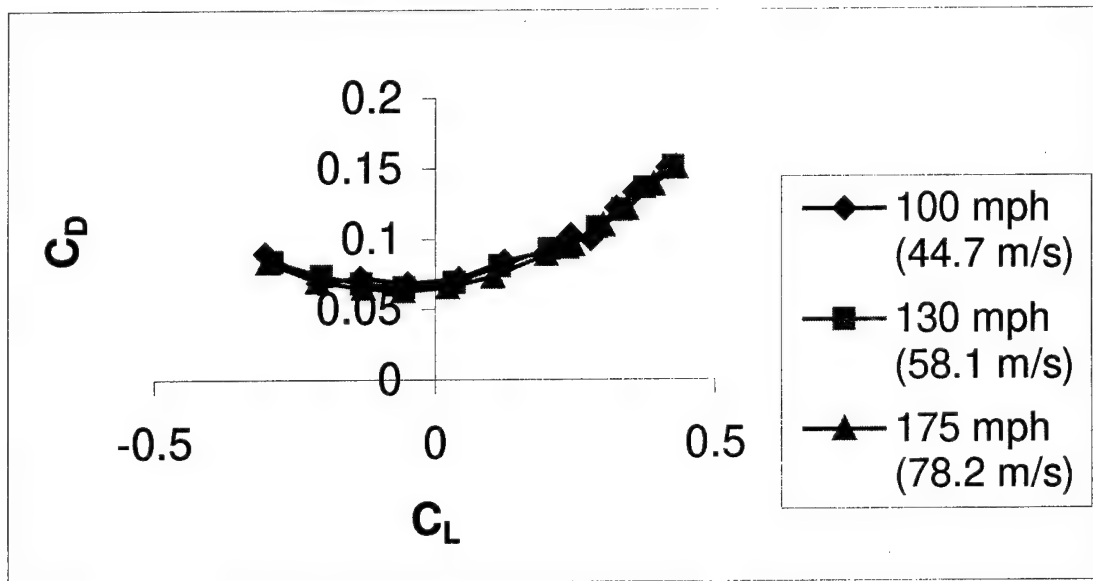
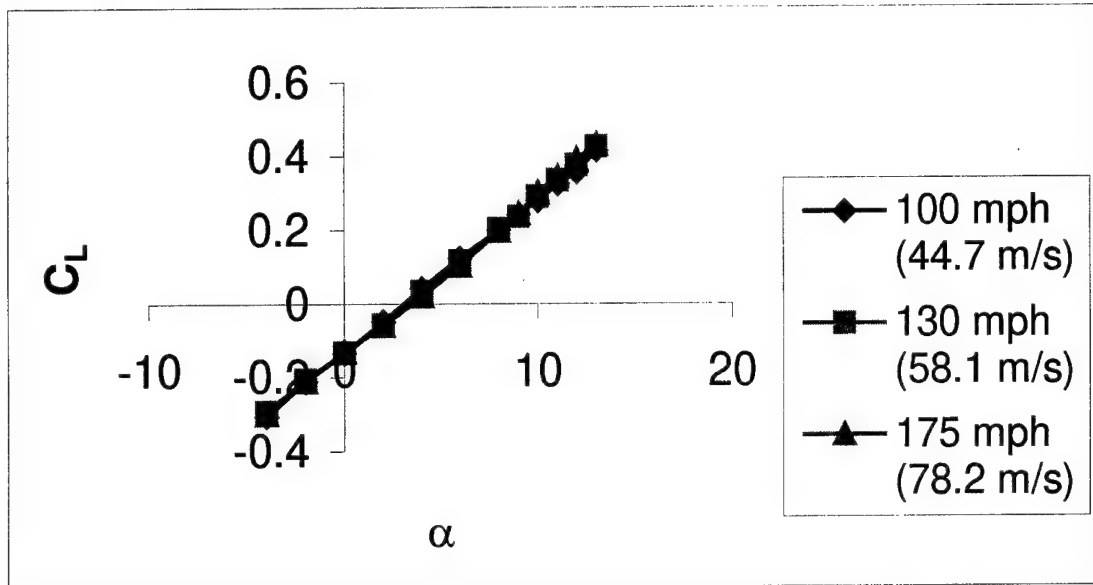


Figure 34: Lift and Drag Relations of the 60° Swept Jointed Wing with Curved Connectors, Positive Stagger

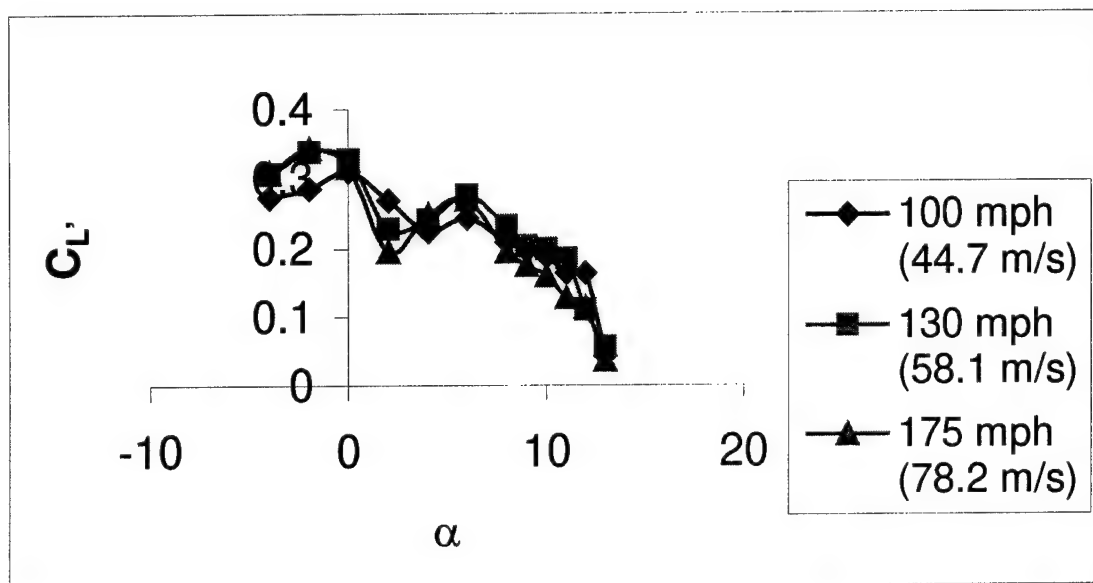
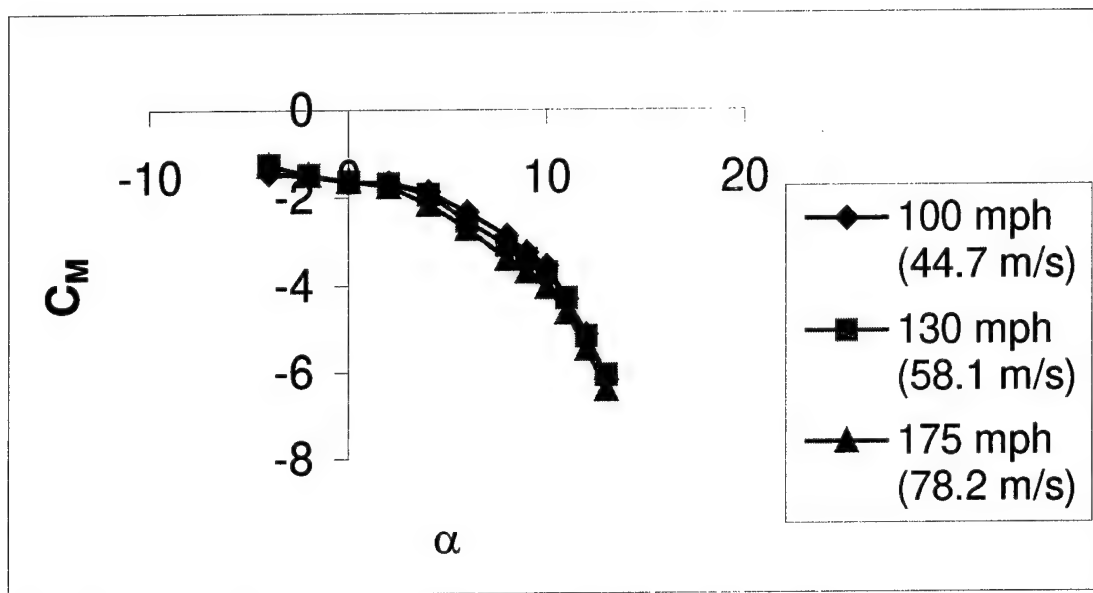


Figure 35: Pitch and Roll Relations of the 60° Swept Joined Wing with Curved Connectors, Positive Stagger

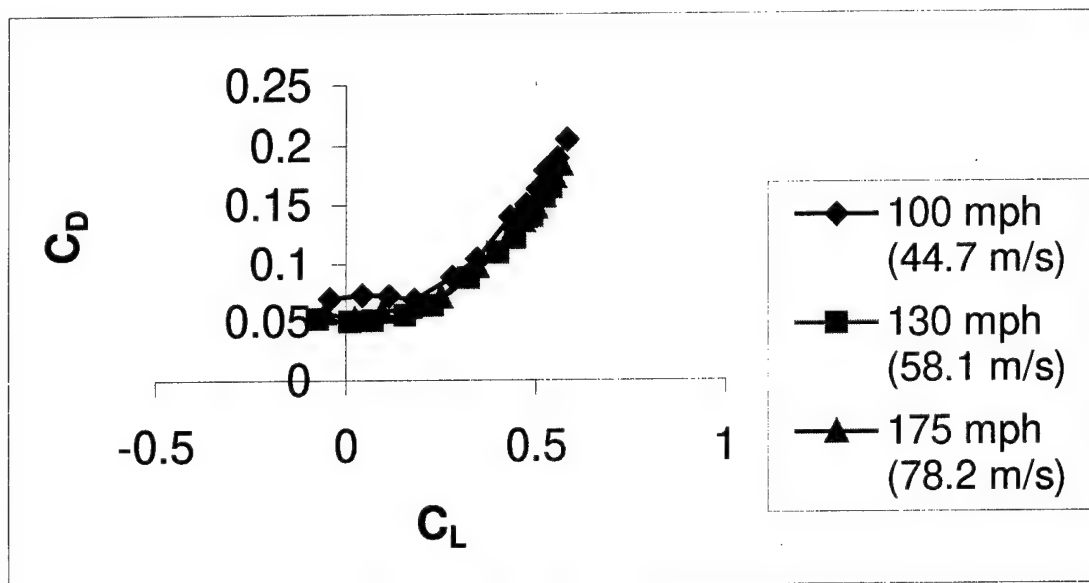
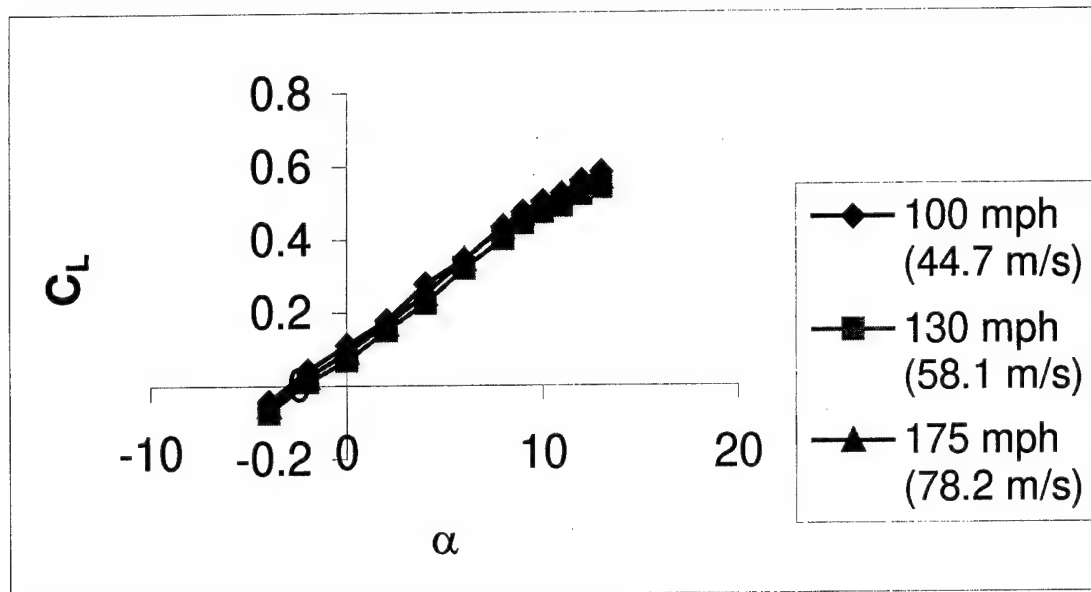


Figure 36: Lift and Drag Relations of the 60° Swept Jointed Wing with Straight Connectors, Negative Stagger

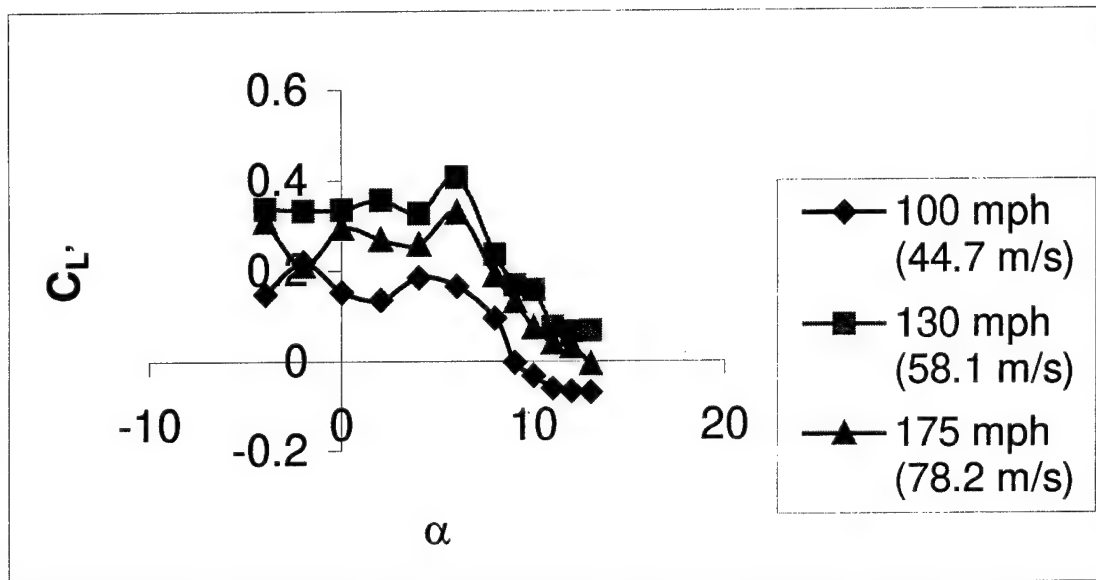
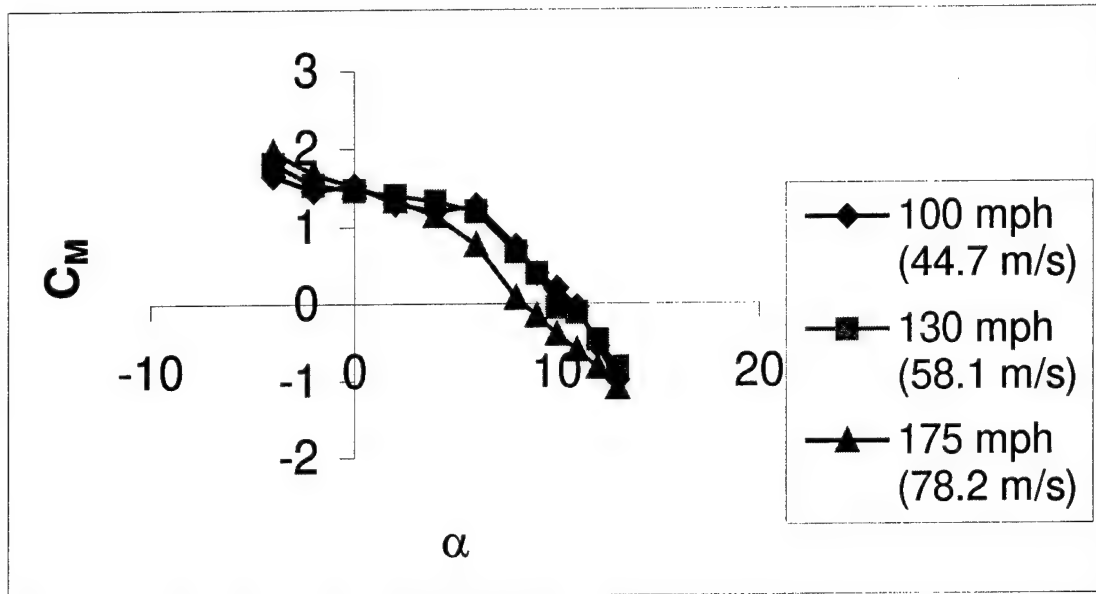


Figure 37: Pitch and Roll Relations of the 60° Swept Joined Wing with Straight Connectors, Negative Stagger

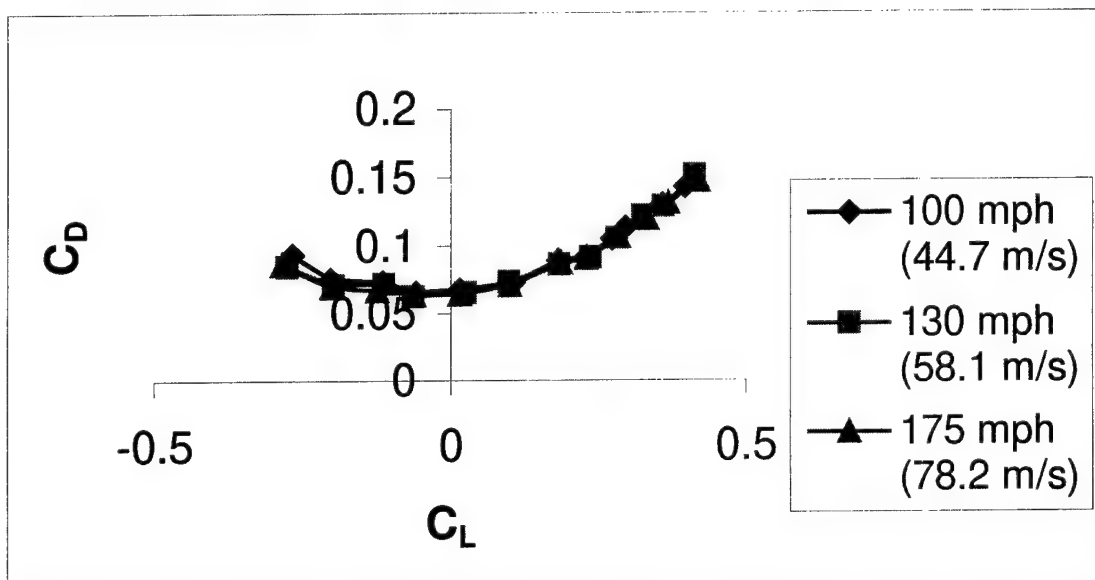
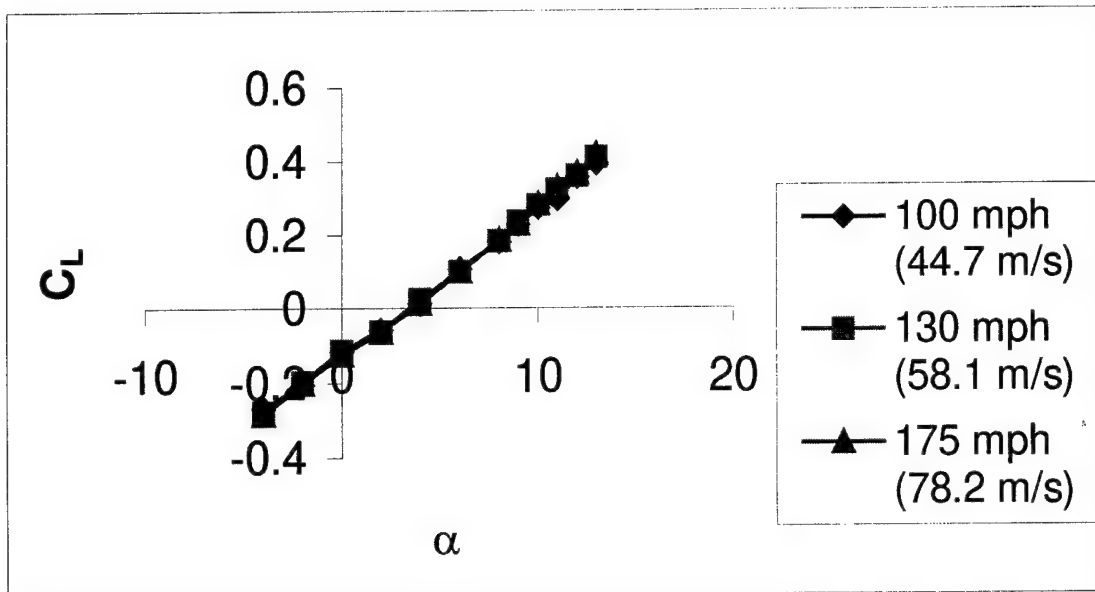


Figure 38: Lift and Drag Relations of the 60° Swept Joined Wing with Straight Connectors, Positive Stagger

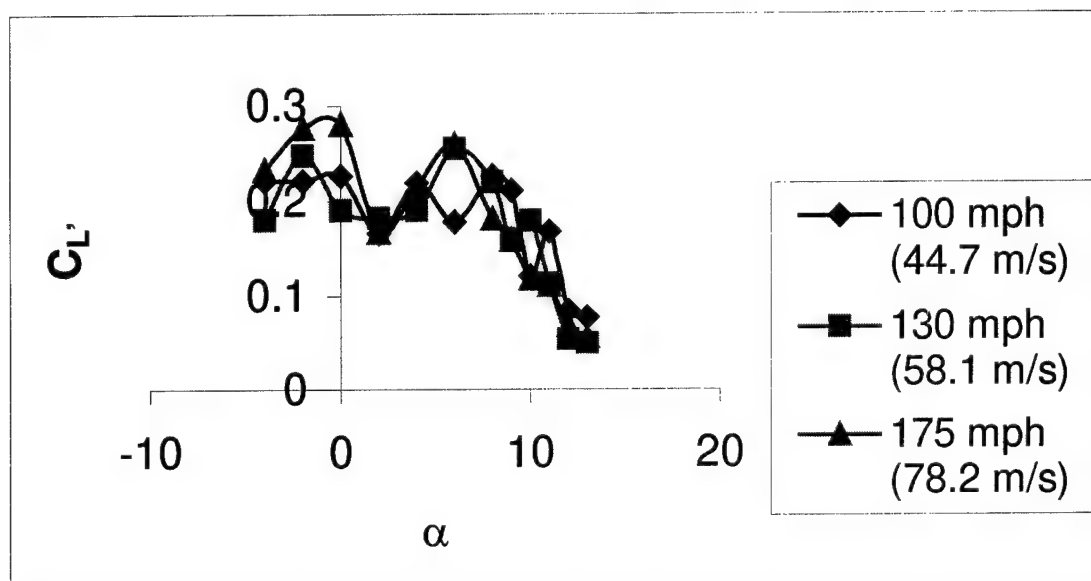
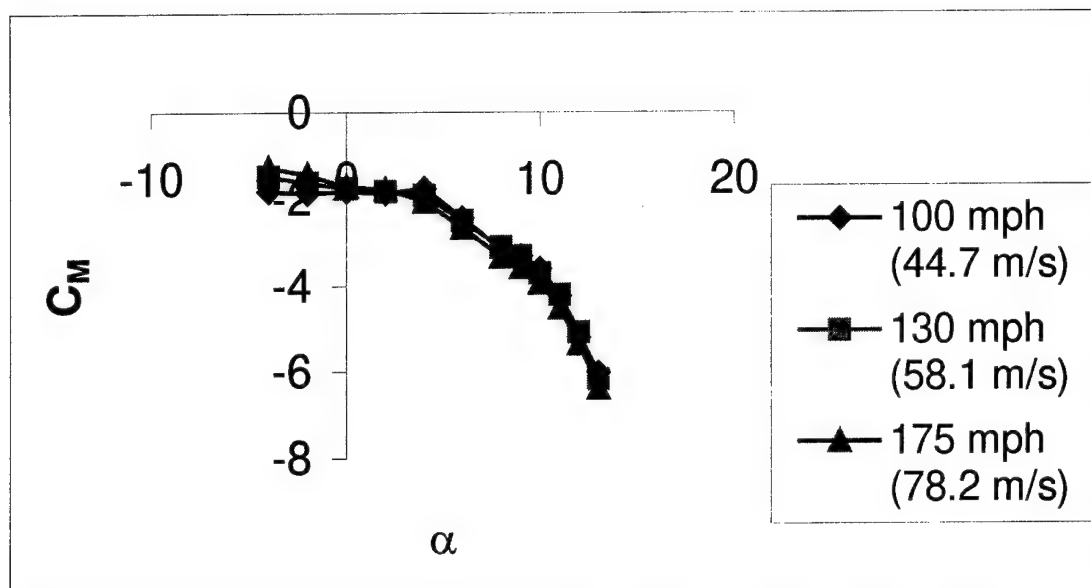


Figure 39: Pitch and Roll Relations of the 60° Swept Joined Wing with Straight Connectors, Positive Stagger

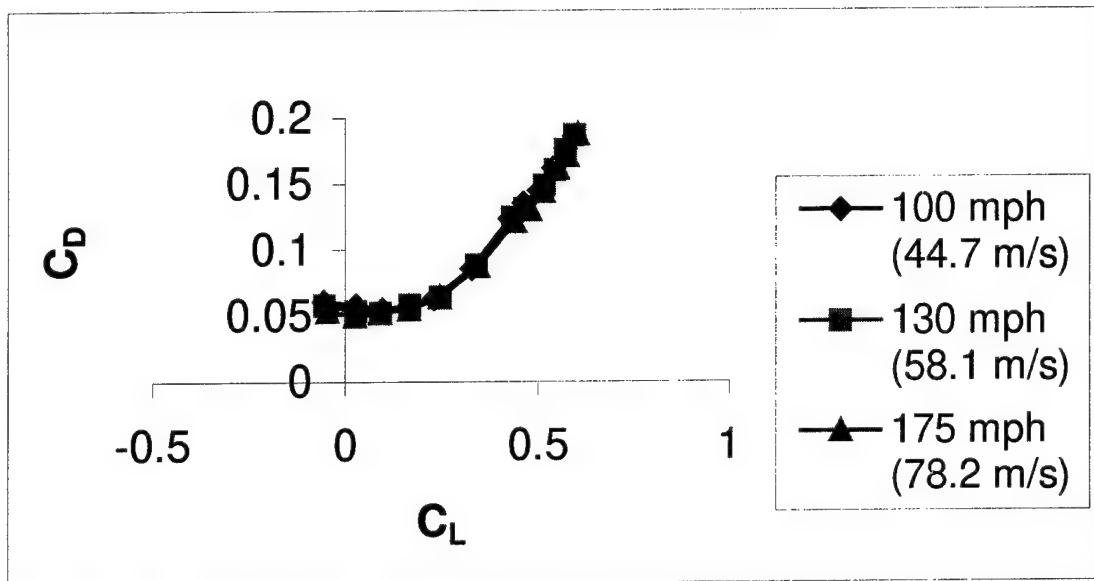
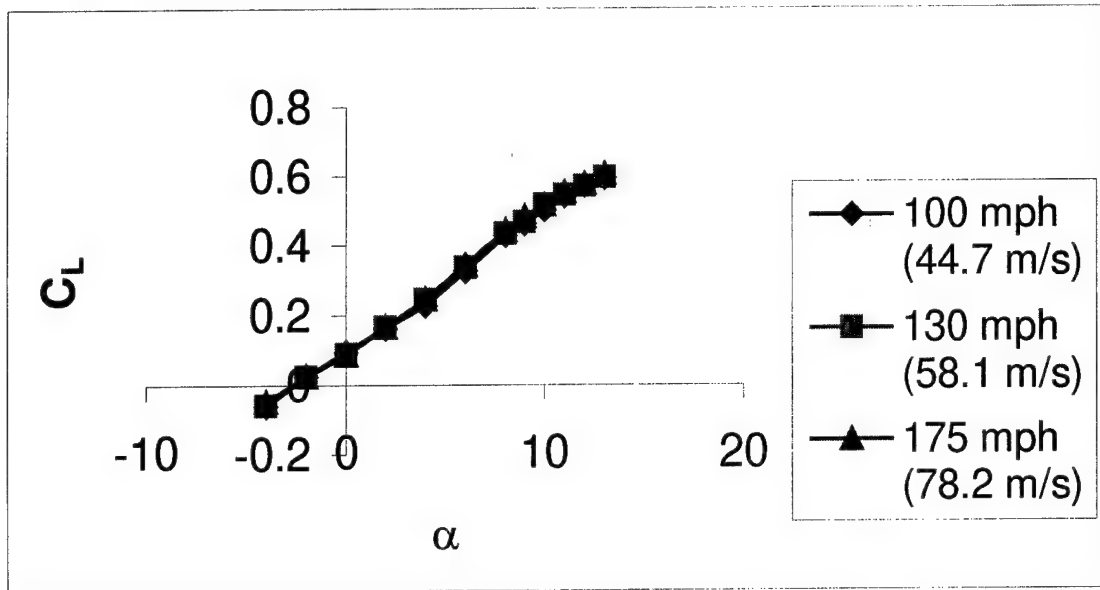


Figure 40: Lift and Drag Relations of the 60° Swept Biplane, Negative Stagger

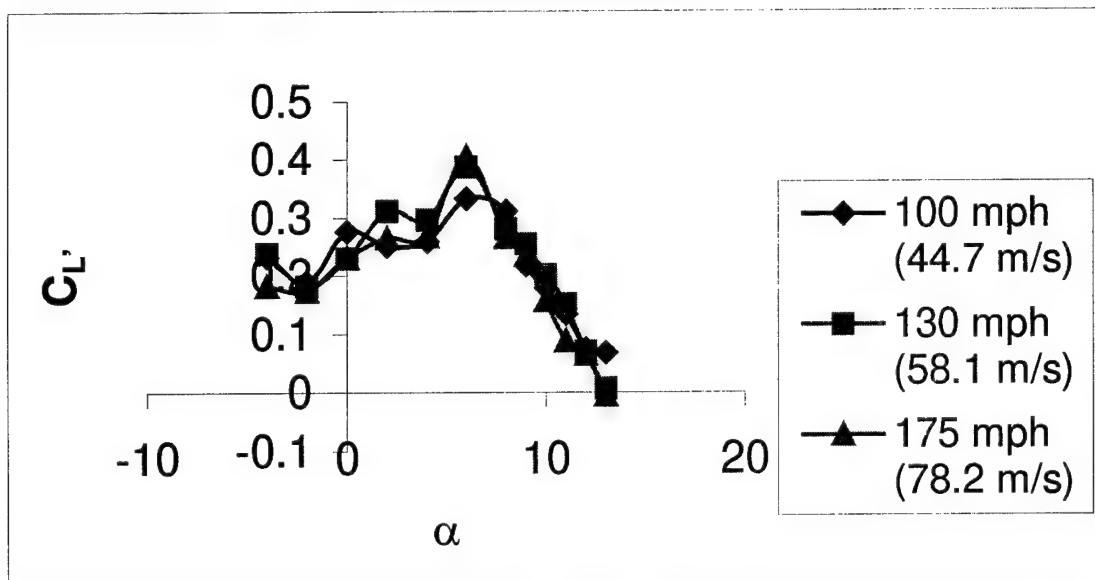
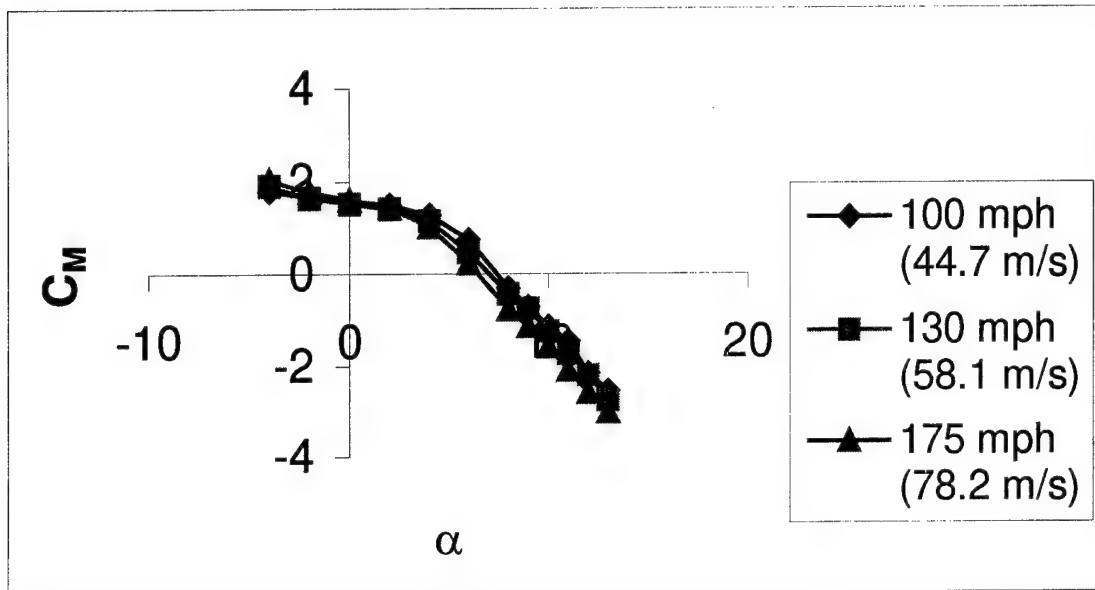


Figure 41: Pitch and Roll Relations of the 60° Swept Biplane, Negative Stagger

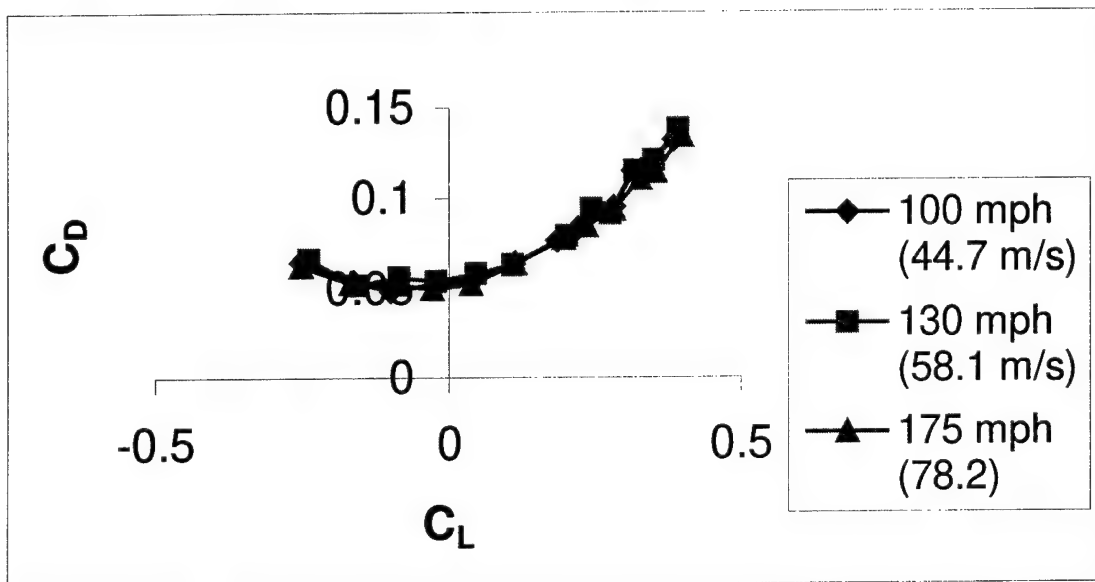
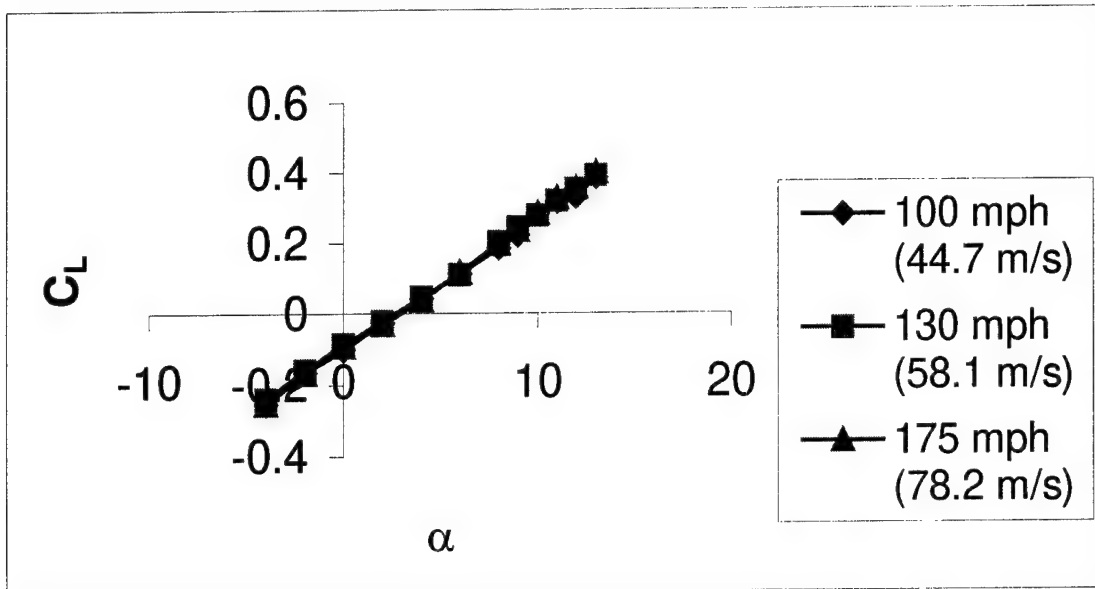


Figure 42: Lift and Drag Relations of the 60° Swept Biplane, Positive Stagger

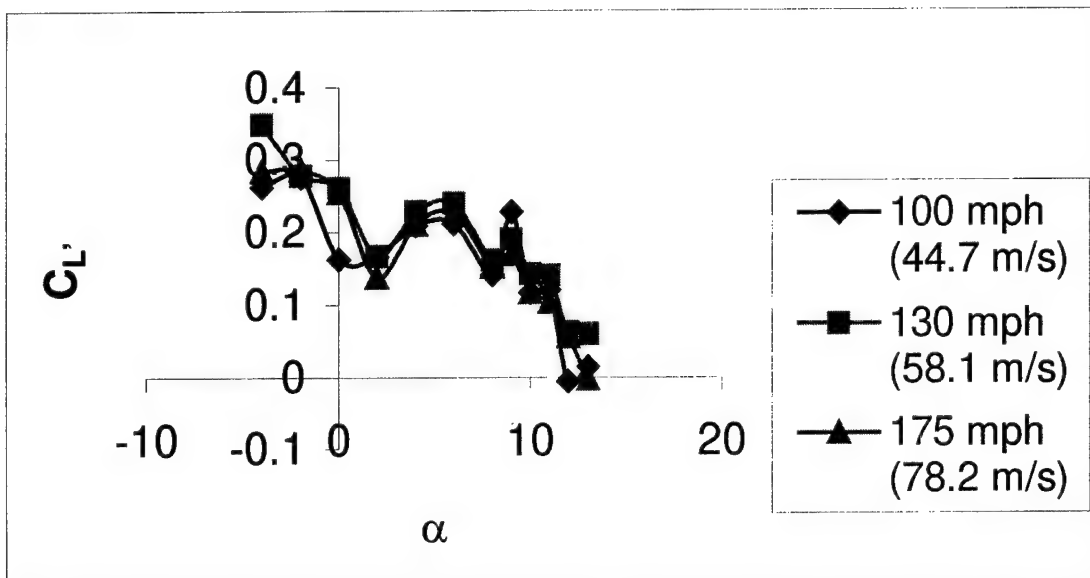
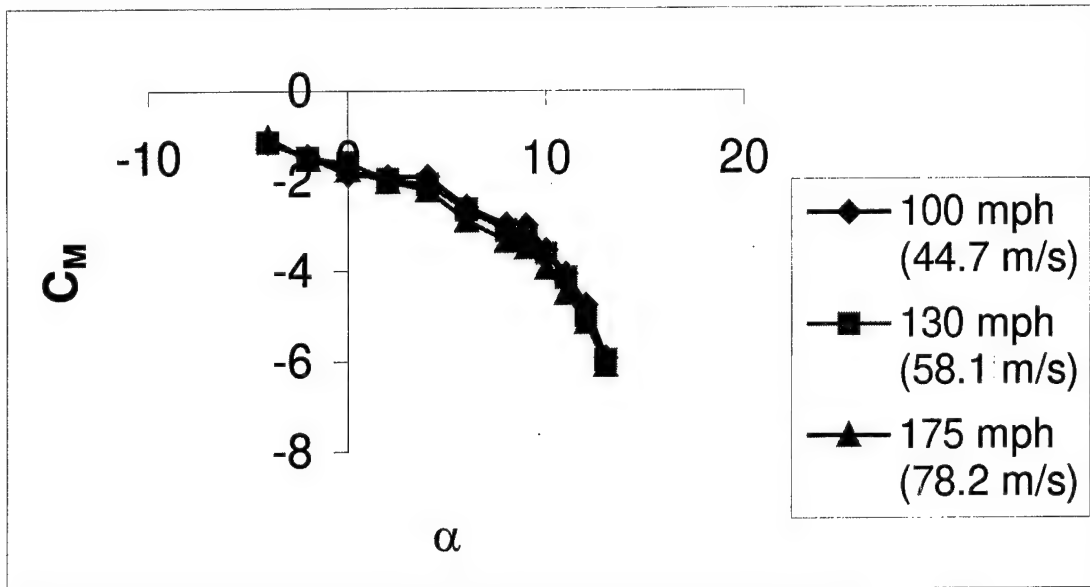


Figure 43: Pitch and Roll Relations of the 60° Swept Biplane, Positive Stagger

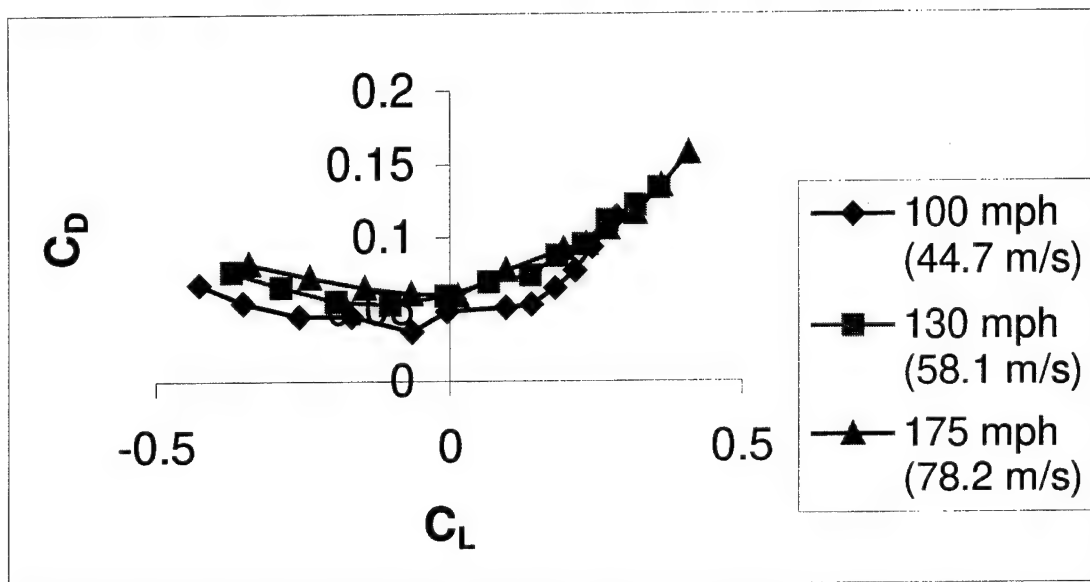
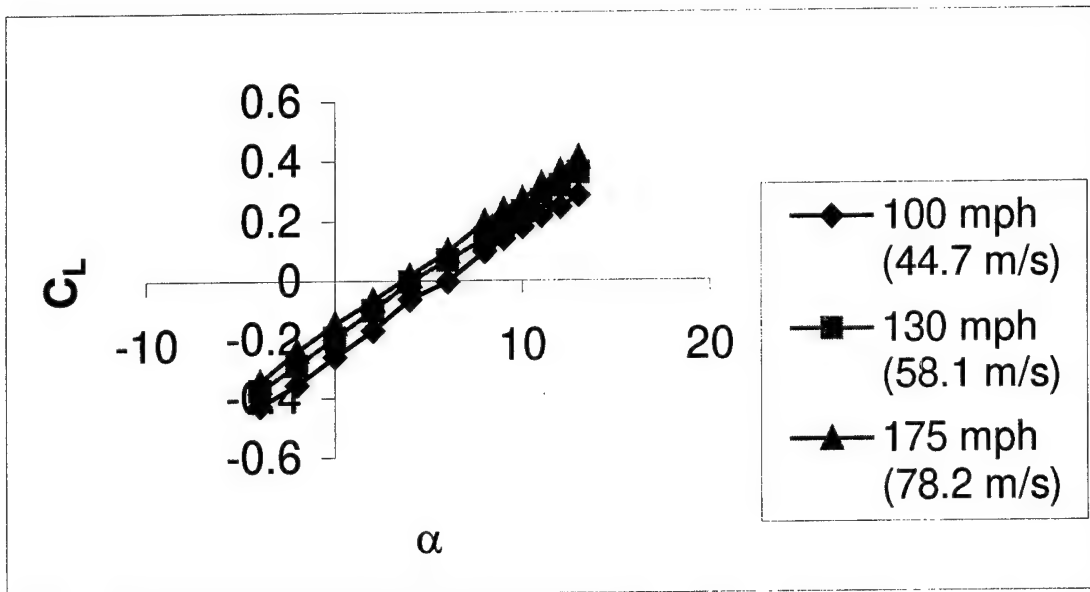


Figure 44: Lift and Drag Relations of the 60° Swept Single Wing Located Aft of the CG, Wings on Bottom

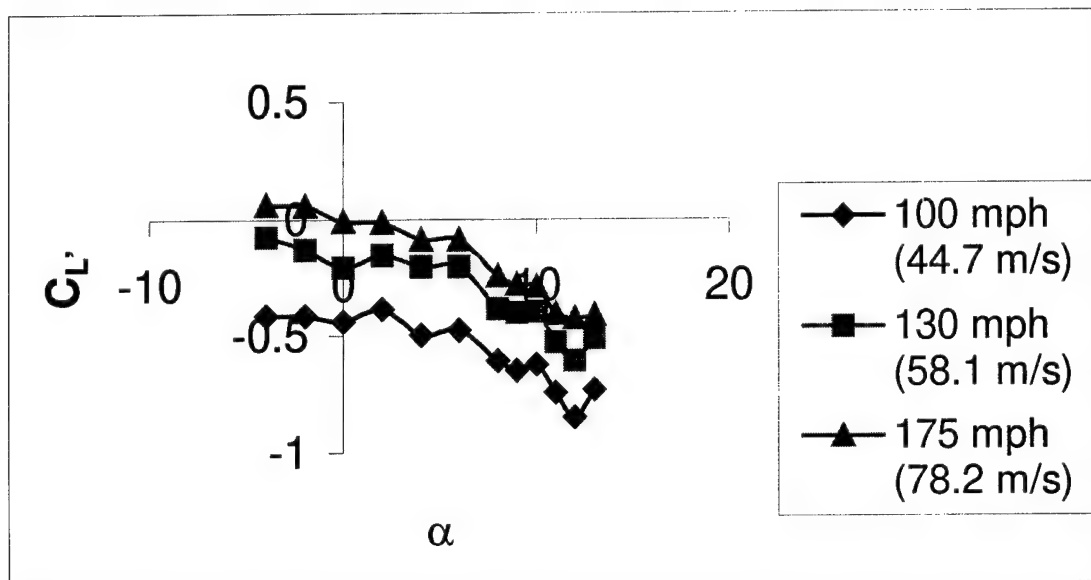
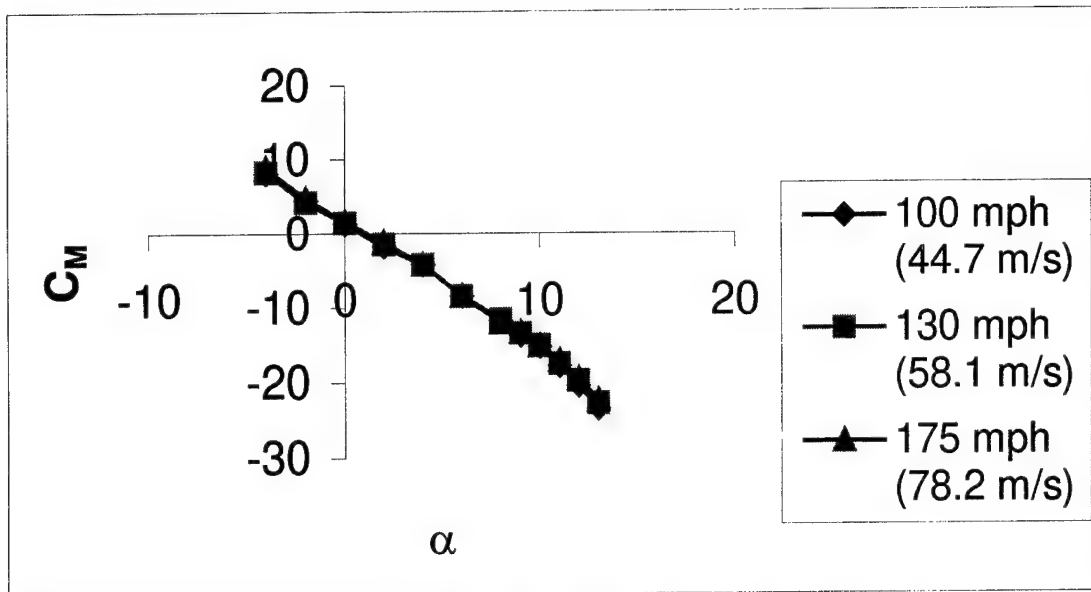


Figure 45: Pitch and Roll Relations of the 60° Swept Single Wing Located Aft of the CG, Wings on Bottom

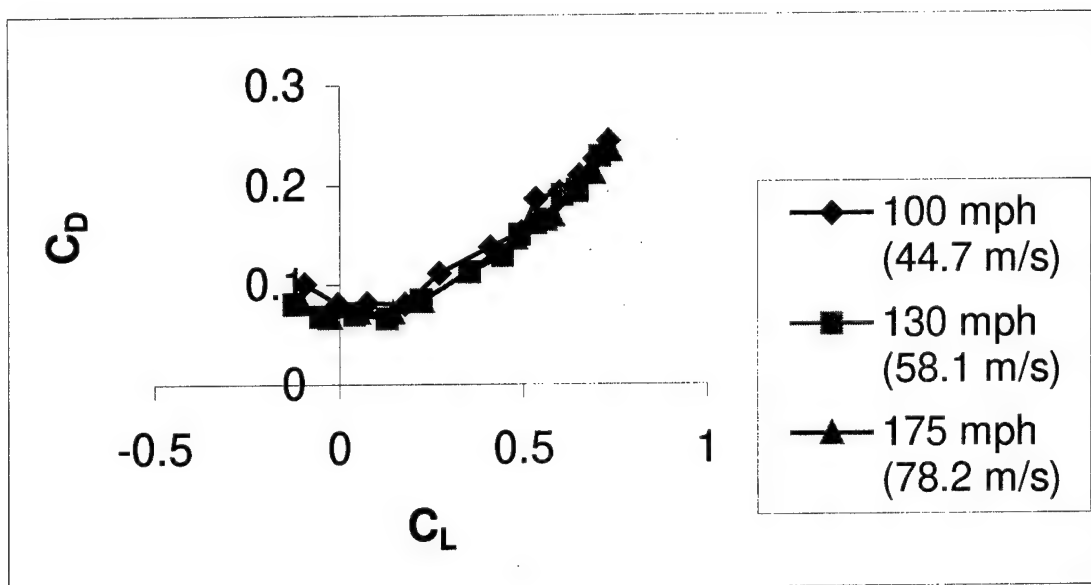
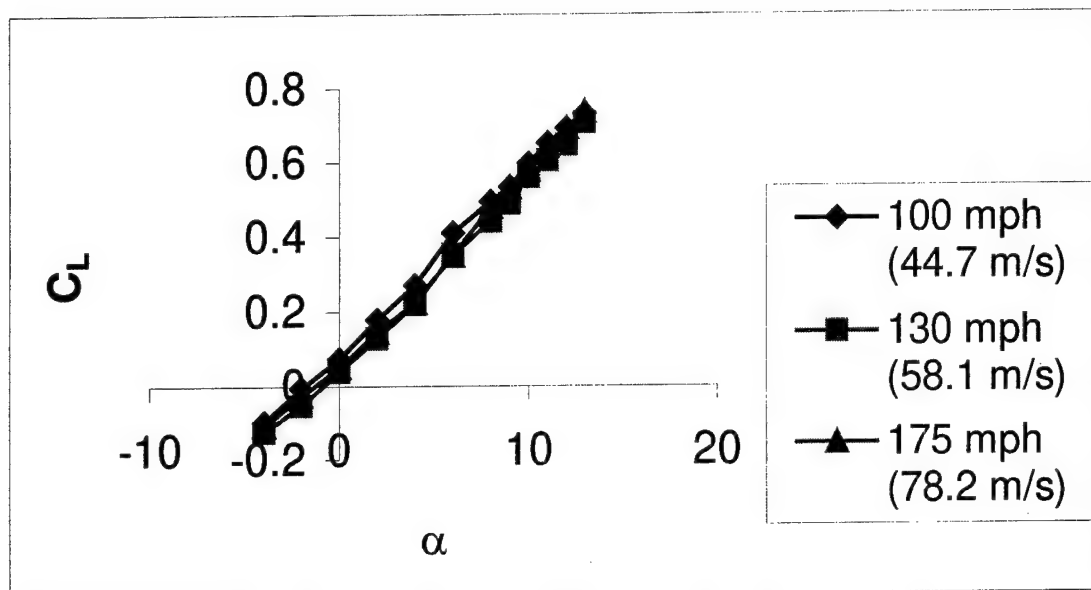


Figure 46: Lift and Drag Relations of the 60° Swept Single Wing Located Aft of the CG, Wings on Top

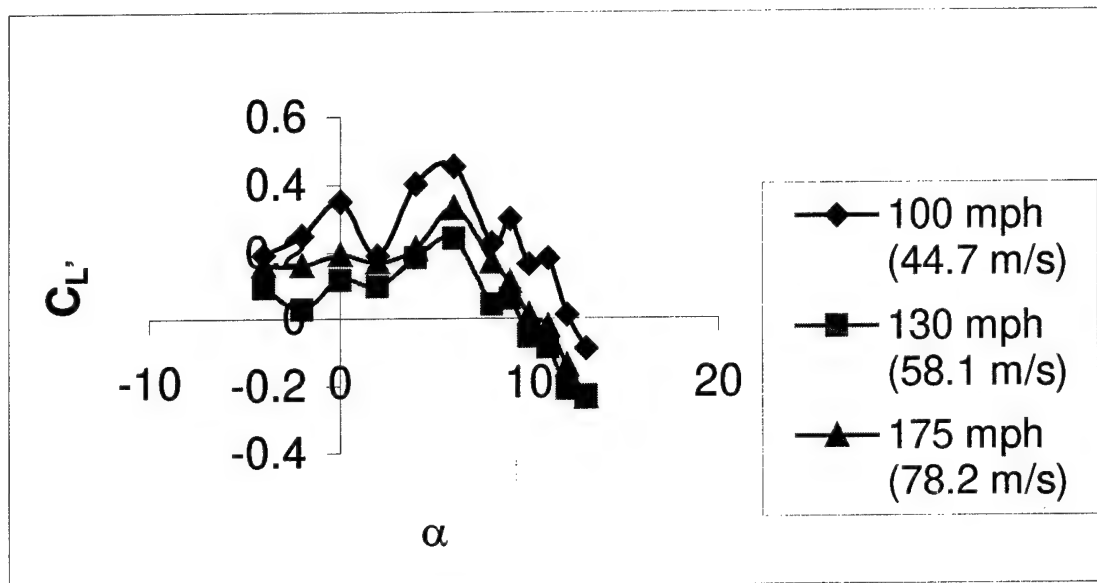
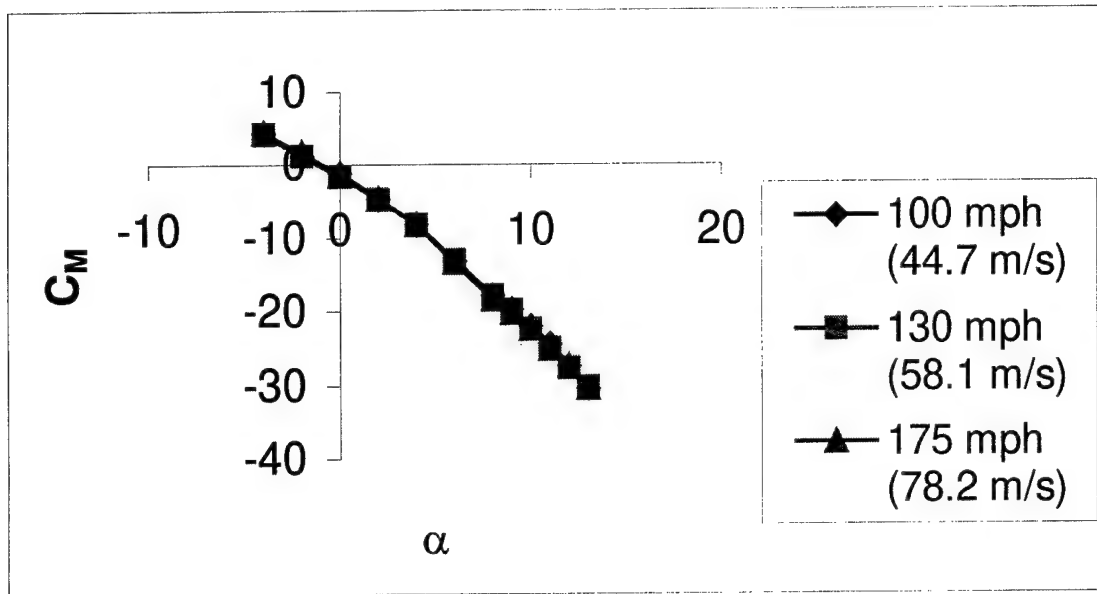


Figure 47: Pitch and Roll Relations of the 60° Swept Single Wing Located Aft of the CG, Wings on Top

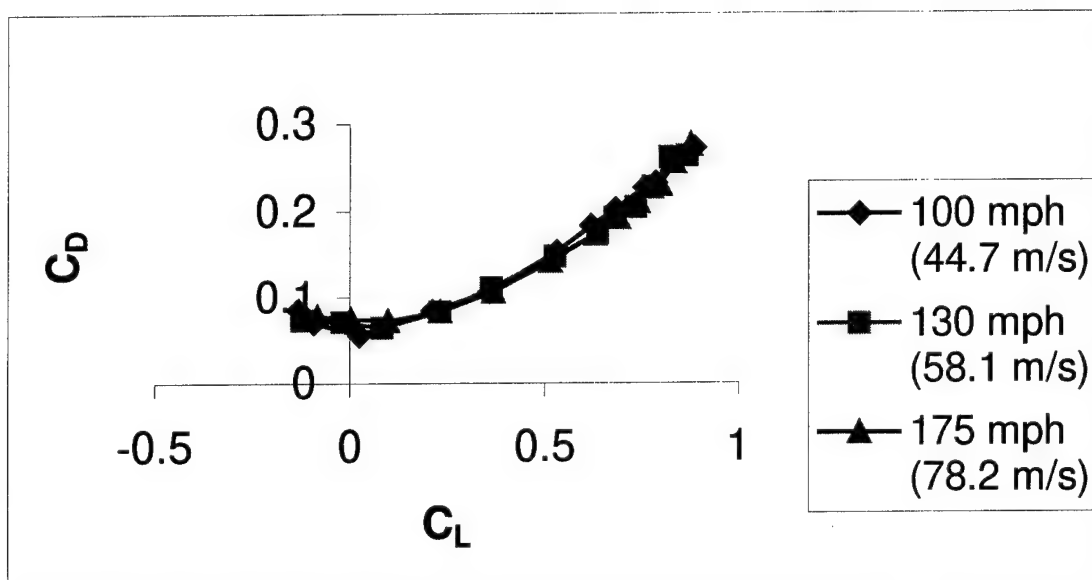
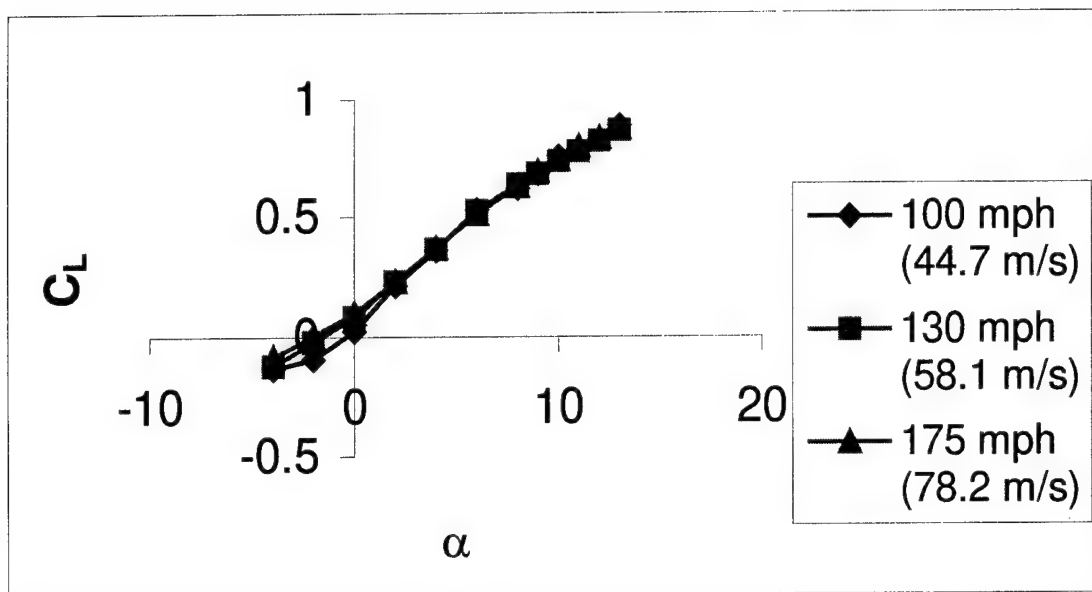


Figure 48: Lift and Drag Relations of the 60° Swept Single Wing Located Forward of the CG, Wings on Bottom

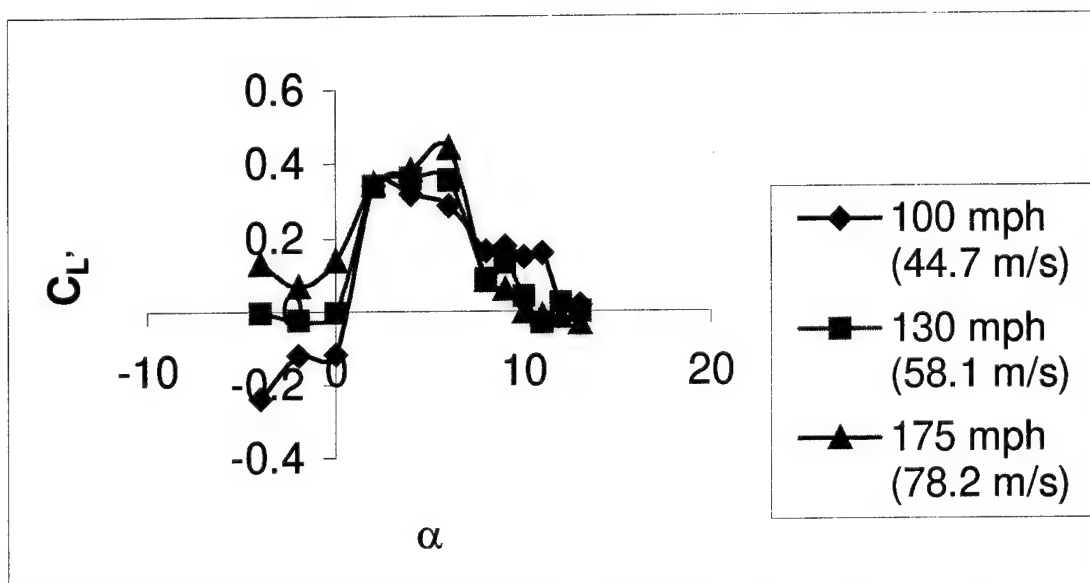
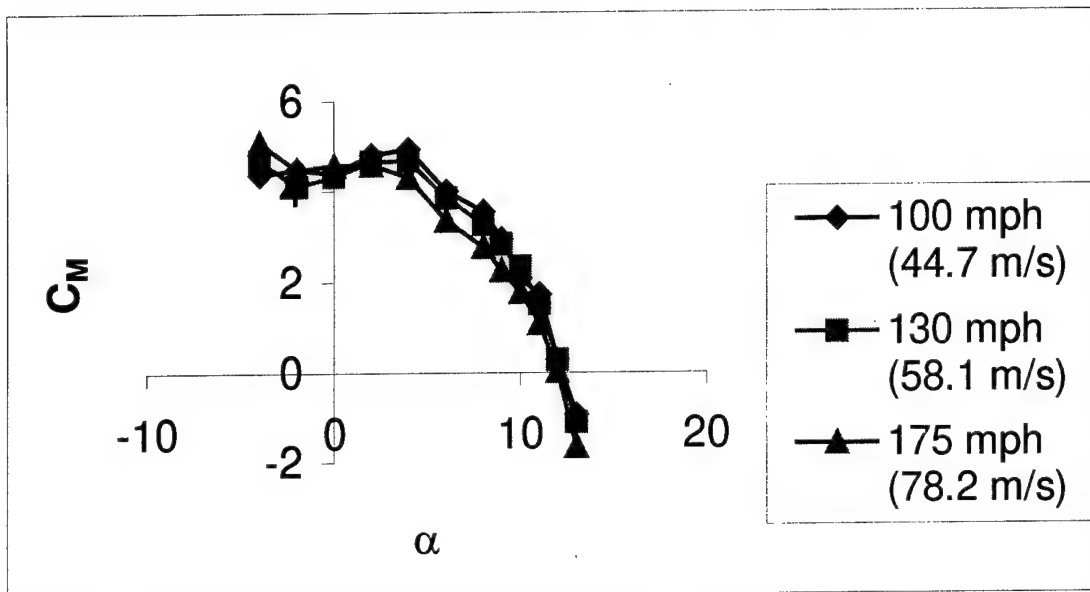


Figure 49: Pitch and Roll Relations of the 60° Swept Single Wing Located Forward of the CG, Wings on Bottom

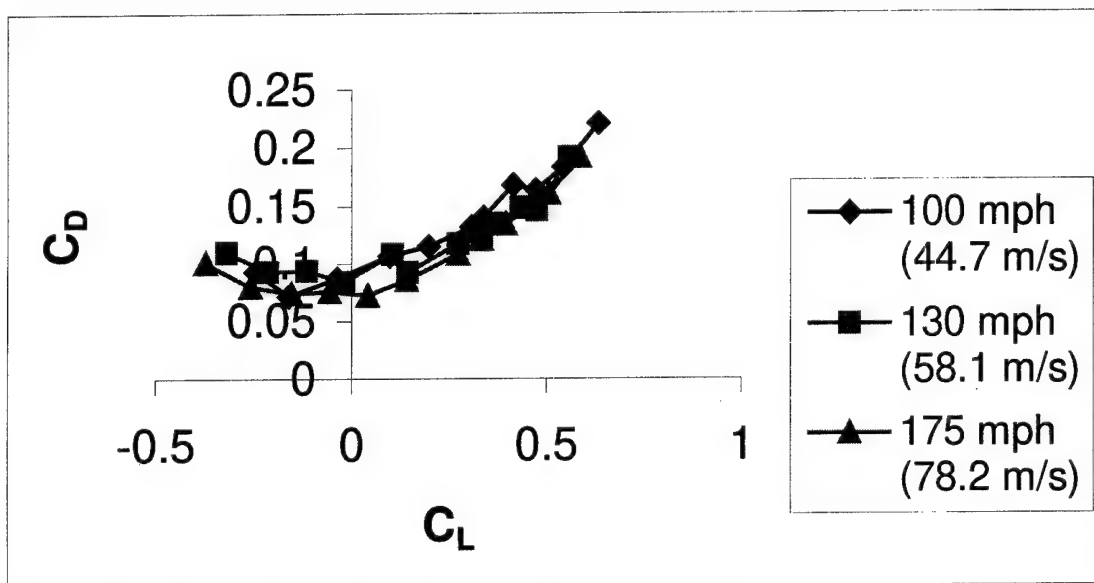
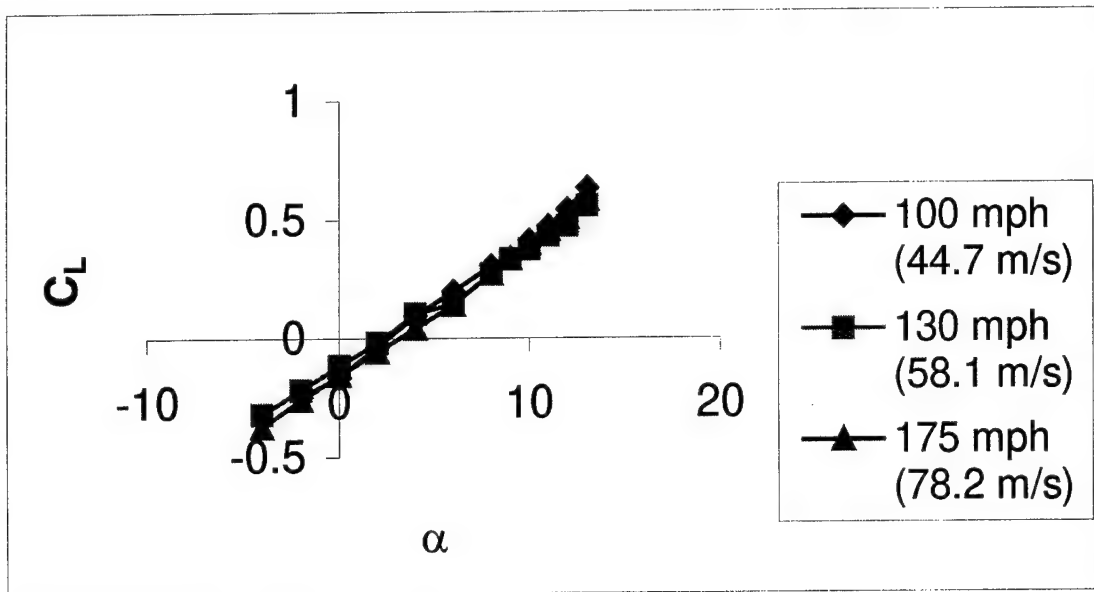


Figure 50: Lift and Drag Relations of the 60° Swept Single Wing Located Forward of the CG, Wings on Top

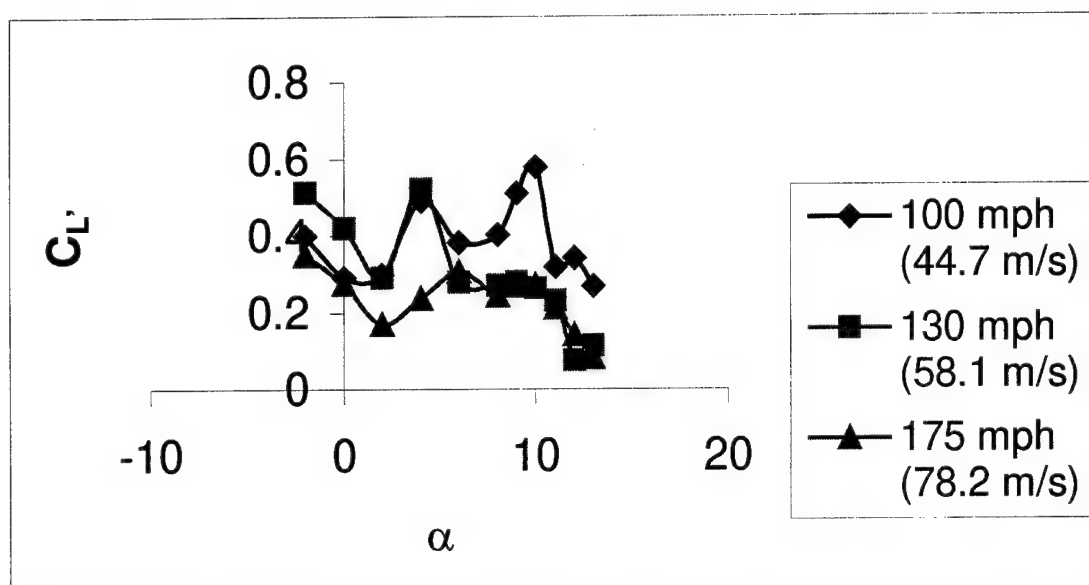
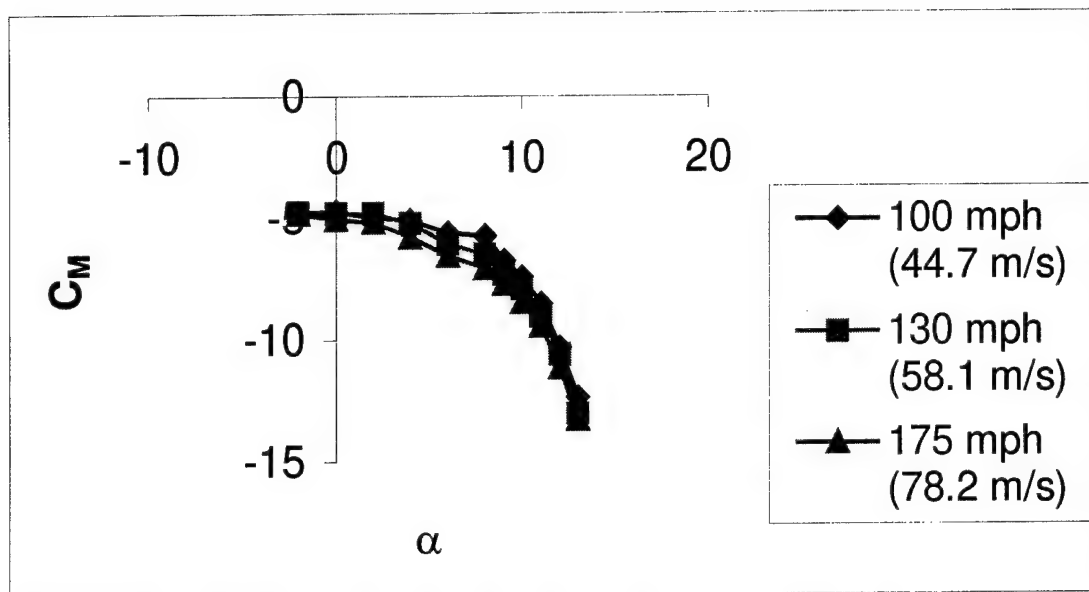


Figure 51: Pitch and Roll Relations of the 60° Swept Single Wing Located Forward of the CG, Wings on Top

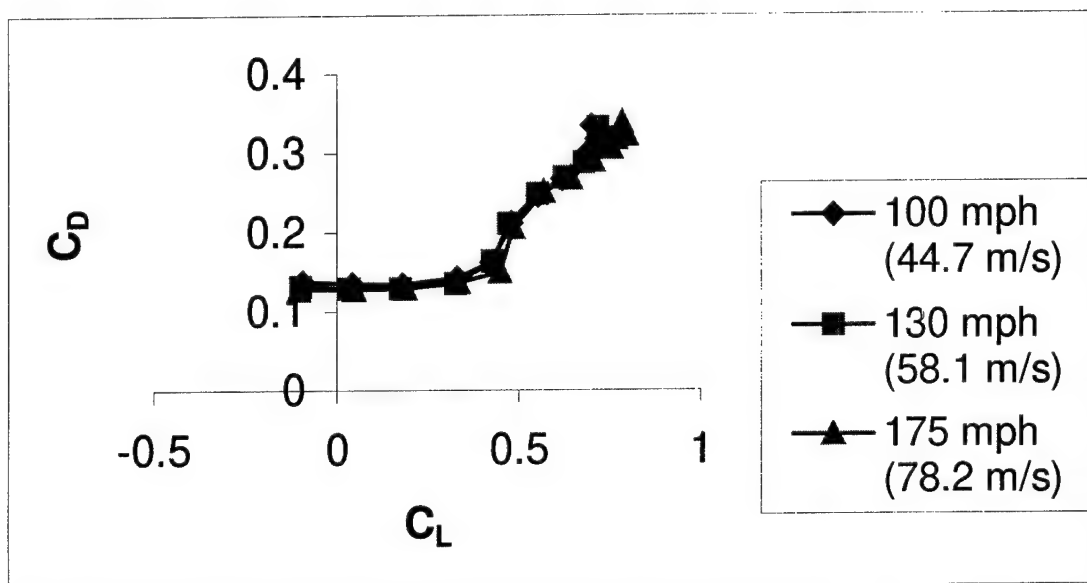
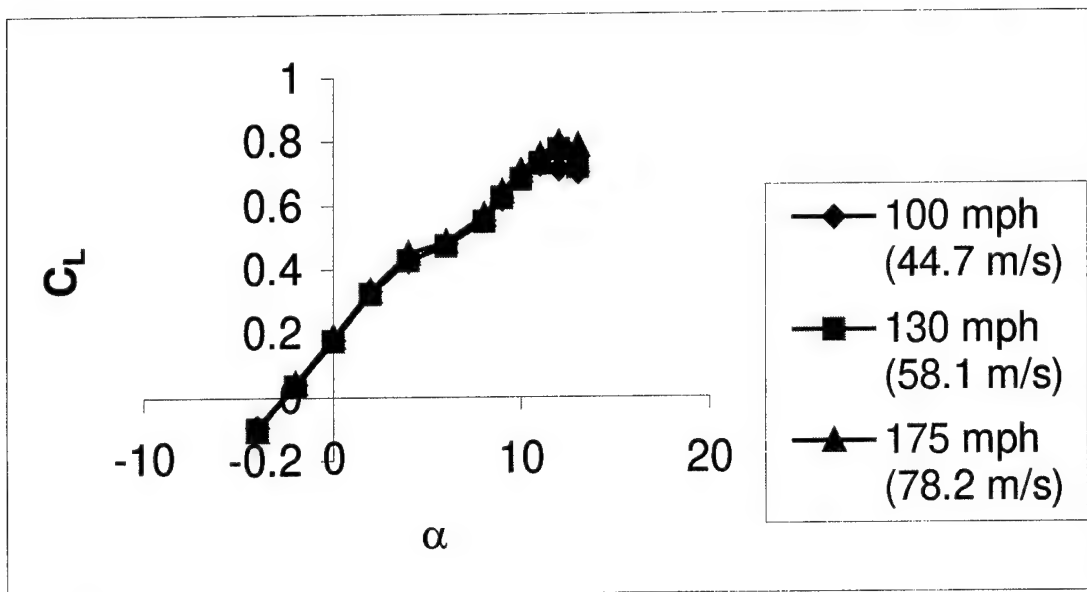


Figure 52: Lift and Drag Relations of the 30° Swept Jointed Wing with Curved Connectors, Negative Stagger

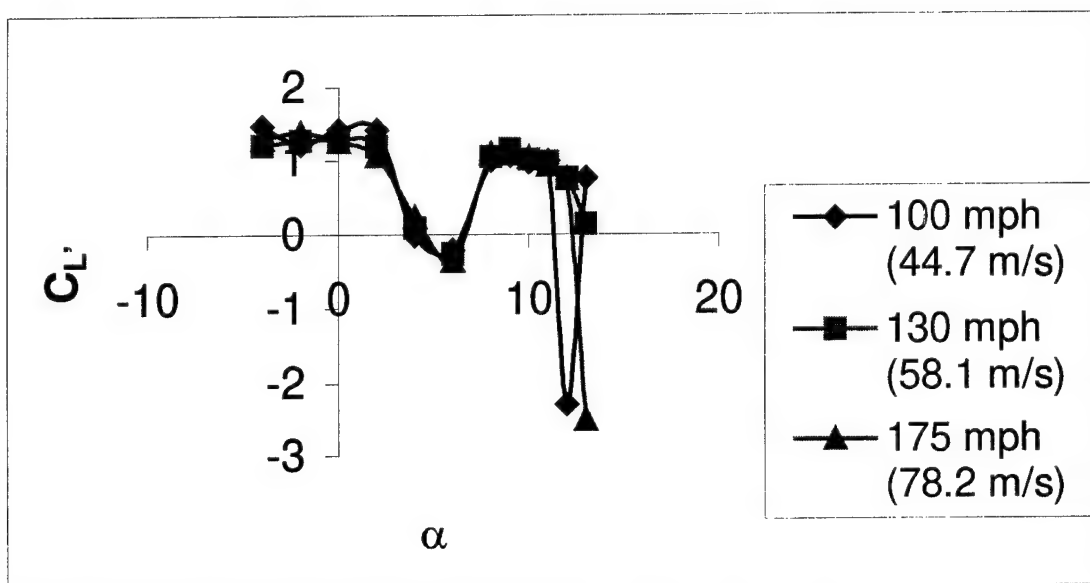
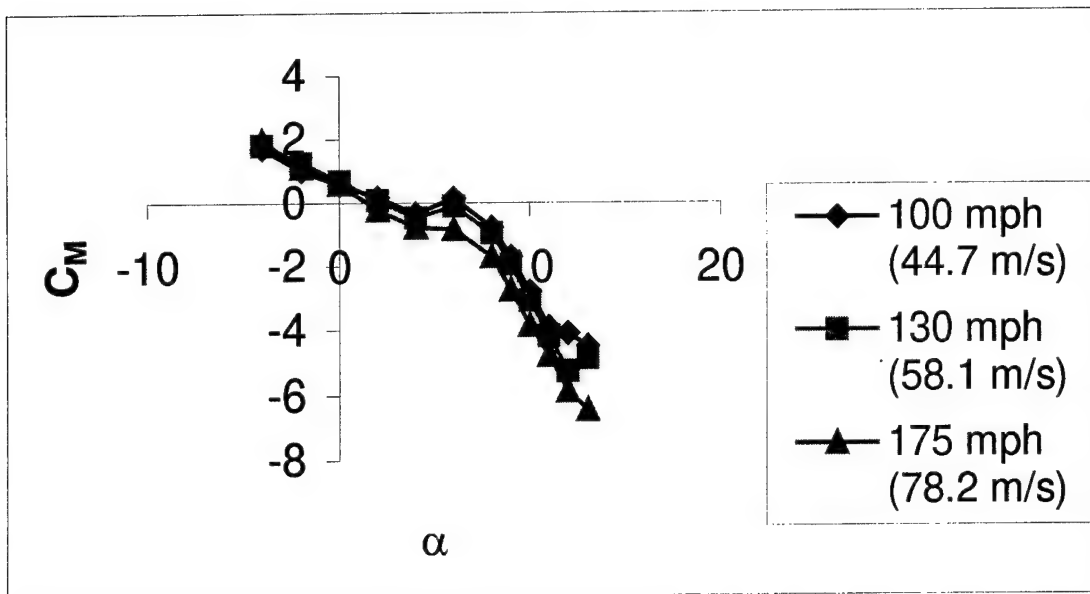


Figure 53: Pitch and Roll Relations of the 30° Swept Joined Wing with Curved Connectors, Negative Stagger

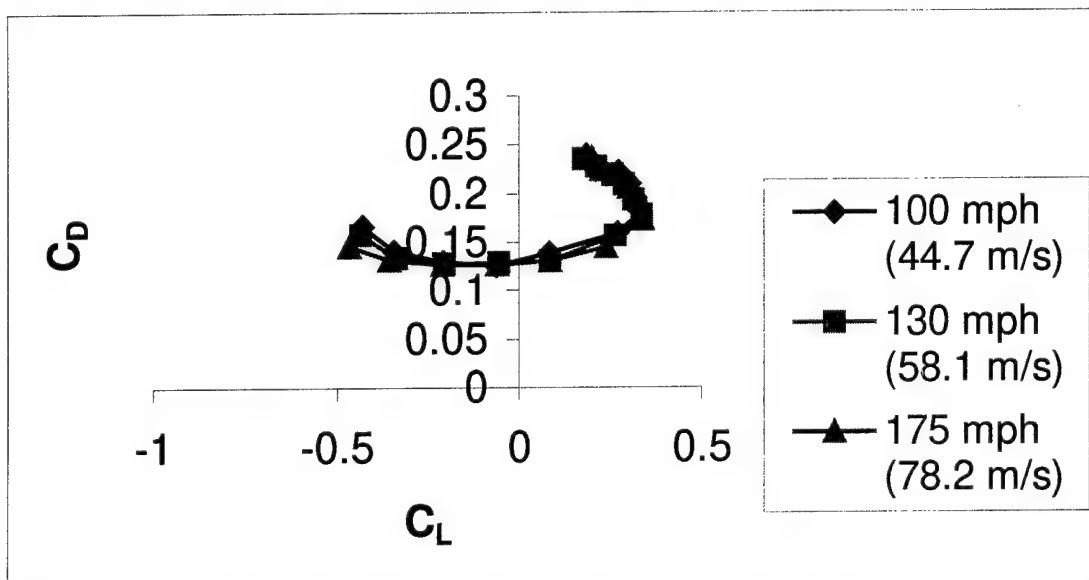
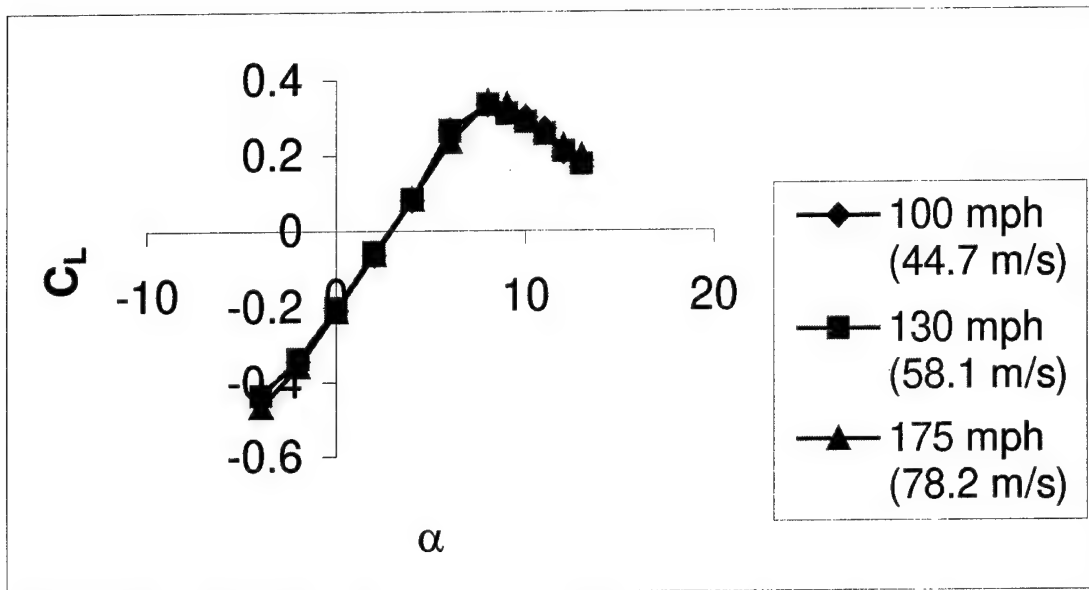


Figure 54: Lift and Drag Relations of the 30° Swept Jointed Wing with Curved Connectors, Positive Stagger

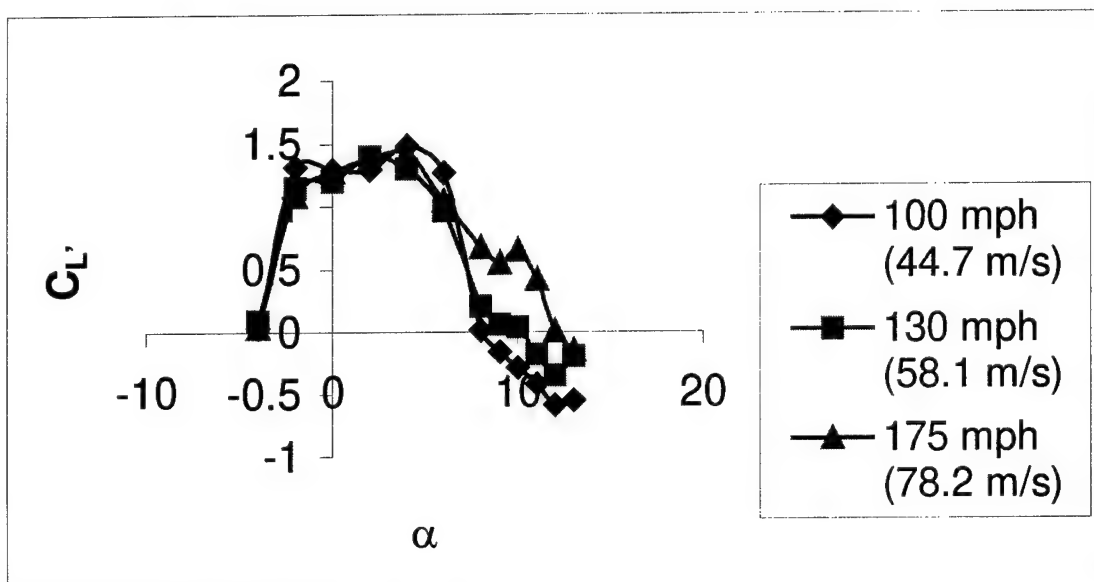
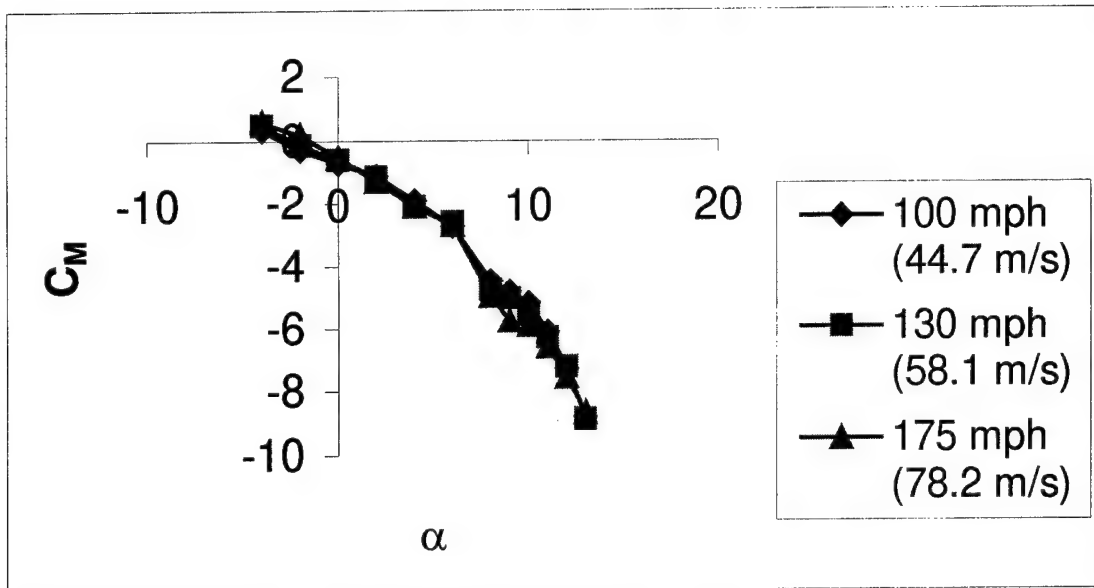


Figure 55: Pitch and Roll Relations of the 30° Swept Jointed Wing with Curved Connectors, Positive Stagger

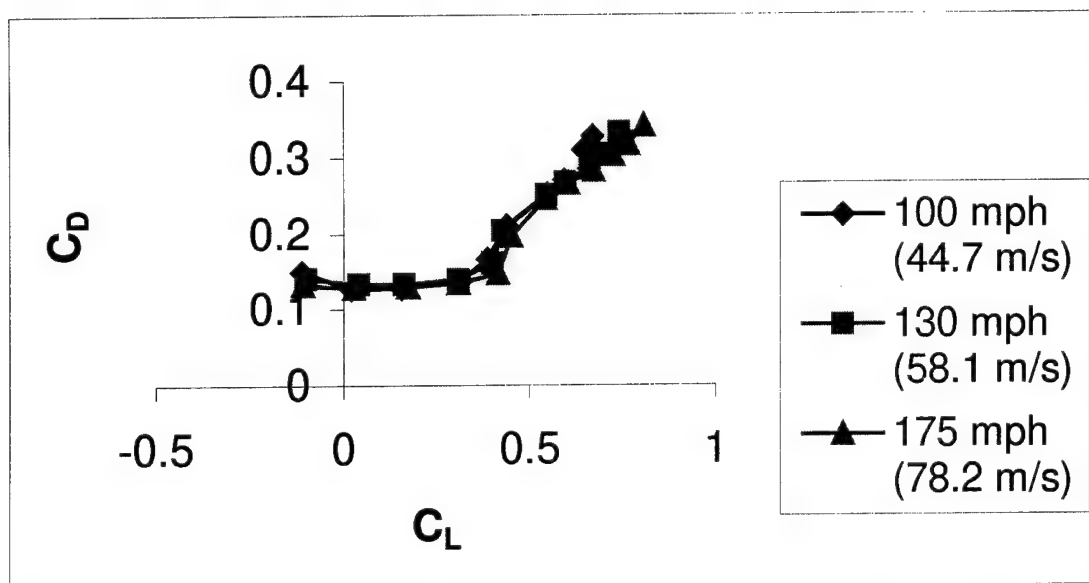
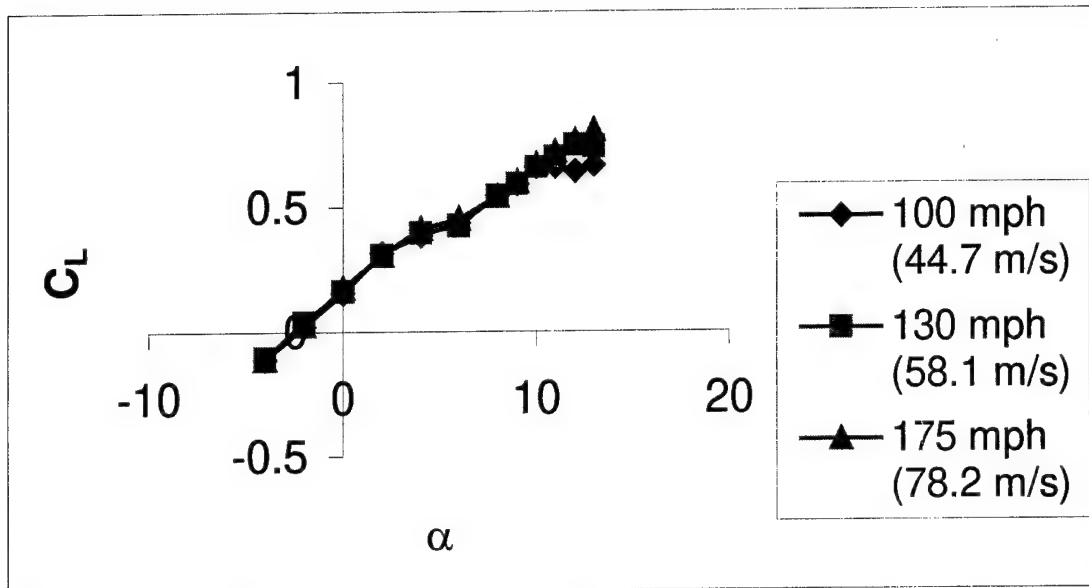


Figure 56: Lift and Drag Relations of the 30° Swept Joined Wing with Straight Connectors, Negative Stagger

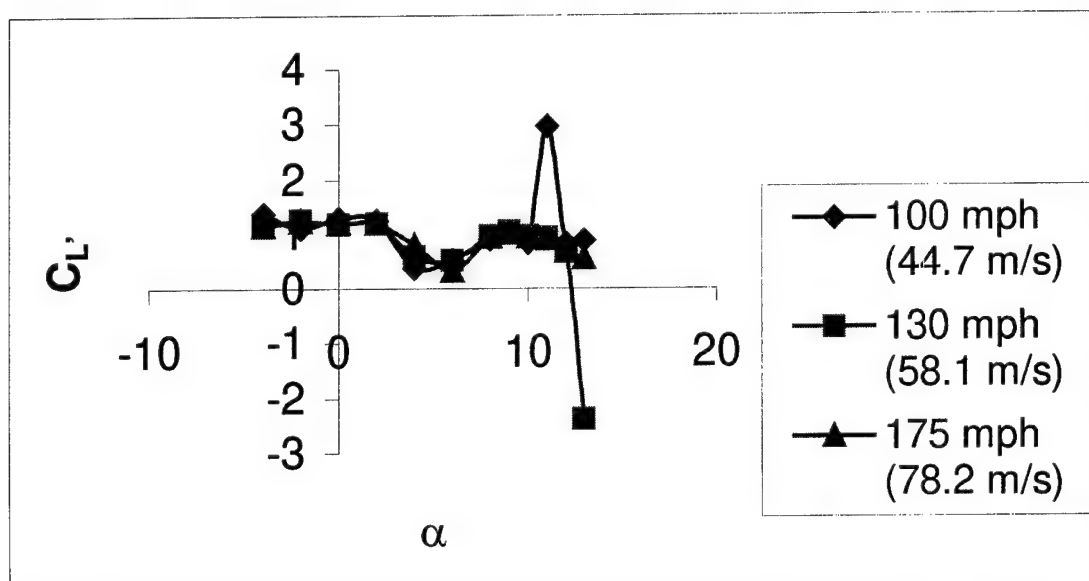
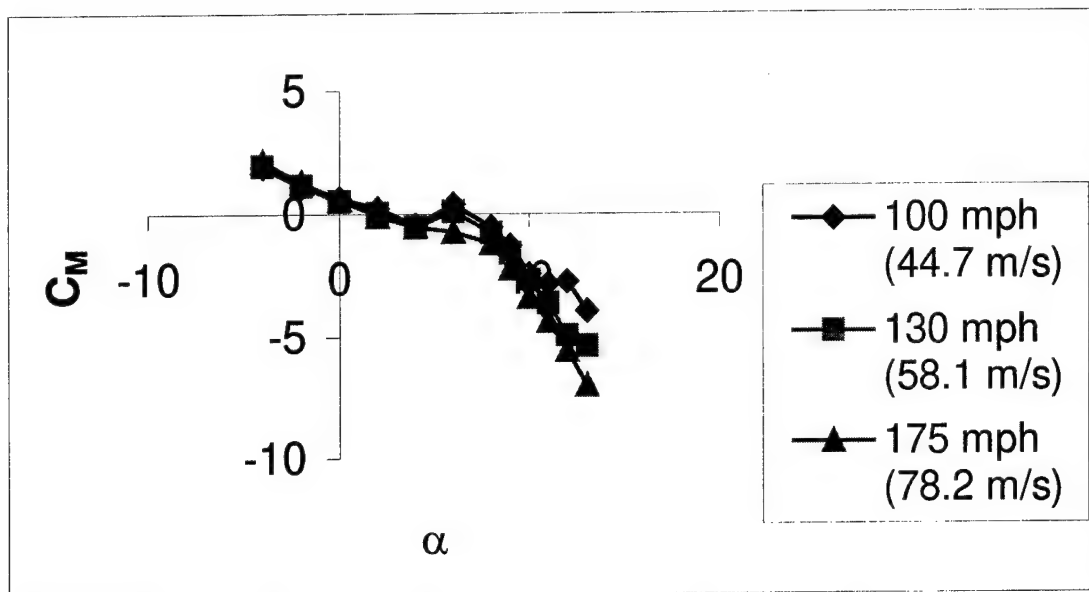


Figure 57: Pitch and Roll Relations of the 30° Swept Joined Wing with Straight Connectors, Negative Stagger

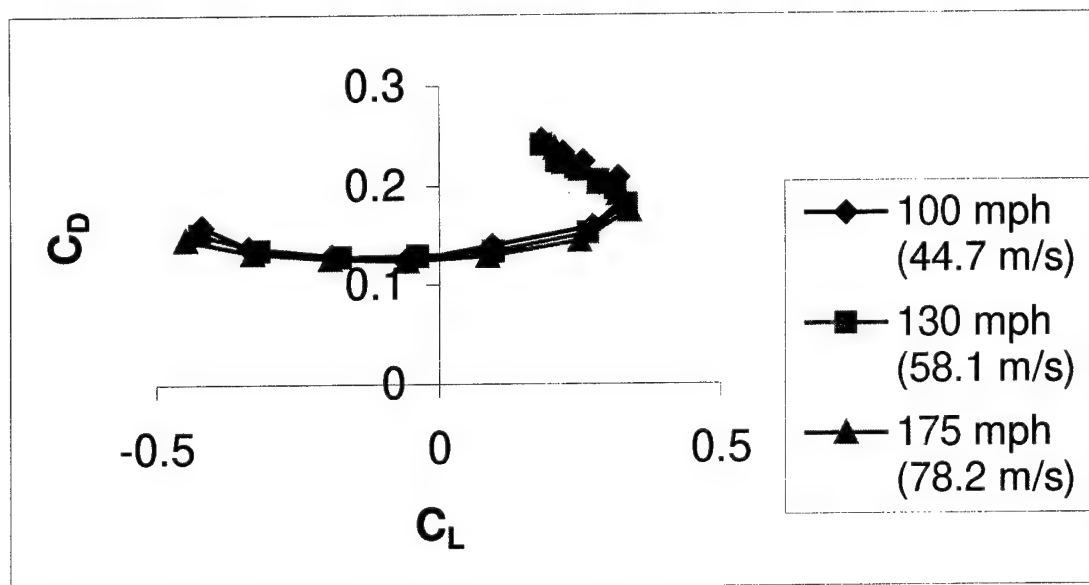
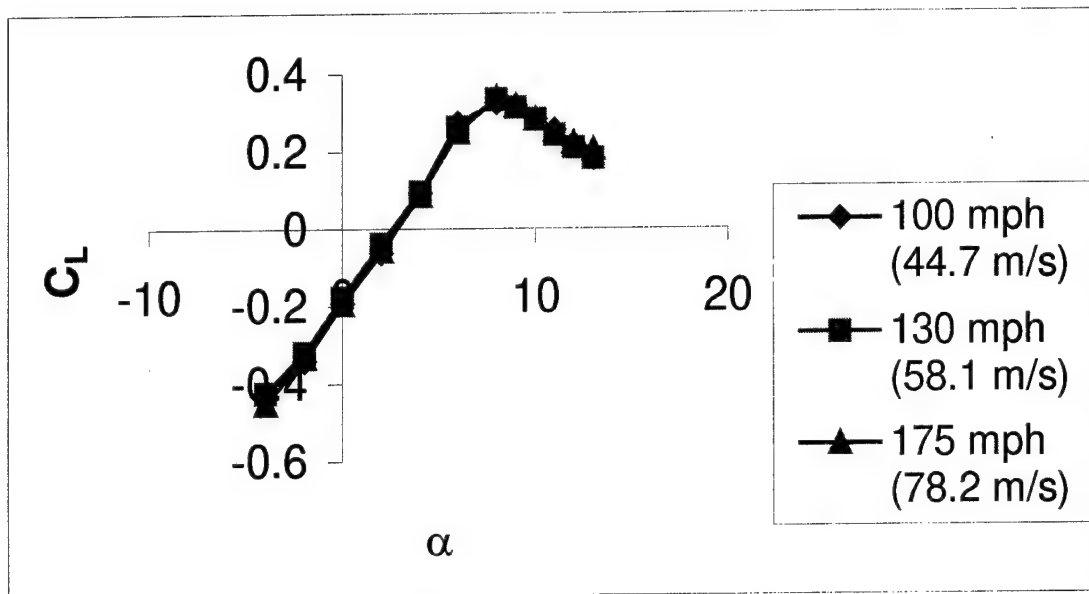


Figure 58: Lift and Drag Relations of the 30° Swept Jointed Wing with Straight Connectors, Positive Stagger

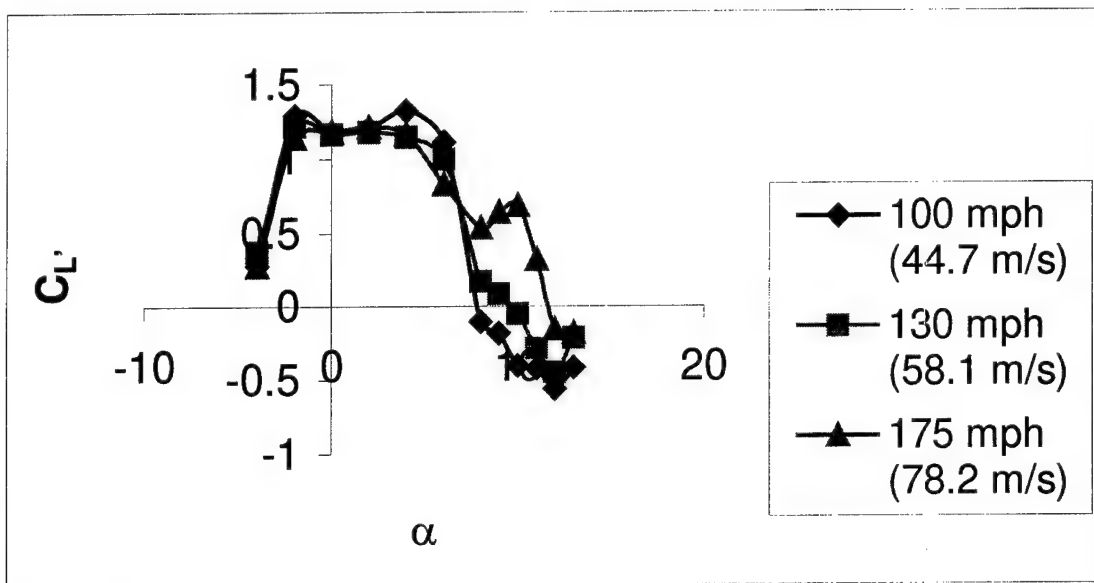
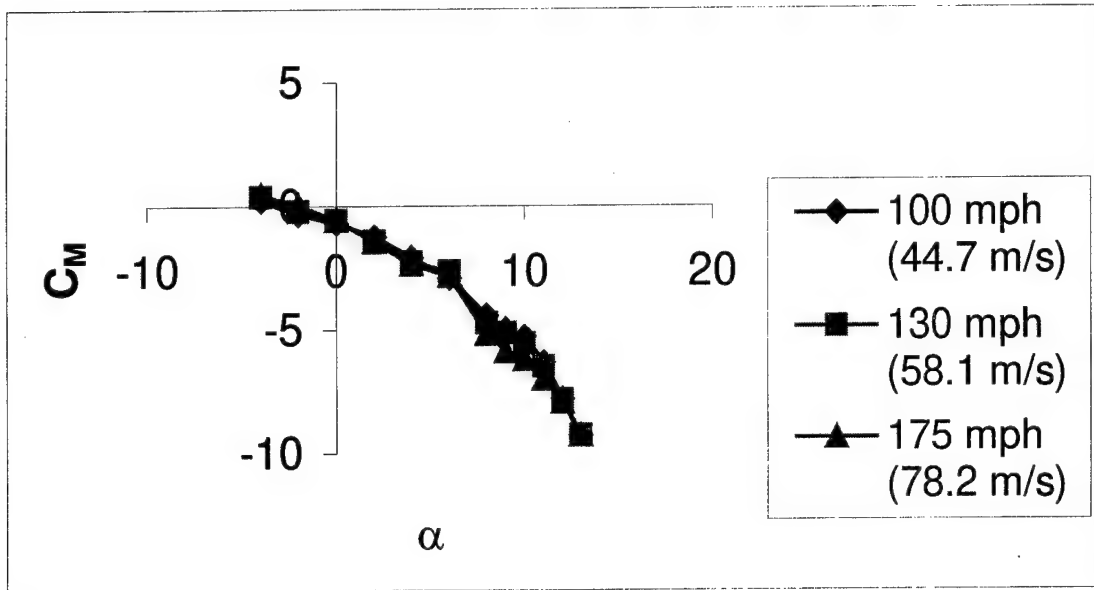


Figure 59: Pitch and Roll Relations of the 30° Swept Joined Wing with Straight Connectors, Positive Stagger

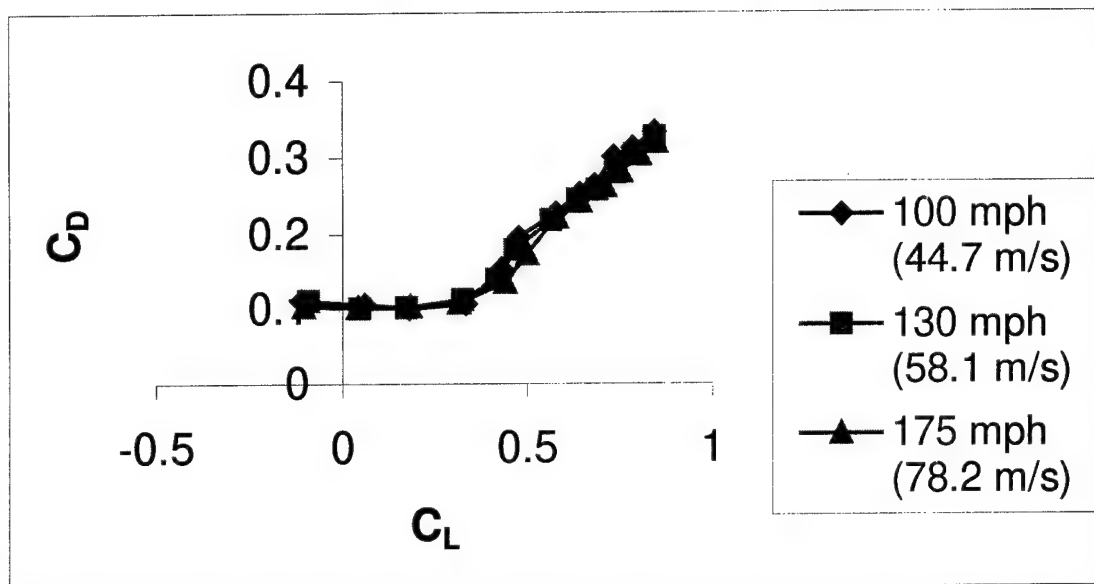
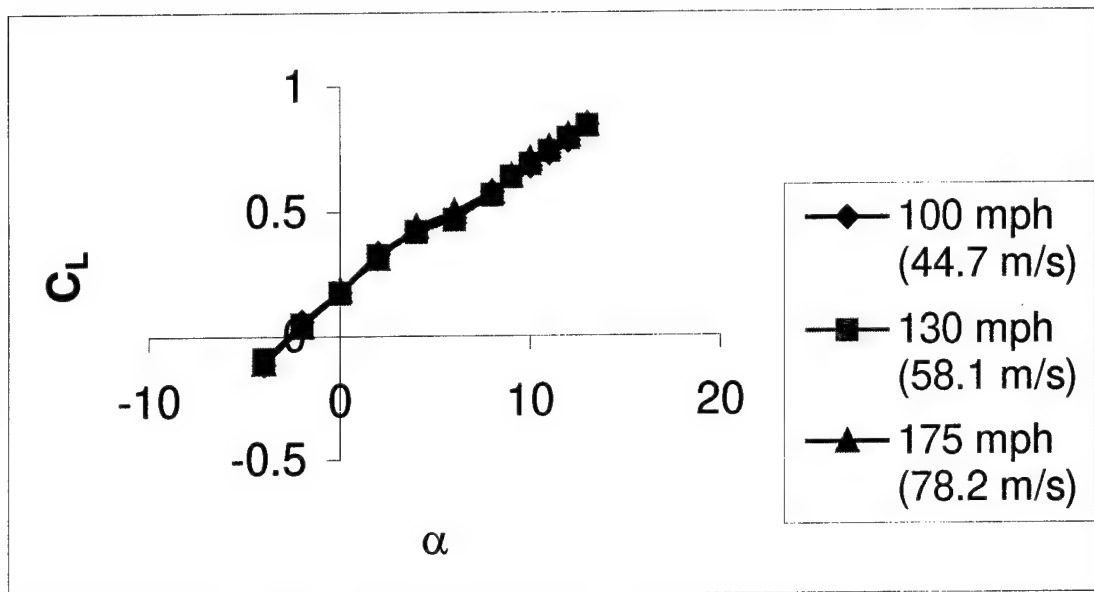


Figure 60: Lift and Drag Relations of the 30° Swept Biplane, Negative Stagger

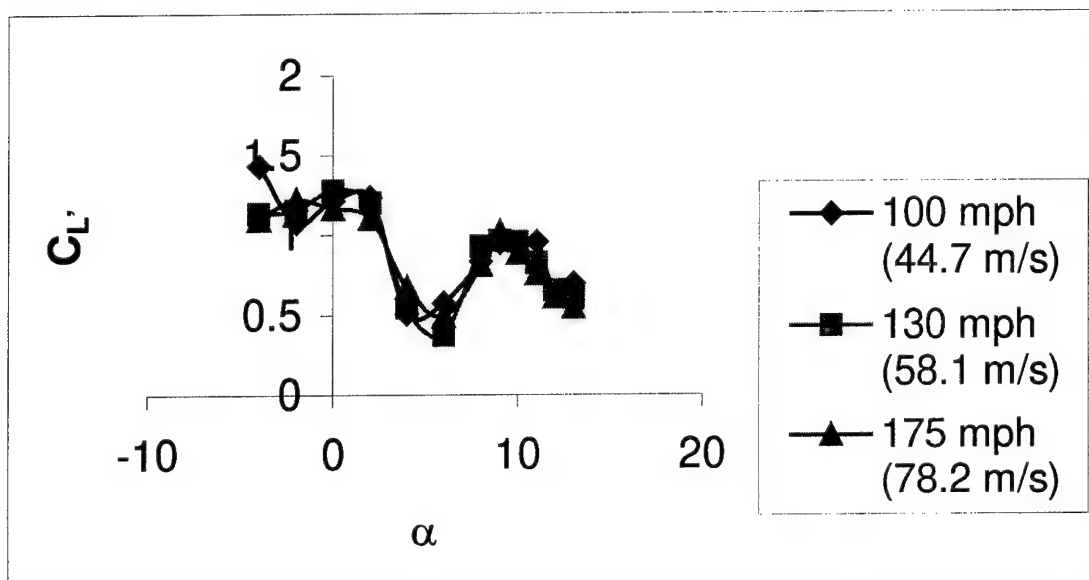
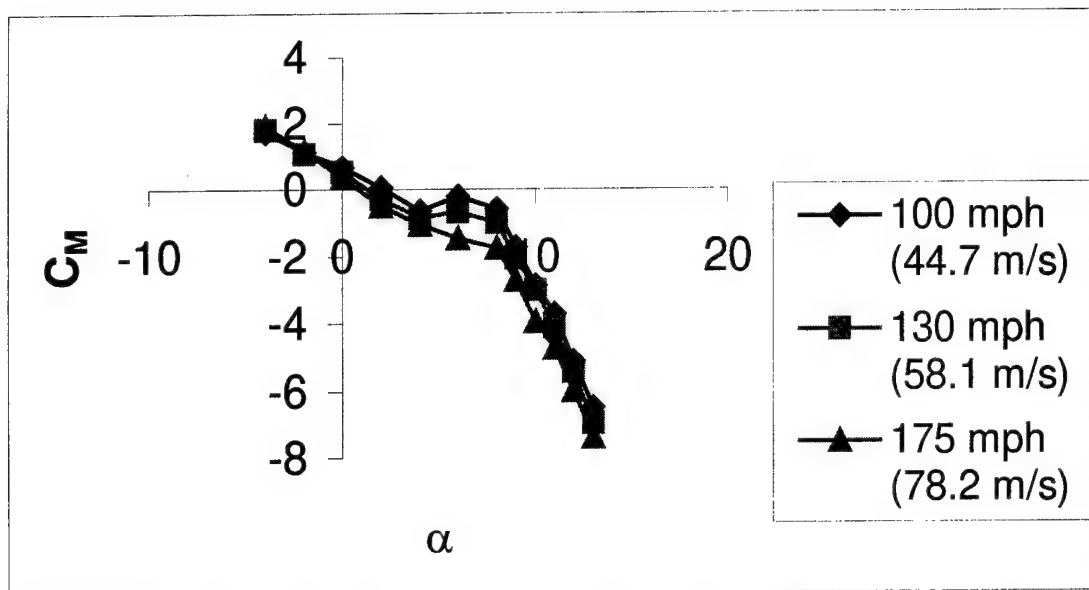


Figure 61: Pitch and Roll Relations of the 30° Swept Biplane, Negative Stagger

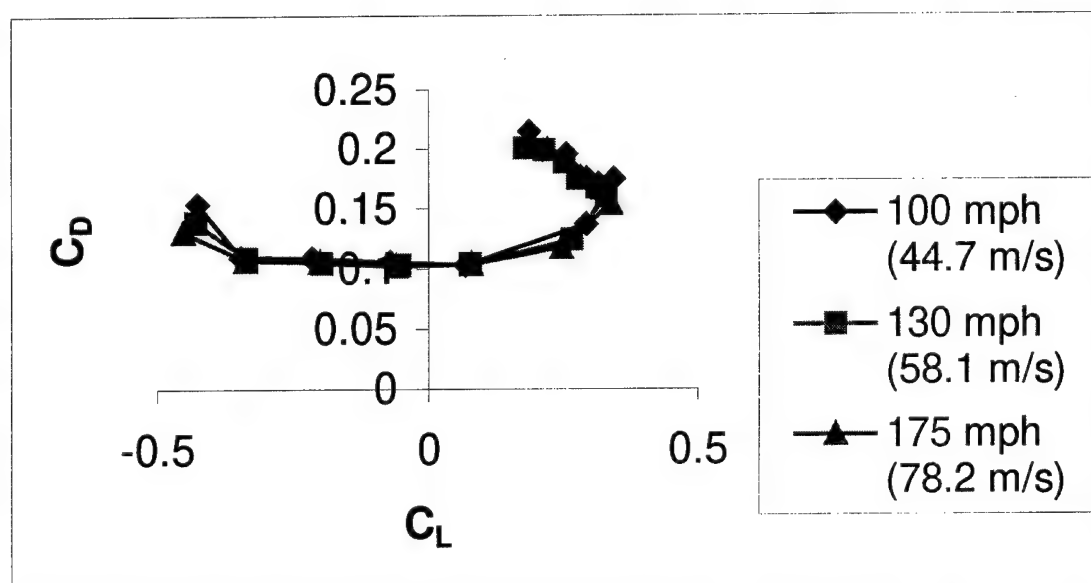
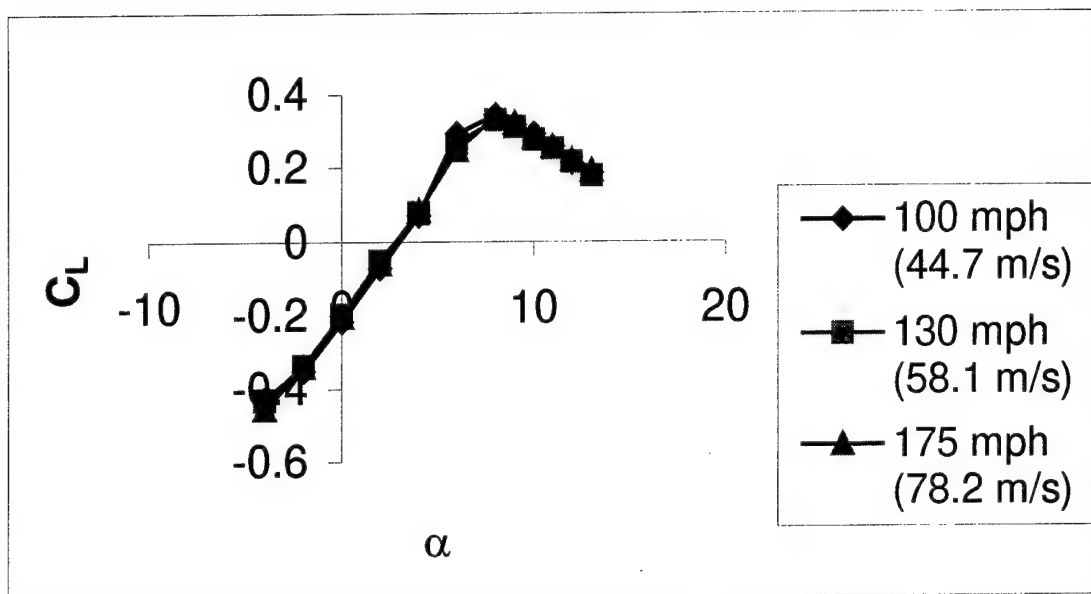


Figure 62: Lift and Drag Relations of the 30° Swept Biplane, Positive Stagger

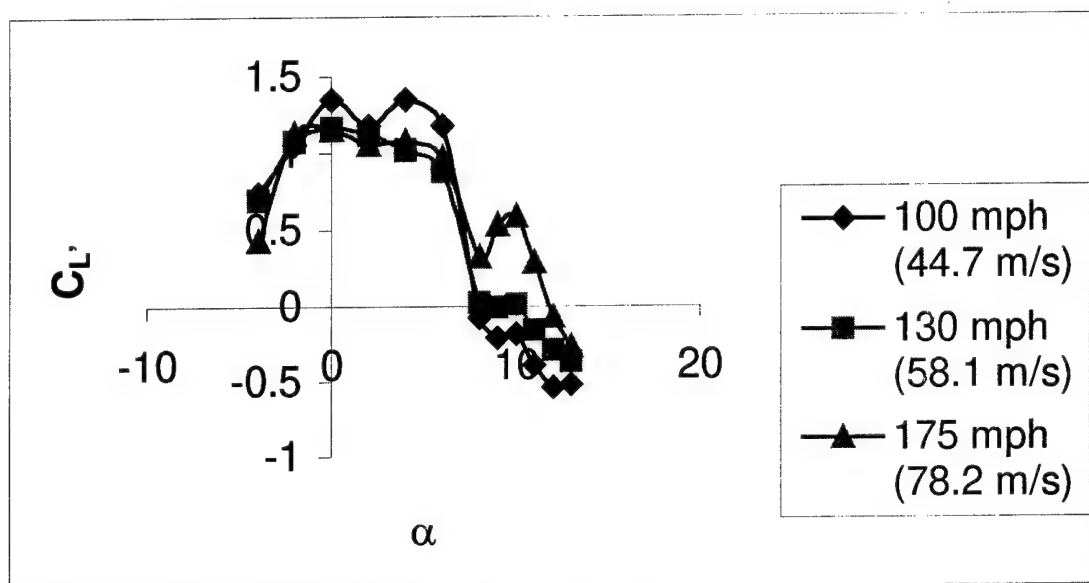
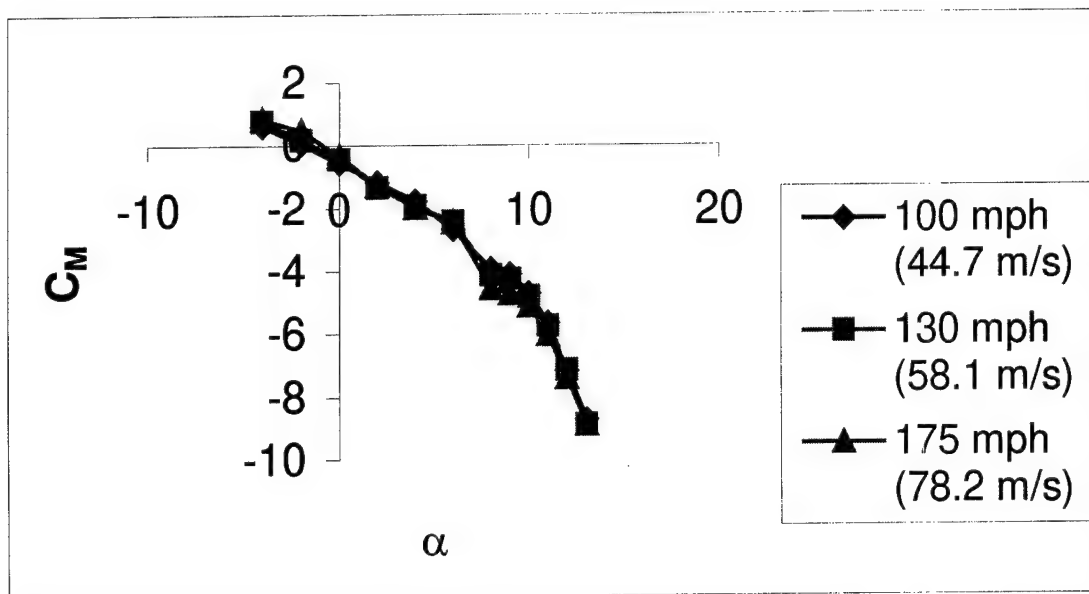


Figure 63: Pitch and Roll Relations of the 30° Swept Biplane, Positive Stagger

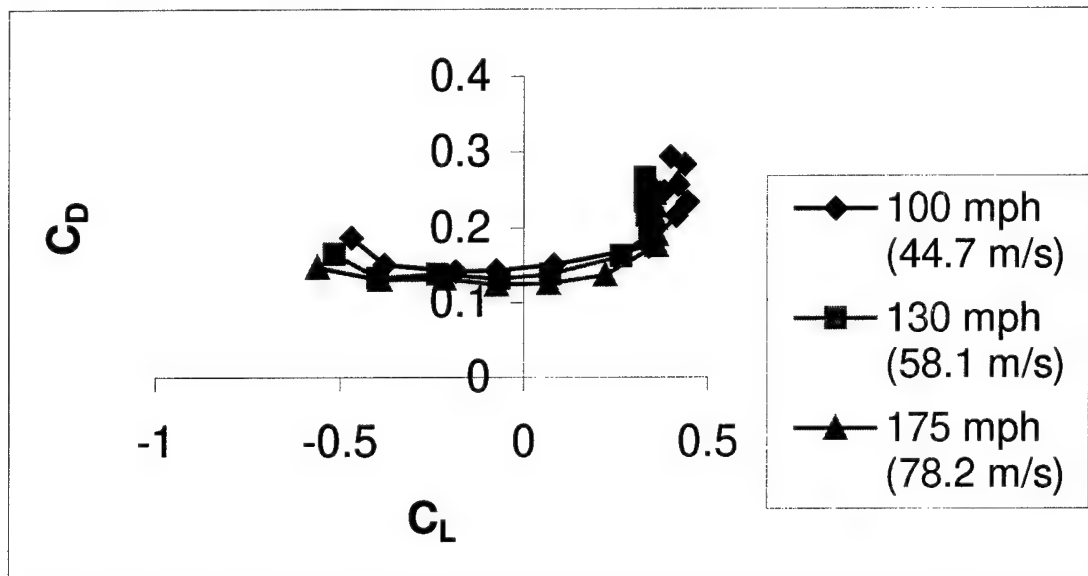
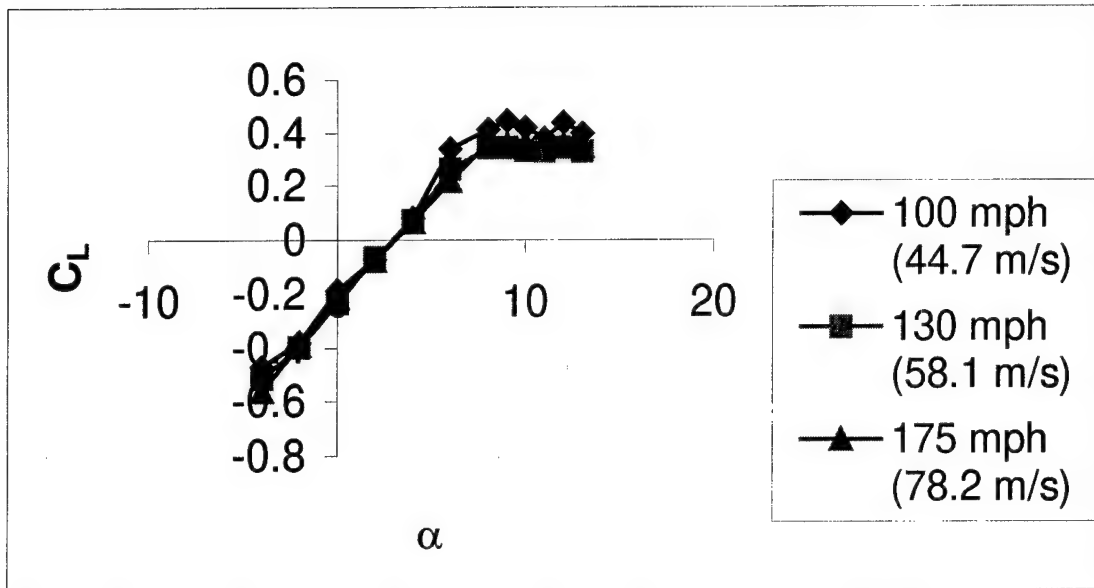


Figure 64: Lift and Drag Relations of the 30° Swept Single Wing Located Aft of the CG, Wings on Bottom

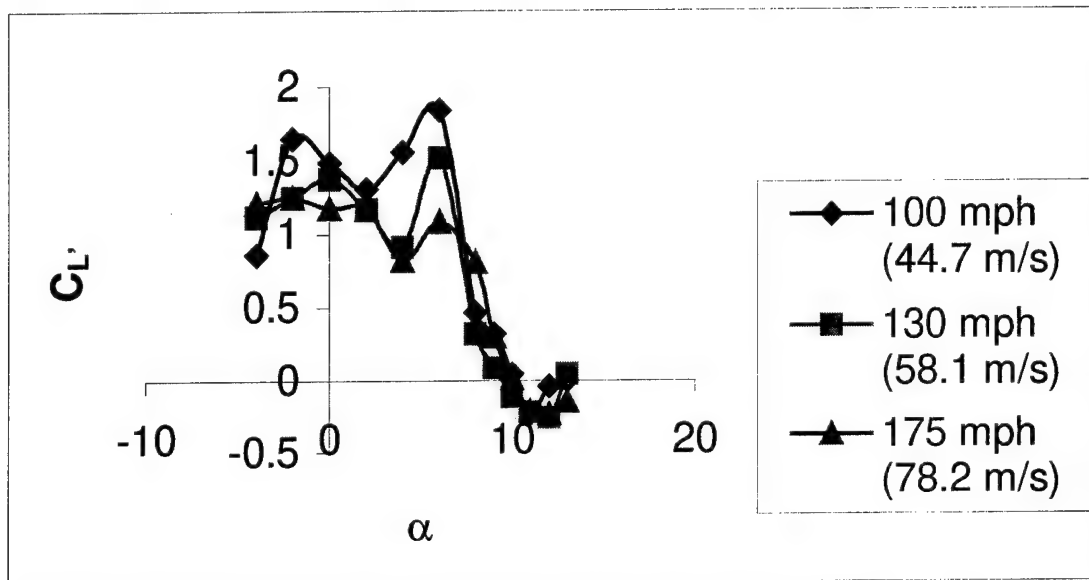
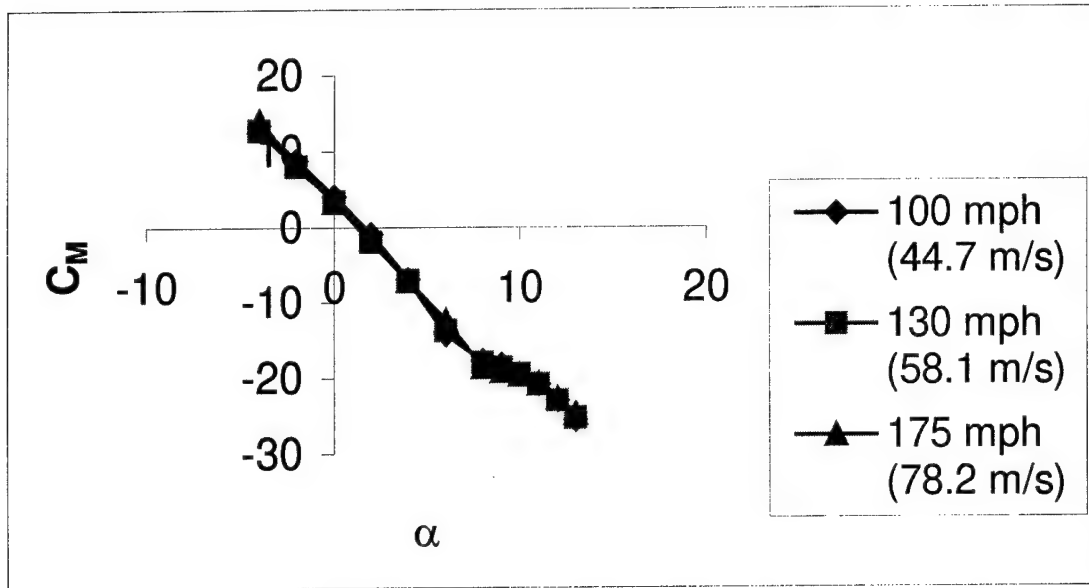


Figure 65: Pitch and Roll Relations of the 30° Swept Single Wing Located Aft of the CG, Wings on Bottom

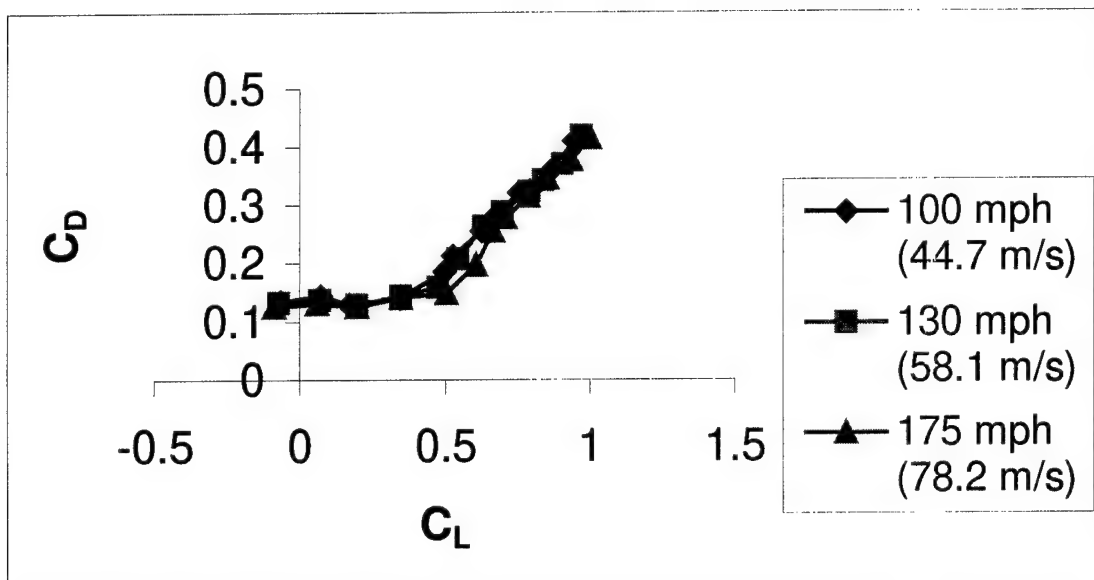
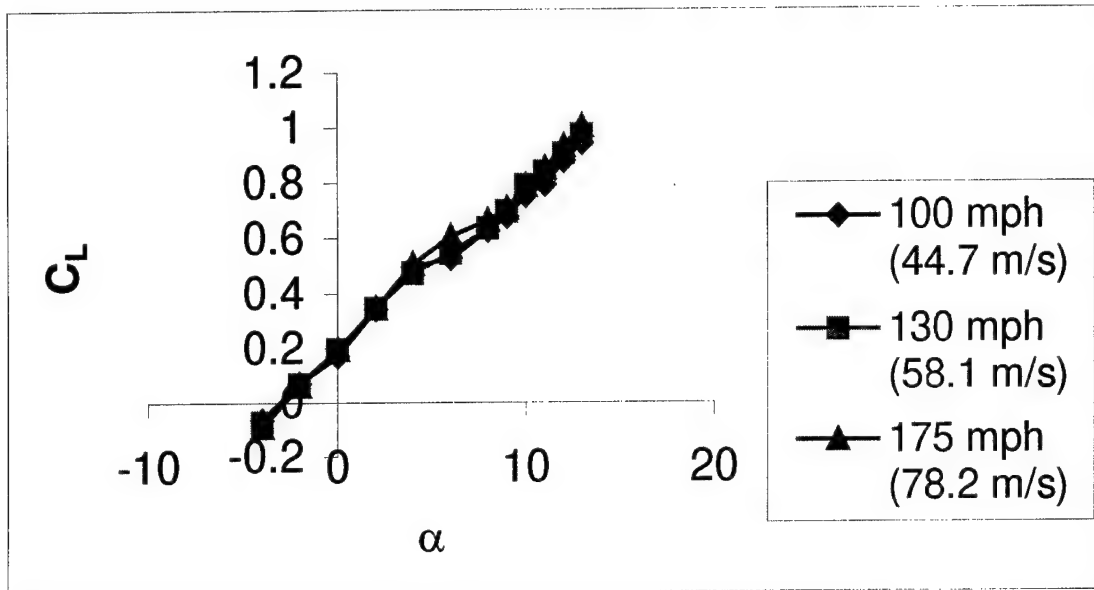


Figure 66: Lift and Drag Relations of the 30° Swept Single Wing Located Aft of the CG, Wings on Top

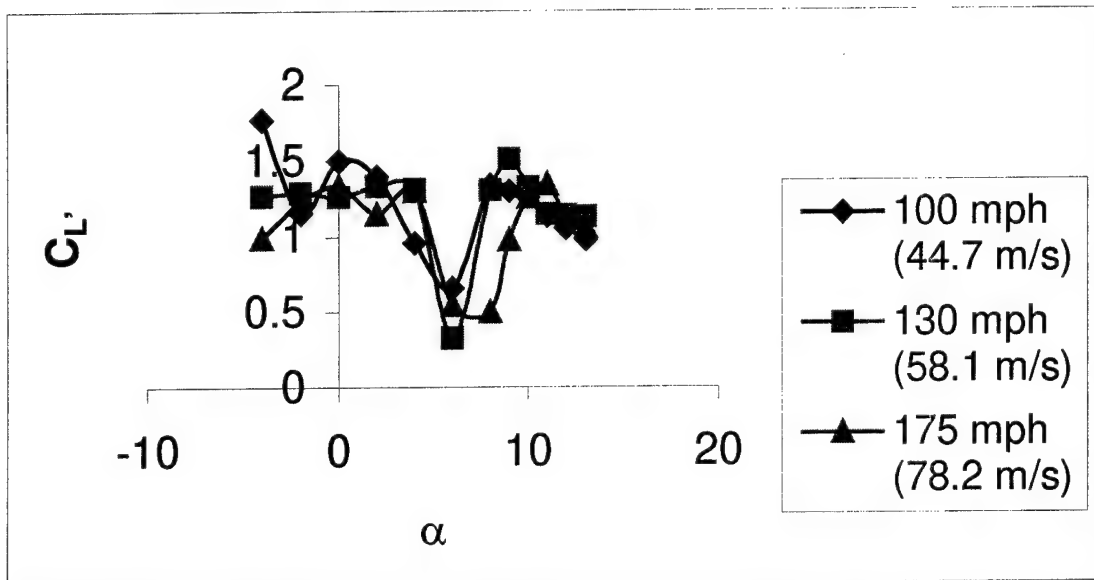
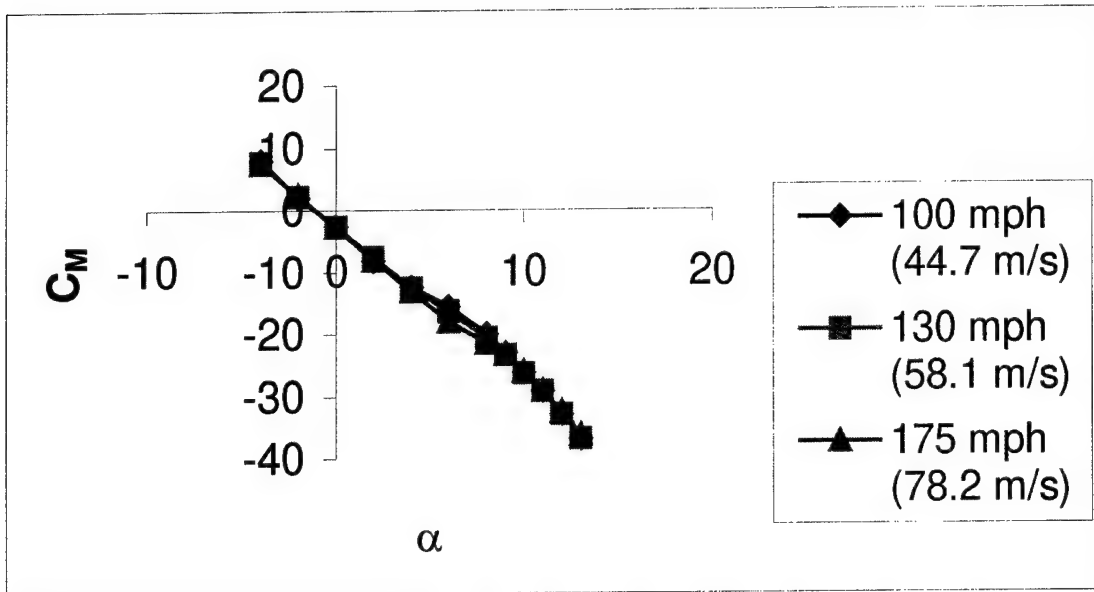


Figure 67: Pitch and Roll Relations of the 30° Swept Single Wing Located Aft of the CG, Wings on Top

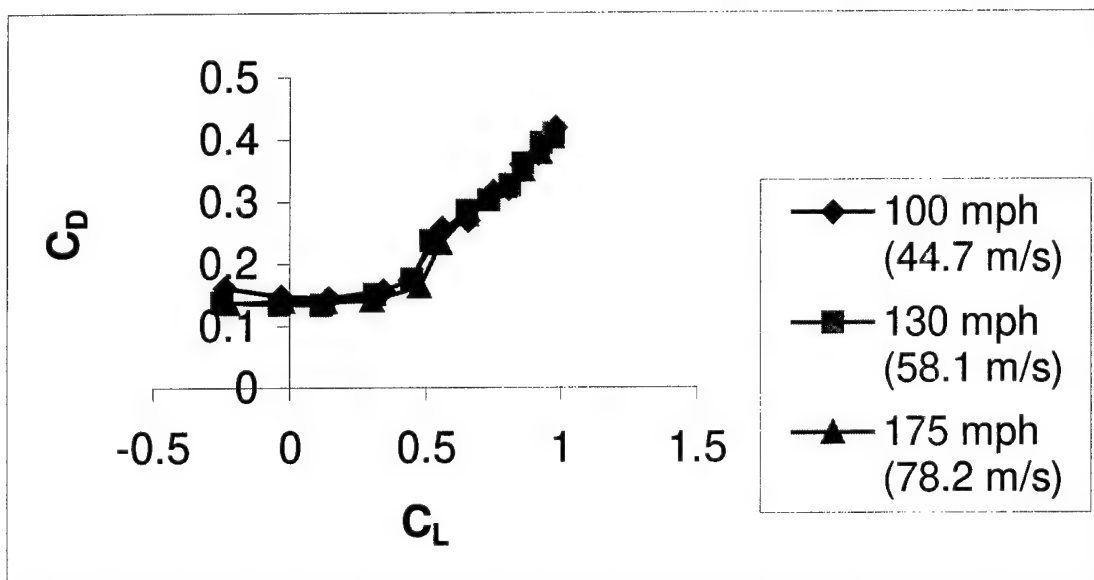
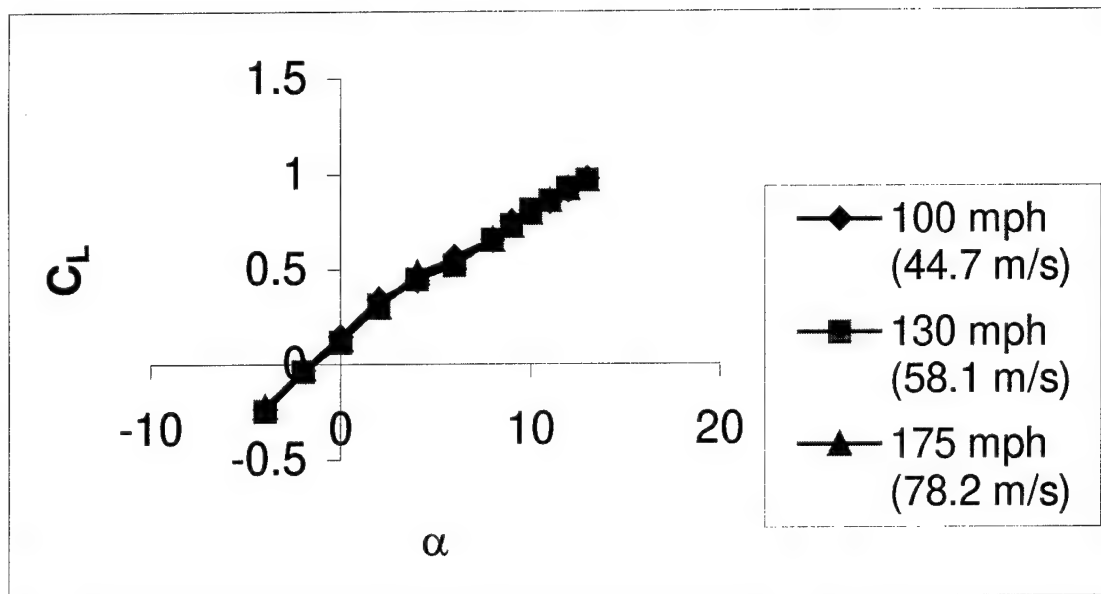


Figure 68: Lift and Drag Relations of the 30° Swept Single Wing Located Forward of the CG, Wings on Bottom

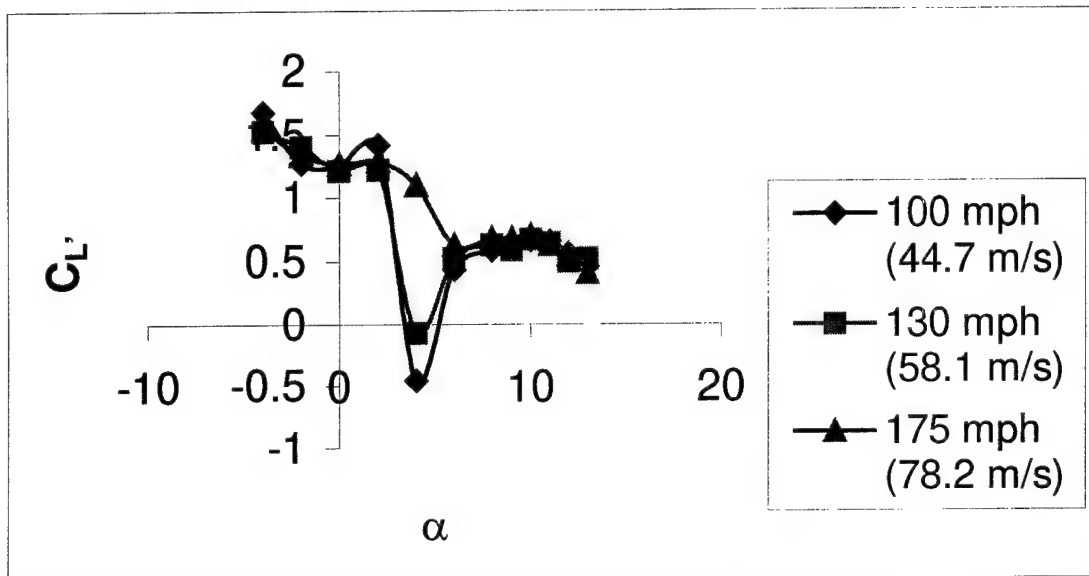
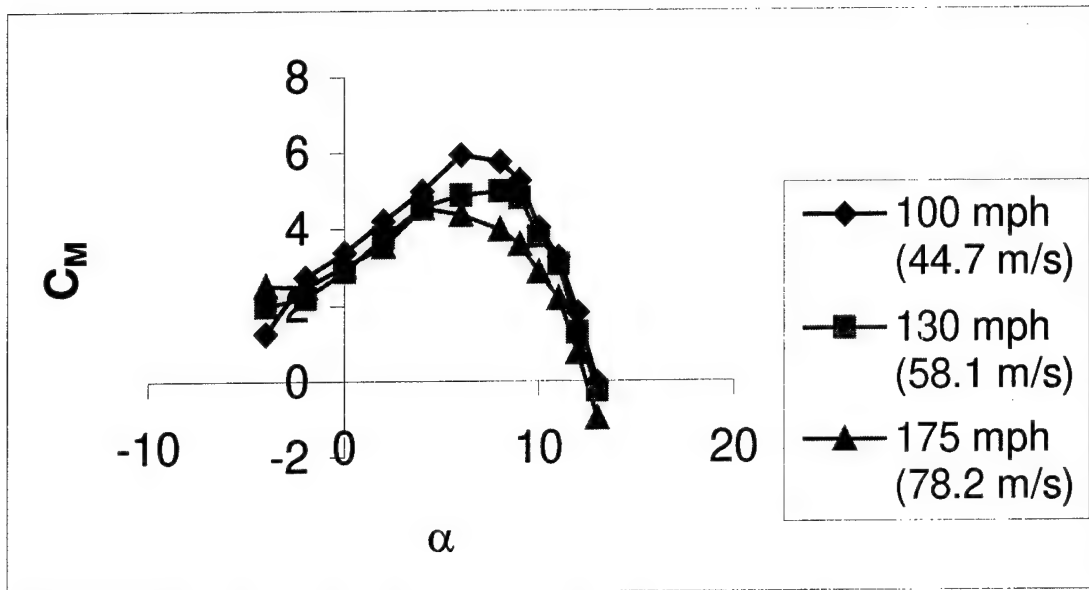


Figure 69: Pitch and Roll Relations of the 30° Swept Single Wing Located Forward of the CG, Wings on Bottom

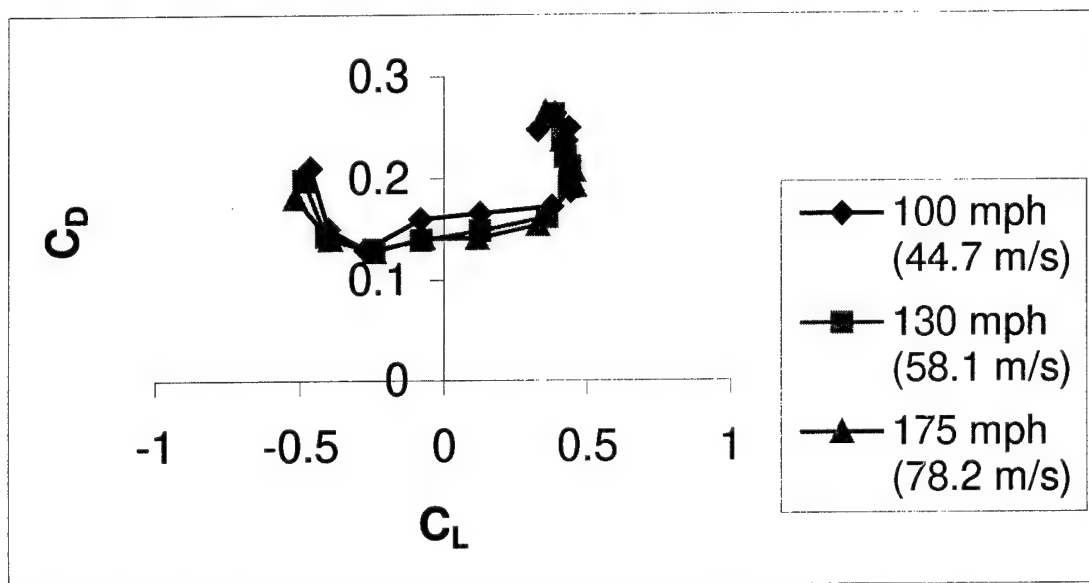
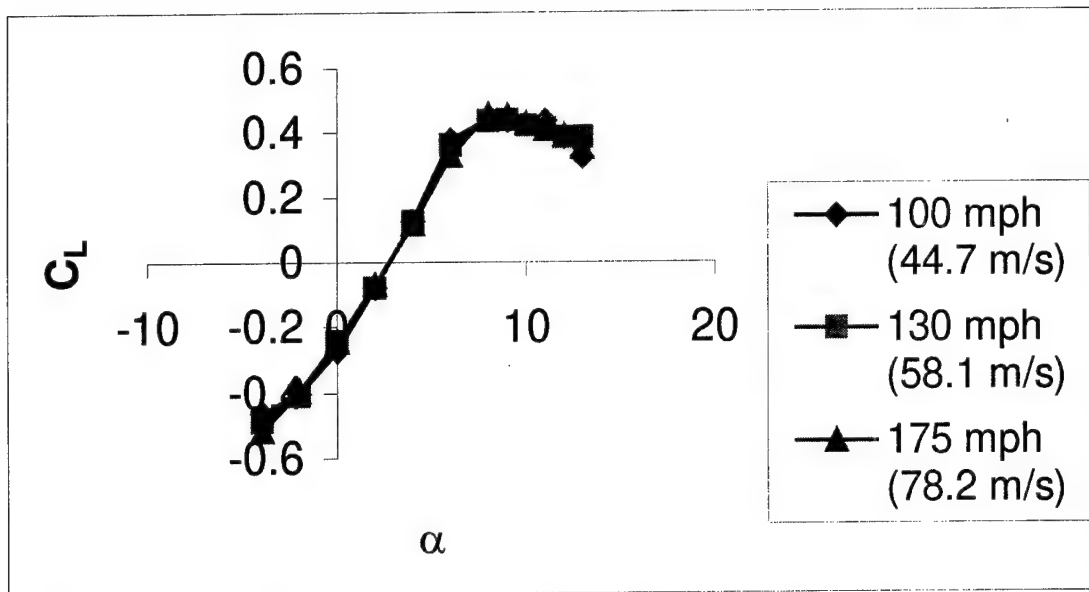


Figure 70: Lift and Drag Relations of the 30° Swept Single Wing Located Forward of the CG, Wings on Top

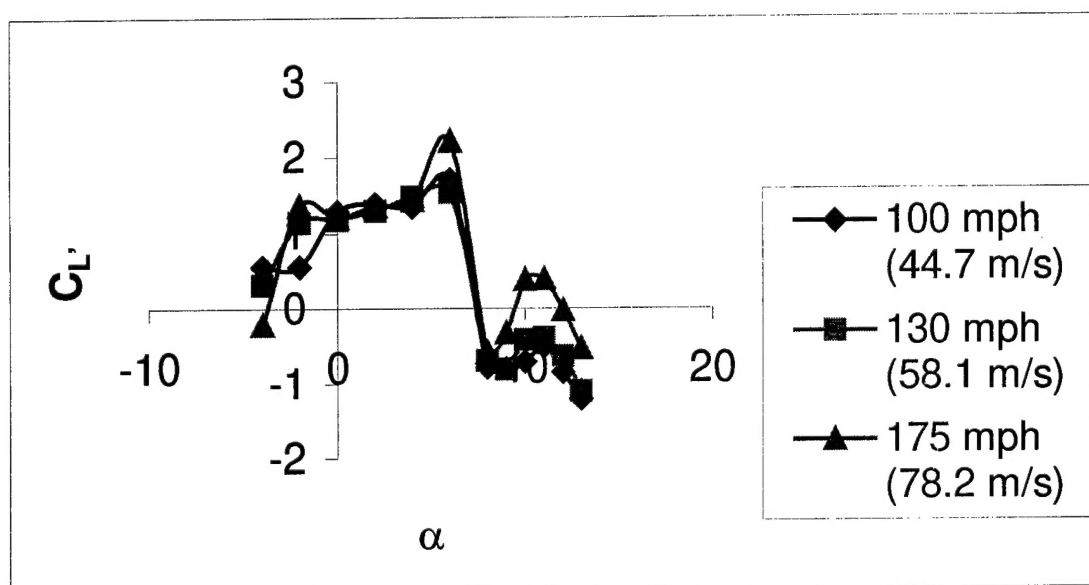
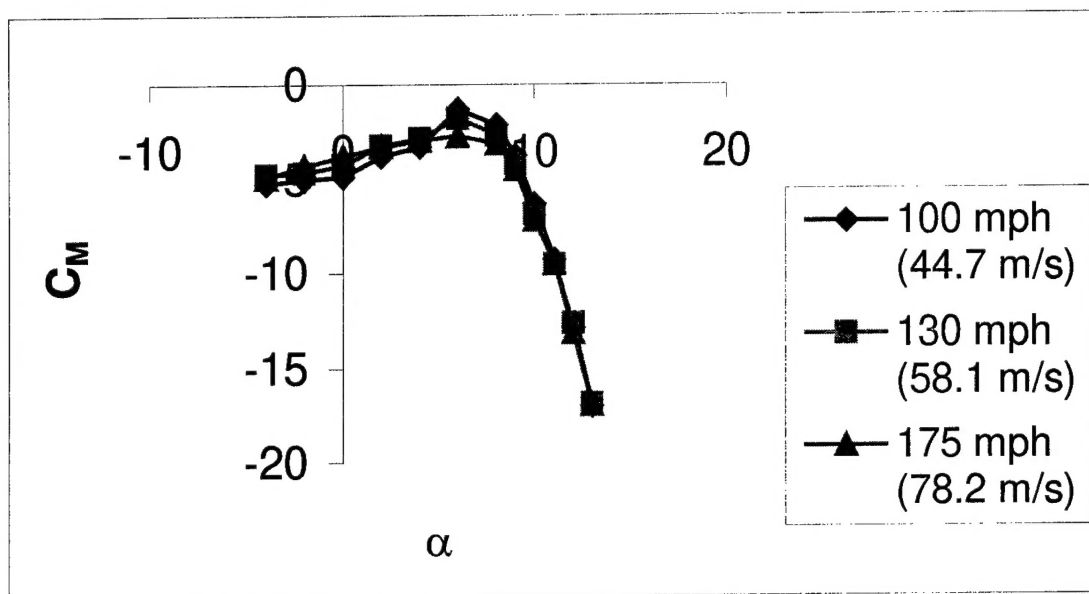


Figure 71: Pitch and Roll Relations of the 30° Swept Single Wing Located Forward of the CG, Wings on Top

Vita

Lt Jennifer Corneille was born in Sault Ste Marie, MI at Kinchloe AFB. She shortly moved to Dayton when her father was assigned to Wright-Patt and has been in the Dayton/Cincinnati area ever since.

Jennifer received a Bachelor's of Mechanical Engineering with a concentration in Aerospace Engineering from the University of Dayton. Upon acquiring her degree, she received her commission in the United States Air Force in May of 1996.

The Manufacturing Technology Division of Wright Laboratory was her first assignment in the Air Force. She worked in the Plans and Programs Office offering support for the SBIR program and coordinating internal and external meetings, including Roadmap. She was also collocated with the Flight Dynamics Directorate conducting ballistic tests on an all-composite wingbox. Jennifer continued to be a participant of the Accelerated Stress Panel, a part of the Armstrong Laboratory, where she was a guinea pig for the centrifuge.

Jennifer received her Master's of Aeronautical Engineering from AFIT in 1999. Upon graduation, she returned to the Materials and Manufacturing Directorate of the Air Force Research Lab. Currently, she is working in the Manufacturing and Engineering Systems Branch where she helps industry effectively use cost and design software.

In July of 1999, Jennifer was assigned to the 49th Test and Evaluation Squadron at Barksdale AFB, LA. As Flight Test Instrumentation Program

Manager, she was involved in testing missiles and bombs dropped by the B-1, B-2, and B-52.

Jennifer enjoys soccer, reading, crafts, having fun, dancing, and smiling.

| REPORT DOCUMENTATION PAGE | | | Form Approved OMB No. 0704-0188 | |
|---|---|--|---|--|
| Public reporting burden for this collection of information is estimated to average 1 hour per response, including the time for reviewing instructions, searching existing data sources, gathering and maintaining the data needed, and completing and reviewing the collection of information. Send comments regarding this burden estimate or any other aspect of this collection of information, including suggestions for reducing this burden, to Washington Headquarters Services, Directorate for Information Operations and Reports, 1215 Jefferson Davis Highway, Suite 1204, Arlington, VA 22202-4302, and to the Office of Management and Budget, Paperwork Reduction Project (0704-0188), Washington, DC 20503. | | | | |
| 1. AGENCY USE ONLY (Leave blank) | | 2. REPORT DATE 15 June 99 | | 3. REPORT TYPE AND DATES COVERED Final; Sep 98 - Jun 99 |
| 4. TITLE AND SUBTITLE Wind Tunnel Investigation of Joined Wing Configuration | | | 5. FUNDING NUMBERS | |
| 6. AUTHOR(S) 1Lt Jennifer Corneille | | | | |
| 7. PERFORMING ORGANIZATION NAME(S) AND ADDRESS(ES) AFIT/ENY 2950 P Street Wright-Patterson AFB, OH 45433-7765 | | | 8. PERFORMING ORGANIZATION REPORT NUMBER | |
| 9. SPONSORING/MONITORING AGENCY NAME(S) AND ADDRESS(ES) Mr. G. L. Winchenbach Air Force Research Laboratory, Munition Directorate 101 W. Eglin Blvd. Eglin AFB, FL 32542-5434 | | | 10. SPONSORING/MONITORING AGENCY REPORT NUMBER | |
| 11. SUPPLEMENTARY NOTES Dr. Milton Franke DSN 785-3636 x4720 milton.franke@afit.af.mil | | | | |
| 12a. DISTRIBUTION AVAILABILITY STATEMENT Unlimited Distribution | | | 12b. DISTRIBUTION CODE | |
| 13. ABSTRACT (Maximum 200 words) The Air Force Research Laboratory's Munitions Directorate is looking to extend the range of its small smart bomb. One proposed idea is to retrofit the bombs with a wing kit, particularly a joined wing configuration. A typical joined wing configuration is one where the wings are positioned in such a way that they form a diamond in both plan and front views. The purpose of this study is to conduct low speed wind tunnel testing of the joined wing configuration to help determine if the joined wing is more beneficial than a single wing configuration. Configurations with differing sweep angles and tip interconnects will be tested in the AFIT 5' wind tunnel. The lift, drag, and pitching moment coefficients will be ascertained. All researched literature indicates that certain joined wing configurations outperform its single wing counterpart. | | | | |
| 14. SUBJECT TERMS Joined Wing Configuration; Wind Tunnel Testing; Range Extension | | | 15. NUMBER OF PAGES 123 | |
| | | | 16. PRICE CODE | |
| 17. SECURITY CLASSIFICATION OF REPORT Unclassified | 18. SECURITY CLASSIFICATION OF THIS PAGE Unclassified | 19. SECURITY CLASSIFICATION OF ABSTRACT Unclassified | 20. LIMITATION OF ABSTRACT UL | |